Application of 3D GPR Imaging in Locating Wat Mo Khlan Archaeological Site in Nakhon Si Thammarat, Thailand

Araya Chansane

A Thesis Submitted in Partial Fulfillment of the Requirements

for the Degree of Master of Science in Geophysics

Prince of Songkla University

2009

Thesis Title	Application of 3D GPR Imaging in Locating Wat Mo Khlan Archaeological Site in Nakhon Si Thammarat, Thailand
Author	Miss Araya Chansane
Major Program	Geophysics

Major Advisor:

……
(Asst. Prof. Dr. Warawutti Lohawijarn)

Co-advisor:

…….....
(Assoc. Prof. Boonlua Phongdara)

Examining Committee:

……...……..
(Dr. Helmut Duerrast)

……...……..
(Asst. Prof. Dr. Warawutti Lohawijarn)

……...……..
(Dr. Sawasdee Yordkayhun)

……...……..
(Dr. Passakorn Pananont)

The Graduate School, Prince of Songkla University, has approved this thesis as partial fulfillment of the requirements for the Master of Science Degree in Geophysics.

…….……..
(Assoc. Prof. Dr. Krerkchai Thongnoo)
Dean of Graduate School

ชื่อวิทยานิพนธ์ การประยุกต์ใช้การสร้างภาพเรดาร์หยั่งลึกชั้นดินแบบ 3 มิติ ในการกำหนดตำแหน่งของแหล่งโบราณคดีวัดโมคลาน จังหวัดนครศรีธรรมราช

ผู้เขียน นางสาวอารยา จันทร์เสน

สาขาวิชา ธรณีฟิสิกส์

ปีการศึกษา 2551

บทคัดย่อ

ได้ทำการวัดและประมวลผลเรดาร์หยั่งลึกชั้นดินแบบสามมิติเพื่อกำหนดตำแหน่งของโบราณวัตถุและโครงสร้างทางโบราณคดีใต้ผิวดินในพื้นที่แหล่งโบราณคดีวัดโมคลาน จังหวัดนครศรีธรรมราช โบราณสถานวัดโมคลานนั้นเดิมเป็นเทวสถานของศาสนาฮินดูลัทธิไศวนิกายขนาดใหญ่ที่มีอายุอยู่ในช่วงพุทธศตวรรษที่ 12 ถึง 14 โดยพื้นที่ศึกษามีขนาด 20 x 33 ตารางเมตร ประกอบด้วย 101 แนววัด แต่ละแนววัดมีความยาว 33.0 เมตร การบันทึกข้อมูลใช้พัลส์สัญญาณเรดาร์ที่มีความถี่กลางเท่ากับ 200 เมกะเฮิร์ต และนำเสนอผลการประมวลข้อมูลในแบบแผนภาพสองมิติ และแผนที่แบบเฉือนตามเวลาและแผนที่ผิวที่มีแอมพลิจูดเท่ากันสำหรับการนำเสนอแบบสามมิติ ผลการศึกษาพบว่าความต่อเนื่องของสัญญาณเรดาร์ผิดปกติทั้งแนวระดับและแนวดิ่งสามารถสังเกตุเห็นได้ชัดเจนด้วยการนำเสนอผลแบบ 3 มิติ โดยการขุดตรวจสอบทางโบราณคดี สัญญาณผิดปกติดังกล่าวเป็นกำแพงโบราณ ซากโบราณสถาน และผิวรอยต่อของชั้นดินปัจจุบันกับชั้นดินโบราณ ดังนั้นลักษณะและขอบเขตทั้งในแนวระนาบและแนวดิ่งของโบราณสถานใต้ผิวดินจึงสามารถประเมินได้จากการนำเสนอผลแบบภาพ 3 มิติข้างต้น

Thesis Title	Application of 3D GPR imaging in locating Wat Mo Khlan archaeological site in Nakhon Si Thammarat, Thailand
Author	Ms. Araya Chansane
Major Program	Geophysics
Academic Year	2008

ABSTRACT

Ground penetrating radar (GPR) measurements and 3D visualization techniques were used in mapping buried archaeological structures in Nakhon Si Thammarat Province, Southern Thailand. The GPR survey was undertaken in an area of the Wat Mo Khlan archaeological site, a Hindu sanctuary of the Saivaism Sect dating back to ca. 7^{th} to 9^{th} century A.D. GPR antennae of 200 MHz central frequency were employed in this study. The measurements were conducted along 101 parallel lines, each 33 m long, in an area of 20 m x 33 m. The processed data were displayed in 2D images and 3D visualizations in time-slices maps and iso-amplitude surfaces maps. Vertical and horizontal continuations of radar anomalies were clearly observed in the 3D visualizations. The anomalies were buried ancient walls, archaeological structure remains, and interfaces between the present and the ancient top soils as verified by ten archaeological tested pits. Therefore, 3D GPR images were proved to be very useful for archaeological mapping, because the shape and boundary of buried archaeological structures can be clearly determined.

ACKNOWLEDGEMENTS

This work has been completed with the help and support from several organizations and people during my study period.

First of all I would like to thank the 14th Regional Office of Fine Arts Department, Nakhon Si Thammarat, for permission to conducting this research, for providing related archaeological information, and for excavation tested pits in the study area. Special thanks to the "*Living Angkor Road*" Research Project and Col. Ph.D. Surat Lertlum for the main financial support during the field work campaign.

Thanks to the Graduate School, Prince of Songkla University, Thailand for financial support to carry out this research project, and thanks to the International Programme in the Physical Sciences (IPPS), Uppsala University, Sweden for the research equipment and interpretation software. Thanks to the "*Development and Promotion of Science and Technology Talents*" (DPST) Project for the scholarship, and research budget to carry out my study.

I would like to express my deepest gratitude to my advisors, Assistant Professor Dr. Warrawutti Loharwijarn and my co-advisor, Associate Professor Boonlua Phongdara for their valuable supervision and suggestions, support, encouragement, guidance, and criticism throughout the course of my study. Thanks also to Dr. Helmut Dürrast for English language corrections of my thesis.

Special thank to Mr. Pongdhan Sampaongen, Mr. Chakrit Sittirit and staffs of the 14th Regional Office of Fine Arts Department, Nakhon Si Thammarat, for their taking care and helping during the periods of fieldwork. Further thanks to Dr. Kamhaeng Wattanasen and Dr. Sawasdee Yordkayhun for valuable suggestions and comments during my research. Many thanks to Mr. Somyot Vitchuvalun for taking care of the field equipment and for his help during my work.

I would never forget my dear friends, Mr. Phongpiyah Klinmanee, Mr. Vongsakorn Aporntip, Mr. Jirapan Sritium, Mr. Sukrit Jonjana, and Mr. Phanuphong Limusanno for their help during my fieldwork period. Thanks to Mr. Apichai Khawtawan, Mr. Prayoot Khawdee, Mr. Santi Ragsawong, Ms. Pitchpilai Khoonphunnarai, and Ms. Atcha Kobwittaya for the practical help and cheerfulness along my study.

I am very grateful to all of my friends in Geophysics Laboratory, Department of Physics, Faculty of Science, Prince of Songkla University, for their practical help, providing the wonderful environment and friendship during the time of my study.

Finally, I would like to express my sincere gratitude and appreciation to my family for their love, cheerfulness, devotion, and encouragement throughout my study.

February 2009

Araya Chansane

TABLE OF CONTENTS

LIST OF TABLES

LIST OF FIGURES

LIST OF FIGURES (Cont.)

LIST OF FIGURES (Cont.)

LIST OF FIGURES (Cont.)

LIST OF FIGURES (Cont.)

LIST OF FIGURES (Cont.)

CHAPTER 1

INTRODUCTION

Wat Mo Khlan is one of the archaeological sites in Tha Sala District, Nakhon Si Thammarat Province, Southern Thailand (Figure 1.1 to 1.2). This site has been proclaimed as a national archaeological site in 1976. This archaeological site is important for the history and archaeology of Nakhon Si Thammarat Province, where a prehistoric human community settled down about 6,500 years ago (Fine Arts Department, 1993).

Archaeological exploration, excavation, and restoration were conducted in the Wat Mo Khlan archaeological site in 1990 and 1992-1993 (Figure 1.3). During that time, many archaeological evidences were discovered such as cultural artifacts and religion related items. These information and other collateral evidences caused archaeologists to believe that there should be other ancient remains, such as walls and building structures, buried in subsurface of the area to the south of the previously excavated and restored Wat Mo Khlan archaeological site (Figure 1.3). To accomplish this expectation, an area to the south of the excavated and restored archaeological walls and buildings has to be investigated. Since the proposed area is quite large in dimension, archaeological excavations are expected to need significant expenses, therefore geophysical investigation was considered as a very useful technique for locating the buried archaeological structures (Lohawijarn, 2005).

Ground penetration radar (GPR) is the most common geophysical method applied for archaeological problems. The GPR can be applied solely or in combination with other geophysical methods, i.e. magnetic, electrical, or seismic methods. Nowadays, application of GPR in archaeological investigations is increasing due to its non-destructive nature, fast operating time, and high-resolution images, which buried features of relatively small size, are easily recognized. Another advantage is the facility of data processing in the field so that the anomalies can be quickly identified. The results obtained from the GPR investigation, including

location, alignment and depth of burial, will be very useful for planning of archaeological excavation pits.

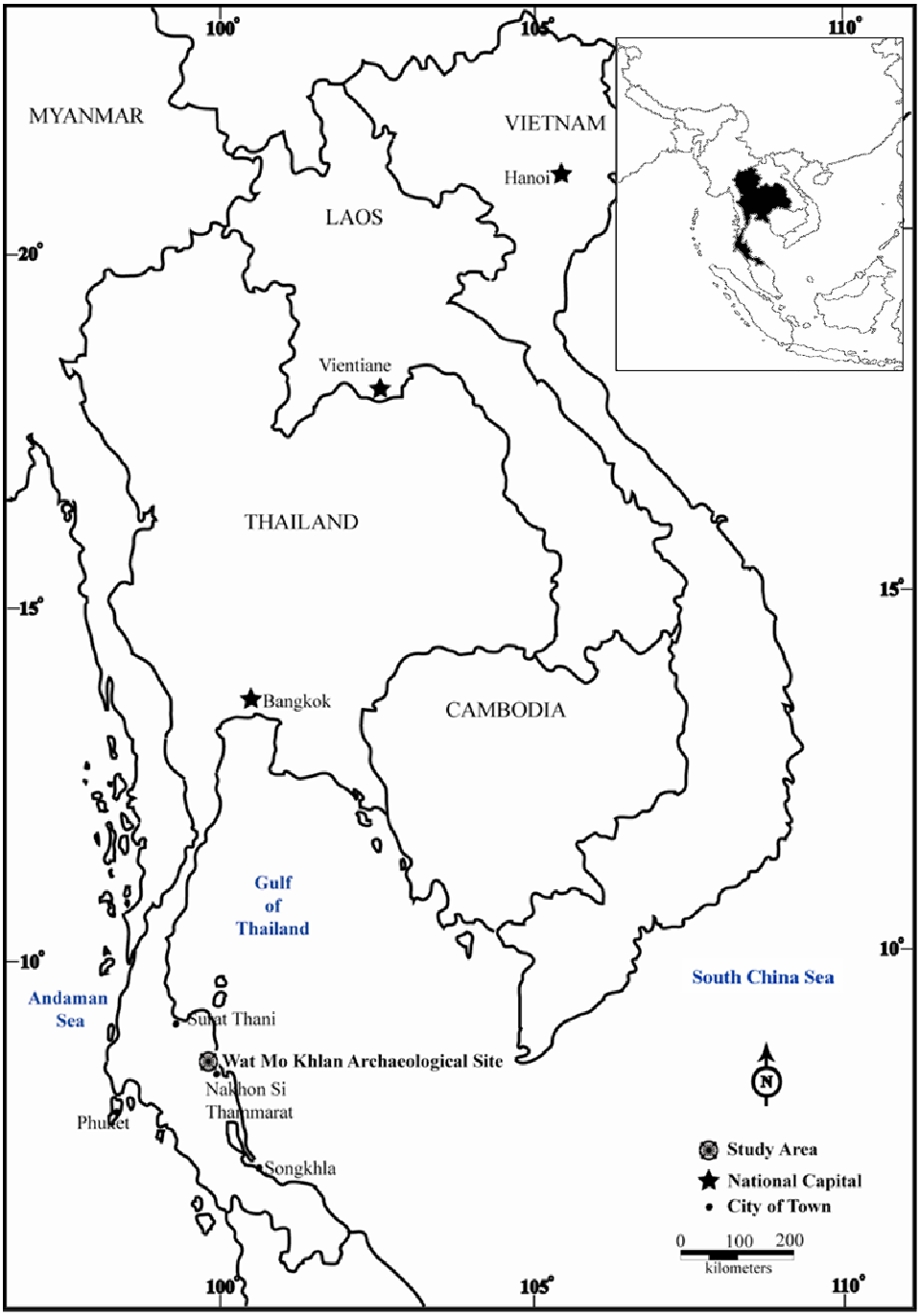

Figure 1.1 Map of Thailand with the location of Wat Mo Khlan archaeological site (modified from http://geology.com/world/thailand-satellite-image.shtml [28 January, 2009]).

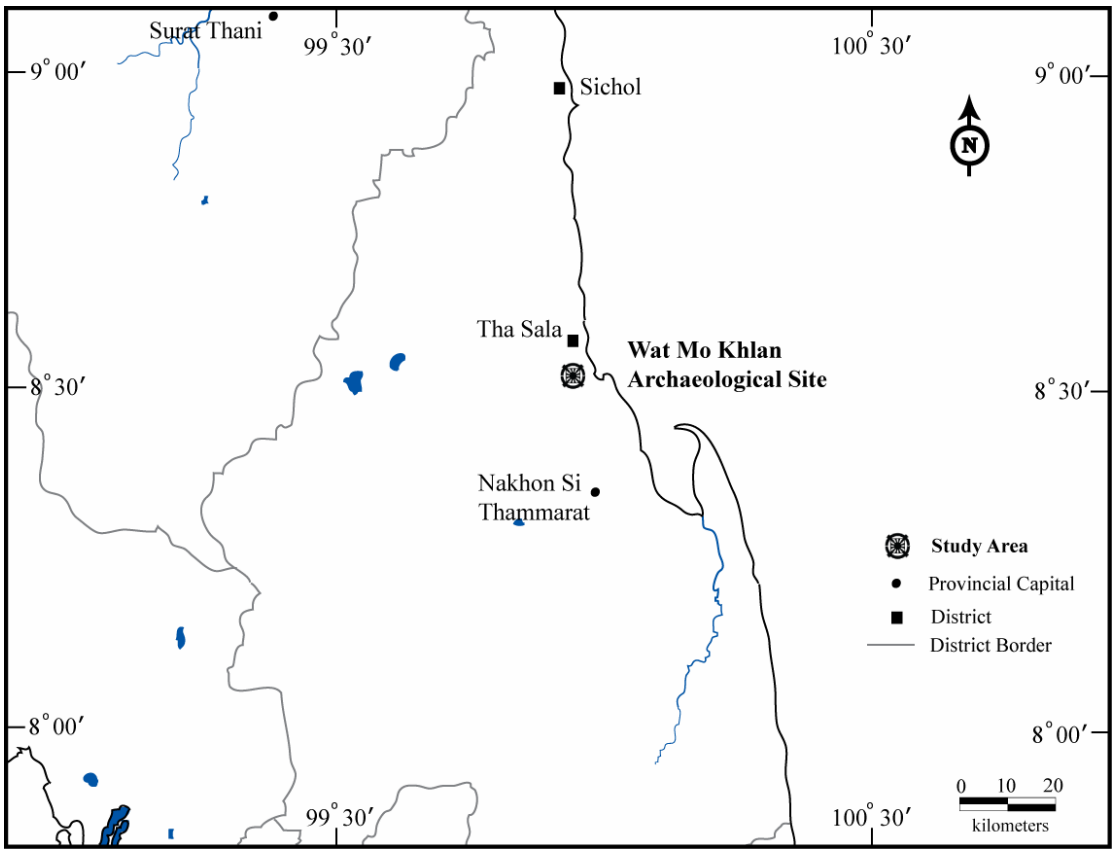

Figure 1.2 The location of Wat Mo Khlan archaeological site (modified from http://maps.google.com/ [28 January, 2009]).

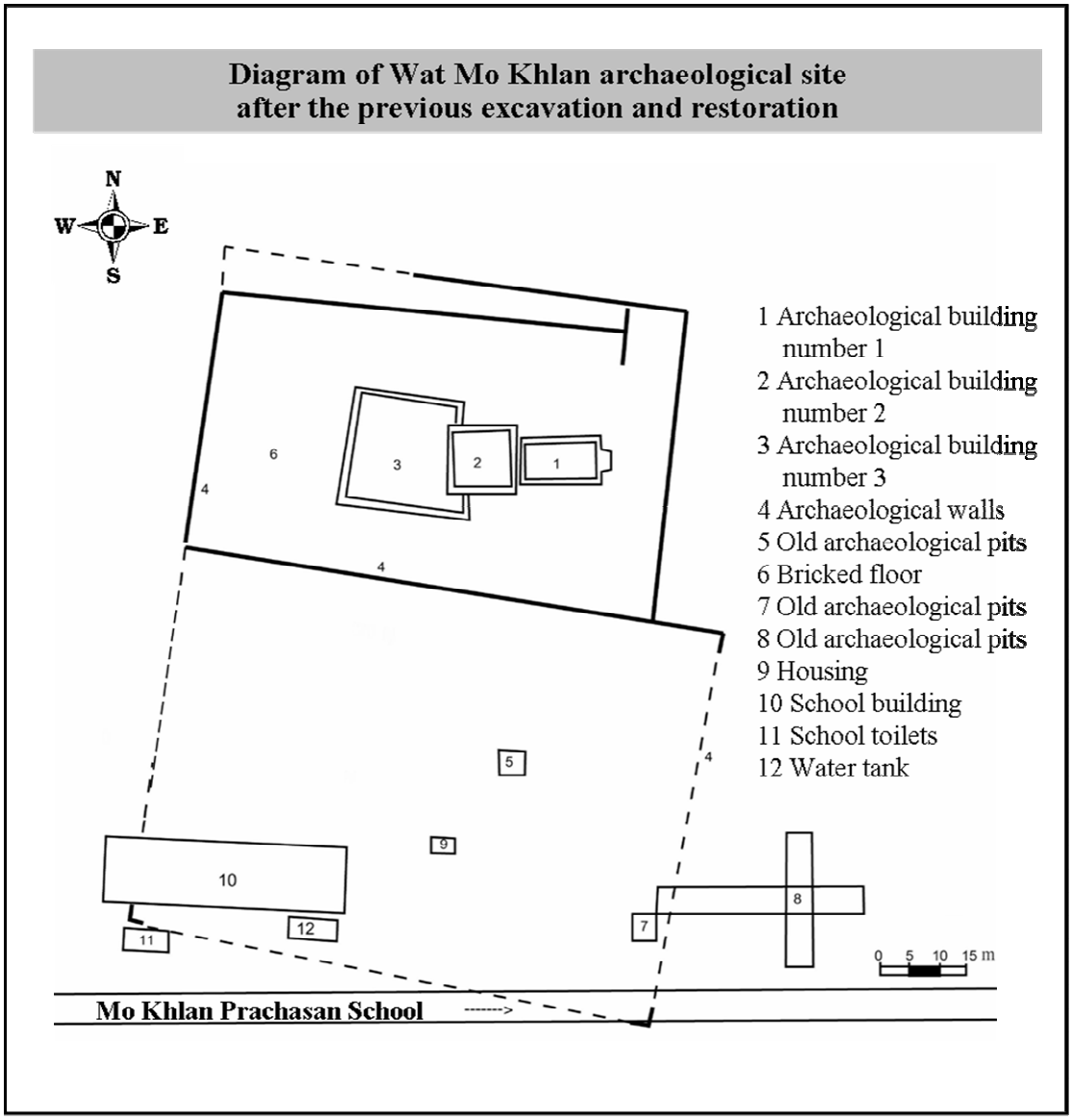

Figure 1.3 Diagram of excavated and restored Wat Mo Khlan archaeological site (modified from Fine Arts Department, 1993).

1.1 Physical base of ground penetrating radar

'Radar' is the acronym of 'radio detection and ranging', a system using short duration electromagnetic waves (Parasnis, 1997). Many different pulse radar devices are available for ground investigations and it is usual to group them as ground penetrating radar or GPR. GPR utilizes the propagation and scattering of electromagnetic waves to image, locate, and quantitatively identify changes in electrical and magnetic properties in the ground. A pulse of radar energy (Figure 1.4a) is generated on a transmitting antenna dipole placed on the ground surface (Conyers, 2001). The energy propagates downward into the ground where portion of it is reflected back to the surface at discontinuity created by changes in electrical properties of sediment or soil, variations in water content, changes in lithology, or changes in bulk density at stratigraphic interfaces. Reflection can also occur at interfaces between anomalous archaeological features, buried pipes, and the surrounding soil or sediment. The greater the contrast in electrical properties between the two materials, the stronger is the reflected signal.

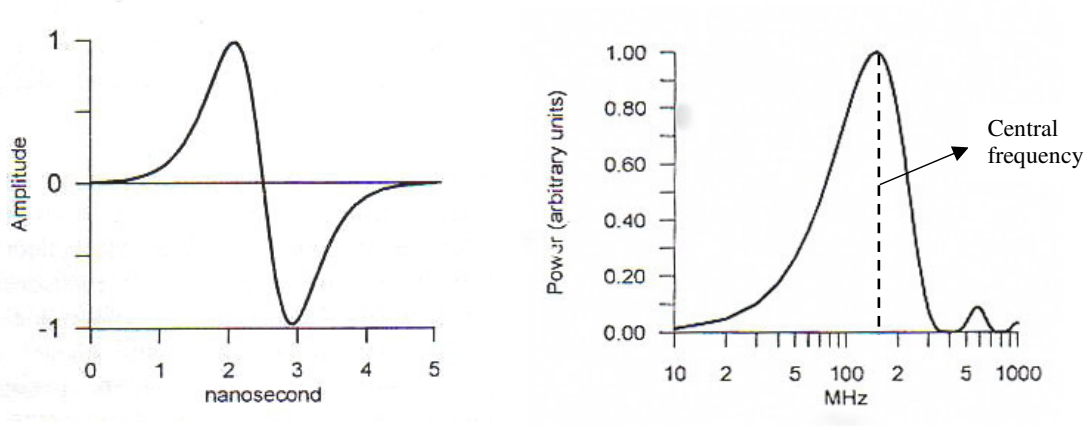

(a) (b)

Figure 1.4 (a) GPR pulse and (b) its power spectrum (from Parasnis, 1997).

1.1.1 Penetration Depth of GPR

The depth of investigation of GPR varies from less than a meter to over 5,400 meters, depending upon material properties which the radar pulse propagates through (Olhoeft, 2006). Detectability of a subsurface feature depends upon contrast in electrical and magnetic properties, and the geometric relationship with the antenna. For the radar pulse that propagating with frequency ω through the medium whose conductivity is σ, and magnetic permeability is μ, the depth of penetration (δ) can be estimated from the following Equations (Parasnis, 1997).

$$\delta = \frac{1}{\sqrt{\pi\mu\sigma\omega}} \tag{1.1}$$

In non-magnetic media ($\mu = \mu_0$), the penetration depth of radar pulse can be calculated from

$$\delta = 503.3\frac{1}{\sqrt{\sigma\upsilon}} \tag{1.2}$$

where υ is the single frequency of the radar pulse (obtained from $\upsilon = \omega/2\pi$), μ and μ_0 are the magnetic permeability of the media and of vacuum, respectively.

1.1.2 Q and loss tangent

The parameter that determines how efficiently an electromagnetic wave propagates in a medium is $\rho\varepsilon\omega$ (where ρ is the resistivity and ε is the dielectric permittivity), often denoted by Q, also written as $\varepsilon\omega/\sigma$.The inverse $1/Q = \sigma/\omega\varepsilon$ is called the loss tangent. If $Q >> 1$, the wave will propagate efficiently without appreciable loss of energy over large distance. If $Q < 1$, the wave is attenuated within a short distance (Parasnis, 1997).

1.1.3 Frequency of GPR

When radar pulses propagating in the ground, it is generally more convenient to consider an electromagnetic wave of single frequency, $\upsilon = \omega/2\pi$, instead of a pulse containing a number of different frequencies (Parasnis, 1997). However, the salient features of the propagation of a GPR pulse are well described if frequency means the *central frequency*, which is surrounded with most of the energy

in the pulse. The power spectrum of radar pulses (Figure 1.4(b)) can be calculated from the following Equation,

$$\left|F(\upsilon)\right|^2 = \frac{\left[1-\cos(\pi\upsilon\tau)\right]^2}{2\pi^2\upsilon^2} \tag{1.3}$$

where $\left|F(\upsilon)\right|^2$ is the power amplitude of frequency υ [arbitrary units], τ is the duration of the pulse [ns], and υ is the frequency of the electromagnetic pulse [Hz].

Based on main antennae frequencies, GPR applications can be divided into two groups; geological applications and engineering applications (Reynolds, 1997). For geological applications, where depth of penetration tends to be more important than very fine resolution, antennae with frequencies less than or equal to 500 MHz are commonly used. For engineering or nondestructive testing applications, antennae with frequencies greater than or equal to 500 MHz and typically as high as 900 MHz or 1 GHz are used.

1.1.4 Reflection of Radar Pulse

During propagation of electromagnetic wave, reflection happens when the wave meets a change in electrical or magnetic properties of material such as the interfaces between media of different impedances. The impedance, Z [ohm], presented by any medium to the passage of electromagnetic waves is expressed by Equation (1.4) (Parasnis, 1997),

$$Z = \omega\mu / k \tag{1.4}$$

where $k = \left(\omega^2\varepsilon\mu + i\omega\mu/\rho\right)^{1/2}$.

Let E_i, E_r and E_t be the amplitudes of the incident, reflected and transmitted electric fields. If the incidence is normal to the interface, the reflection and transmission coefficients are given by

$$R = \frac{E_r}{E_i} = \frac{Z_2 - Z_1}{Z_2 + Z_1} \quad \text{and} \quad T = \frac{E_t}{E_i} = \frac{2Z_2}{Z_2 + Z_1} \tag{1.5}$$

where the subscripts 1 and 2 refer to the two media on either side of the interface and the wave is supposed to be incident from medium 1. Normal incidence implies that the same antenna is used for transmission and reception of the signals. However, if the

offset between the antennas is very small compared to the distance to the interface, the incidence may be assumed to be normal. In non-magnetic media, $\mu_2 = \mu_1 = \mu_0$, the reflection coefficient can be expressed as

$$R = \frac{\left(\omega\varepsilon_1 + i\sigma_1\right)^{1/2} - \left(\omega\varepsilon_2 + i\sigma_2\right)^{1/2}}{\left(\omega\varepsilon_1 + i\sigma_1\right)^{1/2} + \left(\omega\varepsilon_2 + i\sigma_2\right)^{1/2}} \tag{1.6}$$

where ε is the absolute permittivity. If both media are non-conducting $\left(\sigma = 0\right)$ with $\varepsilon_1 = \varepsilon_{1r}\varepsilon_0$ and $\varepsilon_2 = \varepsilon_{2r}\varepsilon_0$, where ε_{1r} and ε_{2r} are relative permittivities, the reflection coefficient can be expressed as

$$R = \frac{\sqrt{\varepsilon_{1r}} - \sqrt{\varepsilon_{2r}}}{\sqrt{\varepsilon_{1r}} + \sqrt{\varepsilon_{2r}}} \tag{1.7}$$

To generate a significant reflection, the change in dielectric permittivity between two media (Table 1.1) must occur over a short distance. These, of course, can be highly variable due to change in clay and moisture content. The greater the difference in relative permittivity of the subsurface materials, the larger is the amplitude of the reflection generated.

1.1.5 Focusing and Scattering Effects

Reflection from a buried surface containing ridges or troughs can either focus or scatter radar energy, depending on its orientation and the antenna location (Conyers, 2001). If a subsurface plane is slanted away from antenna or convex, most energy will be reflected away from the antenna, and very low reflection amplitude will be recorded. This is termed radar scattering. On the contrary, when the buried surface is tipping toward the antenna or is concave, reflected energy will be focused, and a very high-amplitude of reflection will be recorded. Figure 1.5 shows examples of focusing and scattering effects when a narrow buried moat is bounded on one side by a trough and on the other side by a mound.

Table 1.1 Typical relative dielectric permittivity (ε_r), conductivity (σ), and radar pulse velocity (V) observed in common geological and some archaeological materials.

Material	ε_r	σ (mS/m)	V (m/ns)	References
Air	1	0	0.30	Davis and Annan, 1989
Ice	3-4	0.01	0.16	Davis and Annan, 1989
Water (distilled)	80	0.01	0.033	Davis and Annan, 1989
Water (Fresh)	80	0.5	0.033	Davis and Annan, 1989
Sand (dry)	3-5	0.01	0.15	Davis and Annan, 1989
Sand (saturated)	20-30	0.1-1.0	0.06	Davis and Annan, 1989
Shales	5-15	1-100	0.09	Davis and Annan, 1989
Silt	5-30	1-100	0.09	Davis and Annan, 1989
Clays	5-40	2-1000	0.06	Davis and Annan, 1989
Concrete	8	NA	NA	Conyers, 2001
Tuff bricks (dry)	3	NA	NA	Brancaccio et al., 2004
Remnants of ancient kilns	7.3-7.8	NA	NA	Hayee-uma, 2002

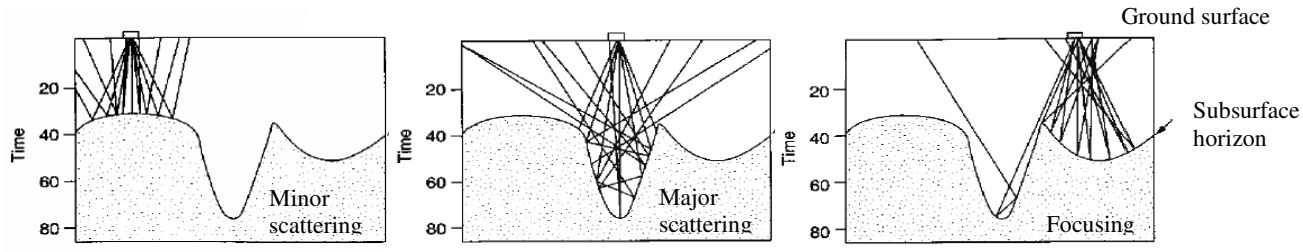

Figure 1.5 GPR ray path reflected from an undulating surface and a deep ditch. Convex surfaces scatter radar energy while concave surface focus. Deep features tend to scatter most of the energy and are hard to be detected by GPR (modified from Conyers, 2001).

1.1.6 Resolution of GPR

Three dimensional objects can be resolved if the reflections from at least two surfaces, usually the top and the bottom interfaces, are distinct (Conyers, 2001). To distinguish reflections from two parallel planes, they must be separated by at least one wavelength of the energy passing through the ground, unless resulting reflected waves from the top and the bottom will either be destroyed or unrecognizable due to constructive and destructive interference. When two interfaces are separated by more than one wavelength, however, two distinct reflections are generated, and the top and the bottom of the feature can be resolved.

Frequency of the antenna is an important resolution factor (Parasnis, 1997). Low frequency antenna received reflected data from a much greater subsurface area, resulted in the low percentage of reflections from small irregular features. Therefore, a reflective profile obtained from reflections of a low frequency antenna produces an average and less accurate representation of a buried surface. In the contrary, a higher frequency antenna provides a greater resolution of subsurface features. High frequency radar waves can resolve very small features but will not penetrate to a great depth, while a low frequency radar wave will resolve only larger features and will penetrate to a great depth. Both point and planar targets are potentially visible with any frequency data depending on a planar surface's thickness, reflectivity, orientation, and depth of burial.

The vertical resolution is the minimum detectable separation in depth between reflection interfaces of a reflector. This type of resolution depends on the antenna frequency, and can be estimated as follows (Parasnis, 1997):

$$d = \frac{V}{2\upsilon} \tag{1.8}$$

where d is the thickness of a layer in the ground [m], V is the velocity of the wave in the media [m/s], and υ is the frequency [Hz] of the electromagnetic wave.

The lateral resolution is the horizontal extent of a reflector. The reflection energy that arrives at the receiver antenna does not come from the single point of incidence but from a finite area of a reflector. Then the lateral resolution, which also depends on frequency, is given by (Parasnis, 1997):

$$a = \frac{V}{2}\sqrt{\frac{t}{\upsilon}} \tag{1.9}$$

where a is the radius of circular area around the point of incidence [m], t is the two-way time [s] and υ is the frequency of the electromagnetic wave [Hz].

1.1.7 The GPR system

The GPR system comprises four main parts; the transmitting unit, the receiving unit, control unit and the display unit. Figure 1.6 shows a schematic diagram of a GPR system. The transmitter generates and sends electromagnetic pulse into the ground. The reflected signal is detected by the receiving antenna. The moveable radar antennas are connected to the control unit by cables. The system records the reflective data digitally and directly at the antenna. The digital signal is sent back through the cable to the control unit and the radargram, including amplitude of the reflected pulses at different arrival time, are displayed at the display unit.

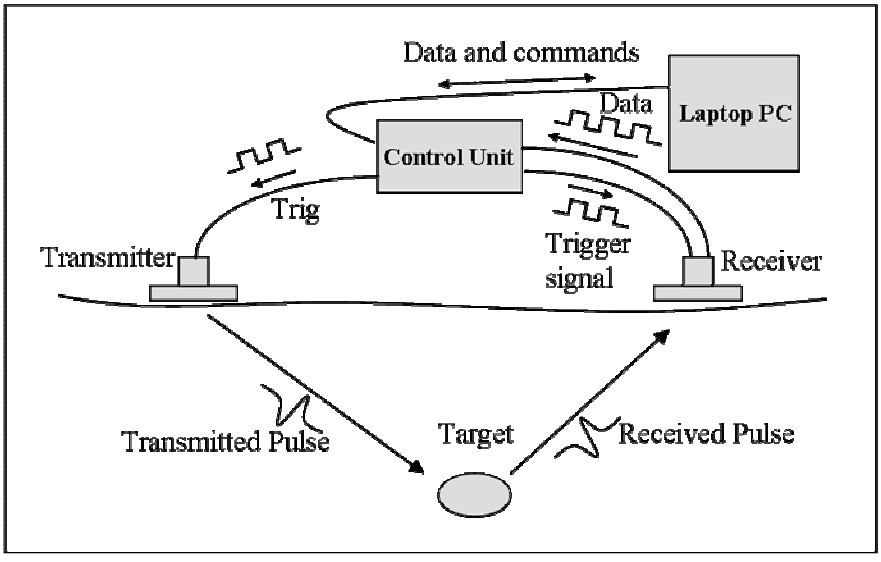

Figure 1.6 Schematic diagram of the GPR system (Modified from Phattanaviriyaphisarn, 2002).

1.1.8 Acquisition parameter

To attain prominently strong and coherent reflection amplitudes, which produces adequate resolution and quality of results, some of the data acquisition parameters have to be considered**.**

1.1.8.1 Minimal antenna separation

When the transmitter and receiver are placed in proximally, the recording signal saturation might be occur. In order to avoid the saturation of the signal that occurs when the transmitter is in close proximity to the receiver, the minimal distance between antennas is made to be equal to one-half the wavelength of central frequency used and direct signals are registered along the transmission time period. (Table 1.2). An appropriate distance between antennas is computed by Equation (1.10) (Avila-Olivera and Garduño-Monroy, 2008).

$$x = \frac{2h}{\sqrt{\varepsilon - 1}} \tag{1.10}$$

where x is the antennas separation [m], h is the exploration depth [m] and ε is the dielectric permittivity.

Table 1.2 Minimal antennas spacing, measuring point interval and maximal recording time window for different central frequencies (modified from Avila-Olivera and Garduño-Monroy, 2008)

Central frequency [MHz]	Minimal antennas separation [m]	Measuring point interval [m]	Maximal sampling interval [ns]
50	2.00	0.50	3.30
100	1.00	0.25	1.67
200	0.50	0.10	0.83

1.1.8.2 Measuring point interval

One of important acquisition parameters is the measuring point interval or trace spacing, which is the distances along which the measurements are recorded. This parameter allows to avoid response overlapping as well as to ensure the

appropriate identification of the objective. In general, the value is from about a quarter to a half of the wavelength of the central frequency used (Table 1.2). Usually a longer interval results in a loss of detail. The measuring point interval can be obtained by the following Equation:

$$\Delta x = \frac{c}{4\upsilon\sqrt{\varepsilon_r}} = \frac{75}{\upsilon\sqrt{\varepsilon_r}} \tag{1.11}$$

where Δx is the measuring point interval or trace spacing [m], c is the propagation velocity of electromagnetic waves in vacuum, υ is the central frequency [MHz], and ε_r is the relative dielectric permittivity.

1.1.8.3 Stacking

Stacking is a procedure that can be used to increase signal/noise ratio of the radar signal. When it is applied in data acquisition, ordinary noise is minimized and the reflected signals are enhanced. The general equipment employed allows a various stacking from 1 to 2048; however, increase in stacking value means increase in the registering time also.

1.1.8.4 Sampling time interval

The recording time interval, or sampling time interval, is the time during which data are recorded at each point. The maximal values are given in Table 1.2 and it can be computed by Equation (1.12).

$$\Delta t = \frac{1000}{6\upsilon} \tag{1.12}$$

where Δt is the sampling time interval [ns].

1.1.8.5 Recording time window

Recording time window is a parameter corresponding to the time length of display data. To compute the time window size the exploration depth must be exceeded for about one-third. In addition, it must be taken into account that as the time window increases a larger amount of data are processed.

The recording time window size can be calculated from:

$$W = 1.3\frac{2h}{V} \tag{1.13}$$

where W is the recording time window [ns], and V is the minimal propagation velocity of electromagnetic waves in the ground [m/ns].

1.1.9 Field Routine

Success of GPR surveys depends on a great extent on soil and sediment mineralogy, clay content, ground moisture, depth of burial, surface topography, and vegetation. With thoughtful modifications in acquisition and data processing methodology, GPR can be adapted to many differing site conditions.

In GPR measurement, the transmitting and receiving antennae are separated with constantly small offset, called common offset configuration. For surface GPR, the dipole antennae are parallel to the ground surface and perpendicular to the survey line (Figure 1.7). When common offset configuration is used in GPR data acquisition (Figure 1.8), the configuration is pulled continuously along the profile. The profiling direction is along the line joining the antenna centers.

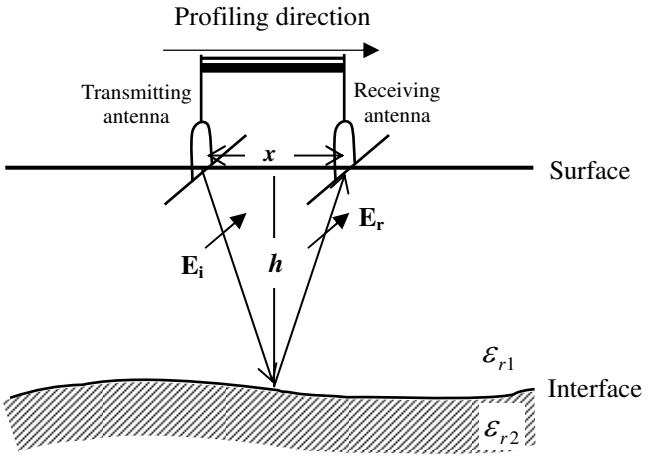

Figure 1.7 Common offset antennae configuration; *x* is the antenna separation; *h* is depth of the reflector; Ei and Er are the incident, and reflected electric fields; and ε_{1r} and ε_{2r} are the relative permittivities in medium 1 and 2, respectively (modified from Parasnis, 1997).

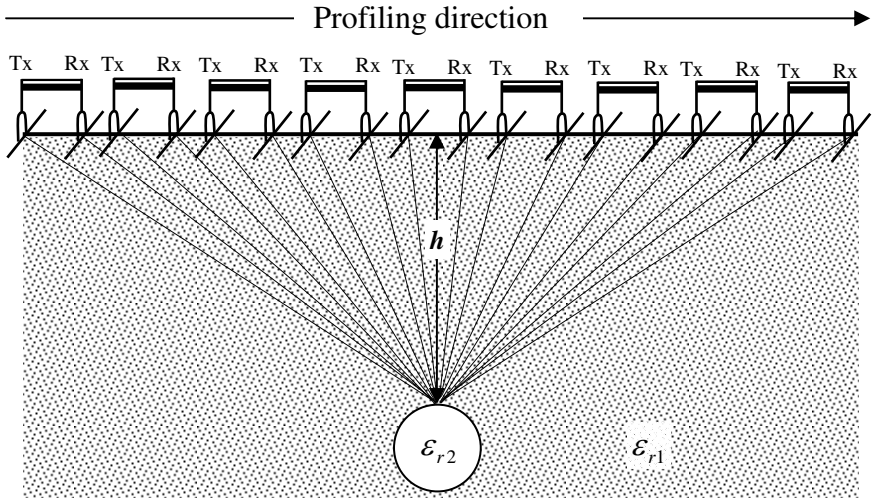

Figure 1.8 Common offset profiling; Tx and Rx are transmitting and receiving antenna; ε_{1r} and ε_{2r} are relative permittivities in medium 1 and 2, respectively.

1.1.10 Velocity and Depth Determination

In GPR measurement, a radar pulse emitted by an antenna is partly reflected and partly transmitted when it meets with an electrical discontinuity, or an interface at which there is a change in electromagnetic wave impedance. If the time for the pulse to go to and return from a subsurface reflector, two-way time, is measured, the depth of the reflector can be determined, provided that the velocity of the pulse in the ground is known:

$$h = \frac{\sqrt{V^2 t^2 - x^2}}{2} \tag{1.14}$$

where h is depth of the reflector [m], V is velocity of the media [m/s], t is two-way travel time [s] and x is distance between transmitter and receiver antennas [m] (Parasnis, 1997).

Basic depth determination depends on the knowledge of radar wave velocity within the survey area. The velocity of radar waves in non-conducting and non-magnetic media can be obtained from Equation (1.15):

$$V = \frac{c}{\sqrt{\varepsilon_r}} \tag{1.15}$$

where ε_r is the relative dielectric permittivity of the media and c is the velocity of light in vacuum (3×10^8 ms^{-1}). The relative dielectric permittivity and the propagating velocity of radar wave of some media are previously shown in Table 1.1.

Another way to acquire velocity of radar propagation in the medium is from the diffraction hyperbola analysis methods. This is a common method for electromagnetic velocity estimation based on the phenomenon that a small object, whose dimensions are smaller than the wavelength of electromagnetic wave introduced in the ground, reflects the electromagnetic wave in almost every direction. Velocity of EM wave can be determined from the hyperbolic parameters as the follow;

$$V_{RMS} = \sqrt{\frac{x_2^2 - x_1^2}{t_2^2 - t_1^2}} \tag{1.16}$$

where x_1 and x_2 are the positions of mid point of antenna, t_1 and t_2 are two-way time of the hyperbolic branch at x_1 and x_2 respectively, and V_{RMS} is an average velocity of EM wave in the medium from the surface to the diffraction point.

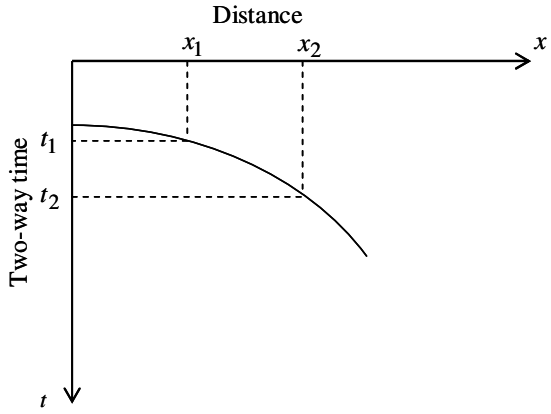

Figure 1.9 The two-way time and distance curve of reflected electromagnetic wave (Singsoupho, 2008).

1.1.11 GPR Display

In GPR data displaying, the scanned digitally recorded intensity values are converted back into analog signals and plotted as "signal voltage versus two-way time" with the downward vertical axis at the measurement point representing the two-way time and the horizontal axis representing distance along the measuring profile. The plot is referred to as a normal-incidence time section. When the velocity of the radar pulse propagating in the media is known, this time section can be converted to depth section where the horizontal axis shows the signal intensity and the downward vertical axis presents the depth (Figure 1.10).

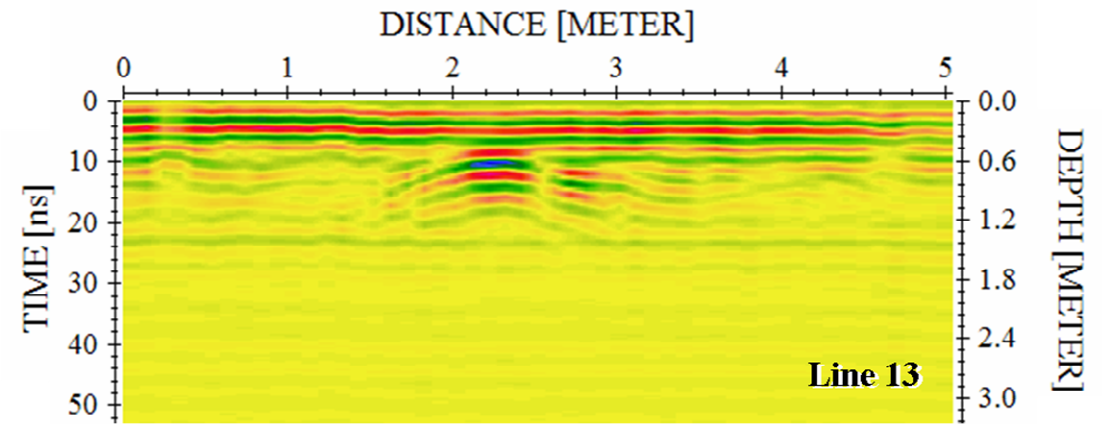

Figure 1.10 An example of GPR section; left axis represents two-way time whereas right axis represents depth by using the expressed velocity in time-depth conversion.

1.1.11.1 2D GPR Images

The standard image for most GPR reflective data is a 2D profile showing the depth on the vertical axis and the distance along the ground surface on the horizontal axis (Conyers, 2001). This image type is constructed by stacking many reflective traces obtained as the antennas are moved along a profile (Figure 1.8). Often, 2D profiles must be corrected to reflect changes in ground elevation. Only after this is done will images correctly represent the real world. Profile depths are usually measured in two-way radar travel time, which can be converted to depth if the velocity of radar in the ground is known. Such velocity can be obtained from both

known velocity information (e.g. Table 1.1) or from hyperbola diffraction analysis as previously mentioned in Section 1.1.10.

Standard 2D images can be used for most basic data interpretation, but analysis can be tedious if many profiles are in the database. In addition, the origins of each reflection in each profile must be defined before accurate subsurface images can be produced. Often, detailed image definition comes only with good deal of interpretive experience.

1.1.11.2 3D GPR Images Using Amplitude Analysis

Primary goal of most GPR surveys is to identify the size, shape, depth, and location of buried remains and related stratigraphy (Conyers, 2001; Acqua et al., 2004; and Heincke et al., 2005). The most straightforward way to accomplish these is by identifying and correlating important reflections within 2D reflective profiles, where hyperbolic patterns revealed the presence of scattered objects. Raw reflective data collected by GPR are nothing more than a collection of many individual traces along the profiles. By plotting reflective traces sequentially in standard 2D profiles, the specific amplitudes within individual traces that contain important reflective information are usually difficult to visualize and interpret. The standard interpretation of GPR data may be sufficient if the buried features are simple, but in complex stratigraphic area and buried materials are difficult to discern, different processing and interpretative methods must be used. The detection of targeted objects in those data, however, is often left to a human operator, due to the presence of intense noise, artifacts, and interfering objects such as stones, etc. This limitation arises because the advantage of the interdependence between aligned views had not been taken.

In order to overcome this limitation, the 3D GPR techniques have been recently applied on the data set of 2D GPR parallel profiles. The 3D location of reflective anomalies can be derived from a computer analysis of all available 2D profiles and reflections are correlated from profile to profile throughout a grid, which can be very time-consuming (Conyers, 2001). Thus, subsurface structures are imaged accurately in stratigraphic studies, fractures and faults detection in crystalline rock, and archaeological surveys.

The 3D visualization provides important information for archaeological applications in displaying complex data in an easily understandable way, therefore, improving the quality and efficiency of the archaeological interpretation.

Time-slices map

One of the sophisticated types of GPR data manipulation is the time-slices map analysis that creates maps of reflected wave amplitude differences within a grid that allowing the remote reconstruction of horizontal subsurface and resulting a series of maps illustrated the 3D location of reflective anomalies (Leucci and Negri, 2006). The arrangement of these amplitude slices in horizontal layers, representing real depths, is in a visual format familiar to archaeologists, analogous to their excavation levels (Figure 1.11). Although the time slices may not be the most suitable visualization technique in the case of great subsurface complexity such as faults or undulating reflectors, however, time slices still remain the easiest and most rapid means to provide a synthetic plan of the anomaly pattern, especially for large areas. For small-size zones a more complete understanding of the subsurface can be achieved by means of various 3D data presentations, side-views and slices parallel to the axis or along arbitrary directions.

Actually, amplitude slices need not be constructed horizontally or even in equal time intervals (Conyers, 2007). They can vary in thickness and orientation, depending on the questions being asked. Surface topography and the subsurface orientation of features and stratigraphy of a site may sometimes necessitate the construction of slices that are neither uniform in thickness nor horizontal in distribution. Arbitrary colors or shades of gray can be assigned in each time-slice in order to show degree of amplitude variation along a nominal scale. Usually there are no specific amplitude units assigned to these color or tonal changes.

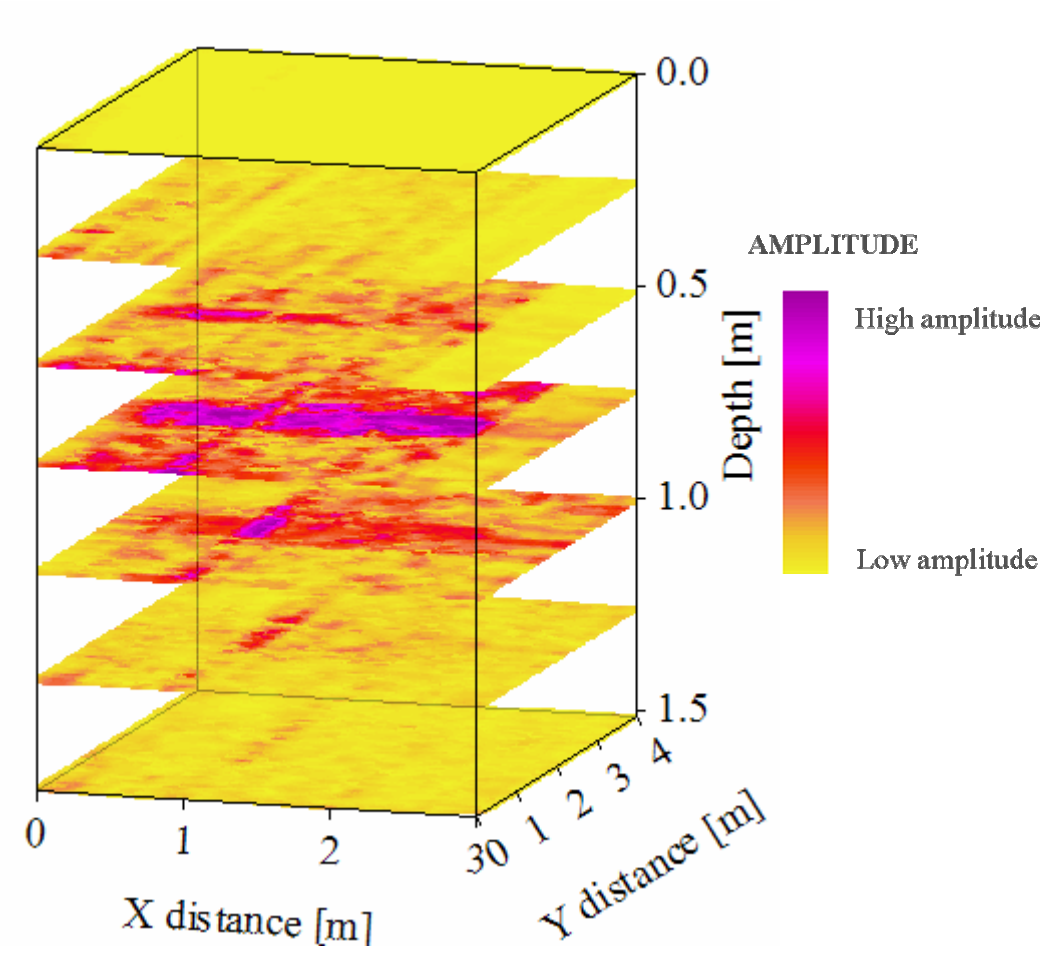

Figure 1.11 An example of 3D GPR image by means of time-slices map.

Iso-amplitude surfaces map

3D image visualization by means of 3D iso-amplitude surfaces map is the other way to present the subsurface below the surveyed area in a 3D cube as shown in Figure 1.12. In the iso-amplitude surfaces map, buried features can be rendered into iso-surfaces, or the interfaces producing the reflections are placed in 3D with a pattern or color assigned for specific amplitudes. To construct the image, certain amplitudes, usually the highest ones, are patterned or colored while others are made transparent. In addition, the map is illuminated by simulating rays of the sun from a given direction in order to enhance the subsurface features. Moreover, the features can be rotated and shaded until desired results are produced (Conyers, 2007).

With this 3D visualization technique, the reflective bodies under the survey plan can be displayed in 3D location, which ease the interpretation.

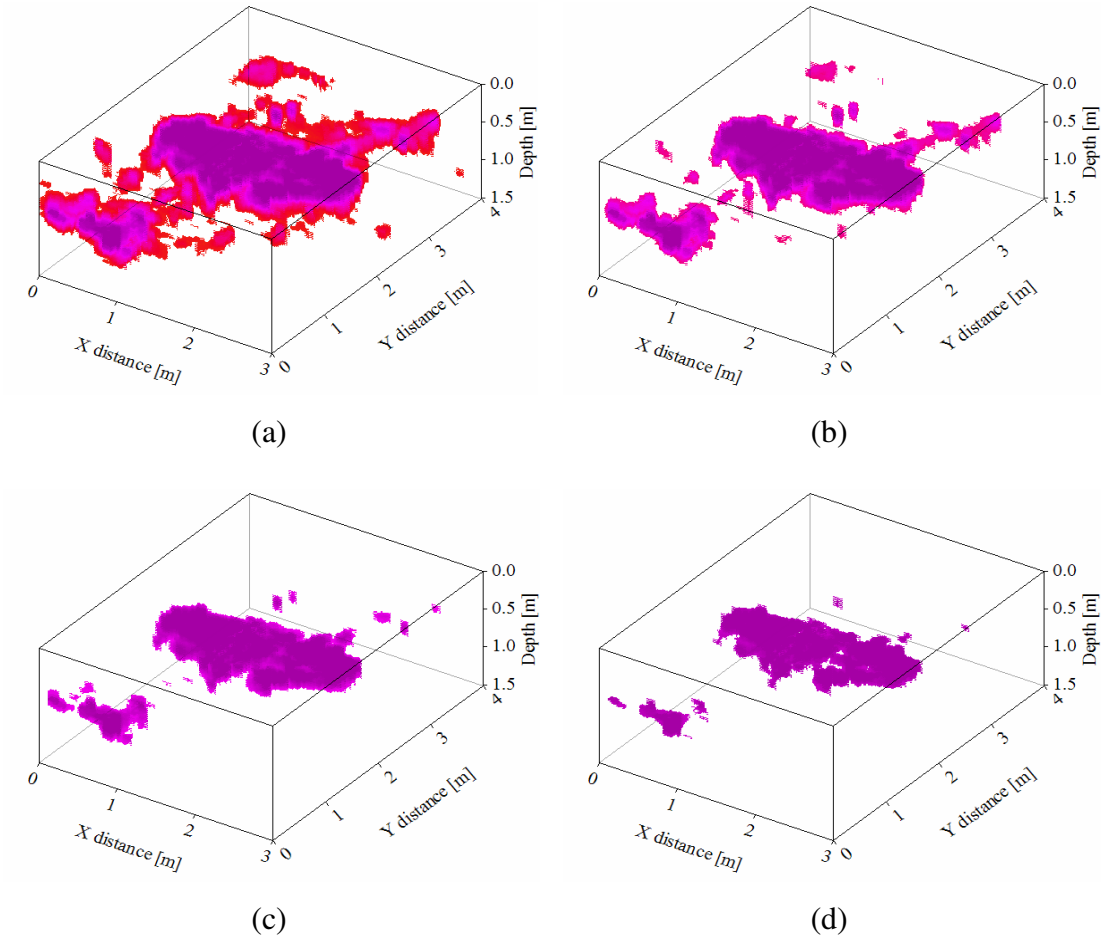

Figure 1.12 Examples of 3D GPR images by means of iso-amplitude surfaces maps of various threshold values; (a) 45%; (b) 60%; (c) 75%; and (d) 90%.

Although the 3D GPR images are produced from hundreds or thousands of reflections in a grid, the sources of the mapped image should be considered with care. Some reflection amplitudes mapped with 2D profiling must be compared to the known situation in order to make sure that the rests represent targeted features (Conyers, 2006).

In many cases, interpretations based only on GPR reflections can be prone to errors. However, many distinctive features, such as standing walls, hard-packed and dense stratigraphic surfaces, are easily recognizable and can be interpreted

with some confidence (more subtle features such as soil composition changes are often difficult to discover and interpret). For this reason, integration of good subsurface information from cores, excavation, probes, or augers with GPR amplitude analysis maps and profiles is always necessary (Conyers, 2006).

1.2 Review of Literature

1.2.1 Detail of study area

Nakhon Si Thammarat, a Province in southern Thailand, is about 610 km south of Bangkok. The city was the administrative center of southern Thailand during most of its history. Originally a coastal city, silting moved the coastline away from the city. The city has a much larger extension in the north to south direction than the west to east direction indicating its original location on a flood-save dune.

Nakhon Si Thammarat is one of the most ancient cities of Thailand, previously named as the Kingdom of Ligor, and contains many buildings and ruins of historical significance. After the fall of the Siamese capital of Ayutthaya in 1767 it regained independence, but returned to its allegiance on the founding of Bangkok. In the 17th century British, Portuguese, and Dutch merchants set up factories in this region and an extensive trade was carried out.

The city of Nakhon Si Thammarat is one of the oldest towns of southern Thailand, but its origins are not fully known. Most historians recognize the Tambralinga kingdom of Chinese records as a precursor of Nakhon Si Thammarat. The town chronicles of this time are hardly separable from legend, but they do tell the abandonment and refounding of the town, which would explain the break in history between Tambralinga and Nakhon Si Thammarat.

References to a country named Poling appear in Chinese chronicles from the Tang dynasty period down to the early Ming dynasty. Many scholars identify Poling with Maling and Danmaling was one of the member-states of Sanfoqi (Srivijaya in Chinese language) in the central part of the Malay Peninsula or today southern Thailand. Consequently, Poling may also be the Tambralingarat (Tambralinga state) that appear in Indian sources. By the end of the 12th century, Tambralinga had become independent of Srivijaya kingdom. Its rapid rise to

prominence since the 13th century till the beginning of 14th century, Tambralinga had occupied the entire Malay Peninsula and become one of the dominant Southeast Asian states. By the end of the 14th century, Tambralinga had become a part of Siam (Thailand) named Nakhon Si Thammarat.

At the time of the Sukhothai kingdom, the Nakhon Si Thammarat kingdom was already listed as one of the kingdoms under control of the Thai, which it has remained during most of its history. It was usually known as Ligor to European merchants in the 16th century. At the end of the 19th century, the kingdom was finally fully absorbed into Siam by converting it into the Monthon Nakhon Si Thammarat. With the abolishment of the Monthon system in 1932, the town now is simply a provincial capital (Wikipedia, 2008).

As mentioned previously that thousands of years ago, a prehistoric human was settled the community down in Nakhon Si Thammarat Province. The community had continuously evolved from vagabond to primary agricultural community. Since the 5th century A.D., Nakhon Si Thammarat had incorporated its own culture with Chinese, Vietnamese, Arabian, and especially Indian cultures. The results of incorporation can be seen as the multicultural articles; through the influences of religion which is an important key of the social organization, arts, and architectures (Sampaongen, 2007).

Religious prospering of this area was sensible and can be realized from the remains of ancient buildings and antiques. These evidences had been found throughout the area of Khanom, Sichon, Muang, and particularly in Tha Sala District. Archaeological architectures and antiques were discovered at many sites and most of them are found beneath soils and vegetations. They are, for examples, the stones, Sivalingas, and Yoniporanas of 12th to 14th century A.D. and head of a Buddha dated 5th century A.D. These artifacts were the articles from the Indian cultural influences found on a mound where original archaeological buildings were buried (Fine Arts Department, 1998).

The Wat Mo Khlan is one of the archaeological sites which emphasize the brilliant history of Nakhon Si Thammarat. This prestigious site is located in Tha Sala District, of Nakhon Si Thammarat Province. This site not only possesses the ancient remains which manifest the evidences of the overlapped construction from

one period to another period, but was also the area where the ancient community has settled before it expanded to the city of Nakhon Si Thammarat. Because the area of ancient Wat Mo Khlan was situated at the inner old flood-save sand dune that stretched continuously from Sichon District, while of Nakhon Si Thammarat was the outer new age sand dune.

Some of the silver coins dated back to the ancient Funan Empire (ca. 4^{th} to 5^{th} century A.D.) were also discovered about 2 km northward from the site. Those coins were as the same age as the coins found in Vietnam, Myanmar, and other archaeological sites in central and eastern Thailand. These indicate the settlement of the ancient people in the area and the connection to other remote societies.

The sanctuary Wat Mo Khlan archeological site has been proclaimed as ancient monument since 1976 by the Fine Arts Department. This site used to be a Hindu sanctuary of the Saivaism Sect dating back to ca. 7^{th} to 9^{th} century A.D. It was firstly discovered in 1934 and many of ancient artifacts were found. The discoveries included stuccos of Buddha image, ancient building remains, ancient ponds, shards of ancient potteries, Sivalingas and Yoniporanas were found during that time. Furthermore, lines made from stone elements of ancient building were also found. It was regrettable that most of the ancient artifacts had lost, but some of Buddha heads were still kept inside the Vihara of the present Wat Mo Khalan temple.

During 1990 and 1992-1993, the Wat Mo Khlan site was renovated by the Fine Arts Department. Most of the extensive site was found beneath the soil-mound covered by congested vegetation. The stone alignments were found in the west and south direction of the archaeological mounds, while 3 archaeological ponds were observed in the eastern part but only one shallow pond is left in the present time. In addition, fractions of limestone and sandstone sculptural arts, such as doorframes, rectangular rock, and pedestal pillars were found. In addition, other archaeological evidences, including metal earrings, obsolete coins, ancient potteries, ancient bricks, and broken pedestals were also discovered at that time.

The archaeological structures found in the series of excavation are as follows;

Archaeological building number 1: This first structure was characterized by a rectangular building with soil-cemented bricked wall of 7 m wide

and 12 m long. The building comprises basements and stairs with the eastern entrance. There were three porches in the northern wall and two of the same features in the southern one. Moreover, it was observed that the later-period structure was built by using materials from the former-period, for examples; two doorframe rocks were later used as porch base in the southern wall. These structures of the ancient building were usually found in the Brahman-Hindu temples.

Figure 1.13 Archaeological building number 1.

Apart from that, the excavation at the archaeological building number 1 revealed parts of the Buddha stucco and triangular roof tiles indicated that this building might be the soil-cemented bricked building with wooden roof structure and was built in a later period for placing the stucco of the Buddha image.

Figure 1.14 Archaeological building number 2.

Figure 1.15 Archaeological building number 3**.**

Archaeological building number 2: The second structure was the square soil-cemented bricked building of 10 m in width and length with two storeys, about 80 m high for the upstairs and about 50 m high for the downstairs. Since materials of the demolished building of former-period were found at the base of the building, this suggested that construction material was re-used in building the building number 2.

Archaeological building number 3: The building was found in damaged conditions as the soil-cemented bricked structure of unknown shape. The discovered remains compose of post holes of the rock pillars on the bricked lines, a rectangular bricked structure of 5.5 m in width and 12 m in length, and trace of stairs and entrances. The remains of the north building comprise three walls of about 12 m in width and 15 m in length. These structures were supposed to be the first Hindu

temple built in this area and their rock-components were later used for building Buddhist temples in a later-period as seen in archaeological buildings number 1 and 2.

Figure 1.16 Archaeological building number 4**.**

Archaeological building number 4: This building was characterized by a square solid soil-cemented brick structure of 6 m in width on each side. According to its appearance, it was presumed to be a square monument which was built in the later period. In addition, two parts of the ancient walls were also found. The northern walls surrounded four ancient buildings and the bricked floor. The stairs and entrances of these walls were placed at the north and the south end of the building. The southern walls surrounded two of rectangular mortar-cemented brick buildings. Surrounding by these walls; presently are the Mo Khlan School, playground and a football field; was presumed to be the residential area of ancient monks where shards of potteries were found and the area separated from the ancient temple by the walls.

During the excavation, several burial jars, biscuit and gloss firing, were also found in this area. Difference in firing process implies difference in nobility.

The Wat Mo Khlan archaeological site, accordingly, comprises two overlapped periods of archaeological building remains in the same area. The Hindu temple (archaeological building number 3) was the representative of the Saivaism that was the former-period doctrine of this area. This assumption was supported by the discovery of Sivalingas and Yoniporanas dated back to 6^{th} to 8^{th} century A.D.

The area was later left and new people who pay esteem for Theravada Sect of Buddhism had come and settled down. These new incoming people built the Vihara (archaeological building number 1), Stupas (archaeological building number 2 and 4) and walls (northern and southern walls). The walls not only used to define the area of the temple but also used to partition the area between monastery and Buddhist temple hall. The stone alignments (stone relics from former Hindu temple) were also included in this period. Patterns and period of the discovered architectures and artifacts indicated that they might be in the Ayutthaya Period (about 14^{th} to 17^{th} century A.D.).

The Wat Mo Khlan archaeological site is the ancient monument that still stays alive in the joint of time that has been changing from period through period, while other contemporary sites had been abandoned since the end of the early history period. Therefore, the Wat Mo Khlan archaeological site is considered to be a valuable historical and cultural heritage (Thongjarienchaikit, 2008).

1.2.2 GPR application

Since the mid-1980s, GPR has become enormously popular, particularly within the engineering and archaeological communities. However, radar has been used for geological applications since the 1960s, especially in connection with the development of radio echo-sounding of polar ice sheets. There is enormous scope for the application of ground penetrating radar and it is extremely exciting to anticipate what might be achieved in the future. For shallow subsurface prospecting, GPR has been used for a variety of tasks, like determining the thicknesses of soil horizons and depth to water table, detecting air-filled subsurface cavities, buried channels, masonry structures and bridge piers, detecting buried objects in

archaeological surveys, determining ice or permafrost thicknesses, studying the condition of the asphalt layer on roads, etc.

In archaeological investigations, which the required depth of penetration is usually very small (commonly less than 3 m), GPR can be used as a first-look technique or as a fill-in method between areas of excavation. The location of buried archaeological structure can be important for at least two reasons. As consecrated ground, it has to be carefully exercised for future development and the archaeological structures should be delineated nondestructively (Reynolds, 1997).

Case History of 2D GPR

Some successful applications of GPR method in archaeological prospecting are listed below;

Ground penetrating radar was used to confirm the location of ancient structures under the Valencian Cathedral, Spain (Gracia, et al., 2000). The aims of the survey were to add information to old maps and documents in the Cathedral Archives and to analyze the extent and importance of potentially destructive moisture areas appeared on the floor. The GPR data successfully located crypts, ossuaries, sepulchers, graves, and the location of ancient walls existed before the final Cathedral expansion. Cultural layers corresponding to the three periods of construction; Roman, Arabian, and Middle Age Epochs, were also identified. Measurements of relative sub-floor moisture were obtained by comparing dielectric permittivity changes and radar velocity differences between materials in humid and non-humid areas.

Hruska and Fuchs (1999) proved that ground penetrating radar is one of the most effective tools for the investigation at the ancient Ephesos, the urban area in Turkey, which is too large to be fully excavated. Two different tasks have been solved by GPR, both as a part of overall area exploration. The first task was detection of sacred roads between the city and the temple of Artemis and the second was mapping of older levels of Tetragonos agora in the city center.

Ground penetrating radar was considered to be a suitable tool for archaeological investigation (Phattanaviriyapisarn, 2002). Nine of eighteen convex-shape hyperbola anomalies, which observed on measured radargrams and later verified by archaeological test pits were identified as the remained portions of ancient

Dutch coffins. Their locations and depths very well agreed with those determined from radargrams.

Ranalli et al. (2004) investigated the historic buildings in Italy by using ground penetrating radar. The GPR measurement was conducted in the preliminary stage of a structural monitoring and restoration project of the facade of the Collemaggio Basilica, amedieval church L'Aquila, central Italy. GPR was demonstrated to be an ideal non-destructive method for mapping ancient structures of high cultural and historical value, and very useful for evaluating the state of conservation of the facade and identifying the thickness of its walls, the forms and its masonry deterioration and the forms and locations of its middle cornice supports. The finding was incorporated in seismic modeling of structures. Hence, the GPR results shine more light on the Collemaggio Basilica facade in view of more effective restoration or conservation projects.

GPR accompanied with other geophysical techniques, such as magnetic and electric methods, are commonly used to identify the archaeological remain in the subsurface. The successes of the application are summarized as follows;

The Olonium Roman site Northern Como Lake was investigated by Arlsan et al. (1999). The electrical survey has been carried out in conjunction with magnetic and GPR investigations. These studies indicated the presence of a number of significant anomalies in sub-areas, which excavation tests have been conducted and brought to a number of archaeological findings.

A combination of ground penetrating radar measurement, the vertical gradient of the earth's magnetic field measurement and the electrical ground resistance mapping successfully located archaeological remains in Nakhon Si Thammarat, Thailand (Lohawijarn, 2005). Anomalous zones of magnetic gradient, highly resistive patches of shallow ground and discontinuities in ground layering observed on ground penetrating radar images associated with the buried archaeological remains as immediately verified by archaeological pitting.

Two prehistoric indigenous culture archaeological sites, Serrano and Morro Grande in Araruama County, Rio de Janeiro, Brazil, were investigated by GPR measurement (Cezar et al., 2001). The archaeological remains in the study area are mainly characterized by pottery artifacts buried within layers of sand and clay.

Several profiles were acquired and the results showed that a radar section acquired on an urn filled with air showed a well-marked feature.

Case History of 3D GPR

Recently, 3D GPR imaging has been favorably and successfully employed for detailed mapping in geological and archaeological investigation as summarized below;

Sigurdsson and Overgaard (1998) proved that GPR offered a simple and rapid means of valuable information for mapping geological and structural variations in limestone. Data from closely spaced radar sections were gathered in two areas in Faxe Kalk's limestone quarry on the island of Zealand, Denmark. 3D visualization of GPR data including side-views and multiple slices greatly improved understanding of the distribution and shape of flint-free limestone units, thereby improving reserve estimations and planning of mining operations in the exploration area.

Noninvasive 3D ground penetrating radar imaging with sub-meter resolution in all directions delineates the internal architecture and processes of the shallow subsurface (Grasmueck et al., 2005). With appropriate acquisition parameters and processing steps, the geometry of fractures in various different orientations and accurately image fractured rock, sedimentary structures, and archeological remains previously unseen were clearly defined.

A prehistoric site in Barbados, West Indies was studied using 3D ground penetrating radar (Whiting et al., 2001). Archaeological features included burials, hearths, ceramic lined wells, and postholes. Artifact middens contained pottery sherds, conch shells, and other marine resource debris. The soil layer at the selected site consists of dry, clean quartz sand. 3D visualization software was used in order to enhance the anomalies, usually large diffractors such as conch shells and rocks, and to assemble the parallel lines into 3D volume. In this case study, the dimensions, distribution, and shapes of time-sliced amplitude anomalies were consistent with those of previously excavated burials, poles, and pit structures. The interpreted data indicated the presence of a circular house structure which was previously unknown at this site.

The ground penetrating radar technique was used to map the subsurface archaeological features in an urban area located in Mesagne, Italy (Leucci and Negri, 2006). The GPR survey was undertaken at two selected locations near a necropolis dating from the Messapian to the Roman imperial age. For the selected areas the processed data were visualized in 3D space by means of the standard time slice technique and iso-amplitude surfaces of the complex trace amplitude. The immediacy in revealing the spatial positioning of highly reflecting bodies makes 3D visualization techniques very attractive in archaeological applications of GPR. The performance of these two techniques in the various different situations allowed insights into their main advantages and drawbacks.

The ground penetrating radar was carried out in an urban area (Lecce, Italy) to obtain a detailed characterization of the most superficial layers, where presumably archaeological structures are buried, and to quickly identify anomalous zones for excavation. The information was obtained only between the ground level and the top of the calcarenitic basement. By recording data along parallel profiles and displaying results with time-slice representation, an unexpected barrel-vault cavity near a wall of the historical building and urban utilities buried in the area in the first half meter of soil was successfully located and subsequently confirmed by archaeological excavations (Basile et al., 2000).

Ground penetrating radar was used to map historic graves including intact or partially collapsed coffins and vertical shafts (Conyers, 2006). 2D analysis of radar reflection profiles can be used to identify both coffins and the vertical shaft features commonly associated with human burials. Spatial analysis of the reflection amplitudes within a grid consisting of many profiles produces 3D maps called time-slices maps of these burial features. The results identify remains for possible excavation and study, and can also be used for statistical and spatial analysis when integrated with historical records.

The 3D GPR imaging can be carried out in combination with other geophysical techniques as the following case studies;

Ground penetrating radar and electrical resistivity tomography (ERT) were carried out at the Temple of Apollo in Turkey in order to map archaeological features, such as voids, walls, or else in the subsurface. Two-dimensional ERT was

used to detect the presence of an active normal fault passing under the Temple of Apollo. In addition, the 2D ERT was also suitable for detecting archaeological features in the clay deposits, while the 3D GPR imaging was suitable for detecting man-made structures located under the Temple of Apollo (Negri and Leucci, 2006).

A combined geophysical survey has been carried out on a Roman archaeological site to obtain information on the vertical distribution of the anomalous bodies (Sambuelli et al., 1999). Magnetic gradient measurements were performed over the whole study area while resistivity tomography and GPR profiles were carried out along some selected profiles. The whole structure of the apse was clearly outlined and further excavation tests based on the GPR results were suggested.

Shaaban and Shaaban (2001) used 2D resistivity and ground penetrating radar to locate buried archaeological relics at the archaeological site of the Tell El Rabi'a in Egypt. High resistive anomalies associated with pillar crowns and wall-like structures of hard limestone and a conductive background of river deposits with differing moisture characteristics were observed on the 2D electrical resistivity profiles. In addition, various high amplitude anomalies corresponded with the presence of thin buried walls, thick buried walls depict buried stone-filled chambers were observed on the GPR results. Therefore 2D resistivity profiling and GPR surveys were recommended as the effective geophysical tools for archaeological investigations.

1.3 Objective

The objective of this research was to apply GPR measurements with the 3D GPR visualization techniques for locating buried archaeological remains and structures at the Wat Mo Khlan archaeological site in Tha Sala District, Nakhon Si Thammarat Province.

CHAPTER 2

RESEARCH METHODOLGY

2.1 Equipment and materials

2.1.1 Field equipments

The Malå system RAMAC/GPR (Figure 2.1) was employed in the present study. The system comprises of the following items;

1) A transmitter unit for sending electromagnetic pulse into the ground
2) A receiver unit for receiving the electromagnetic pulse reflected back from the subsurface
3) A control unit for controlling the sending, receiving and storing signals
4) A display unit, a portable PC computer, for displaying the radargram both time of the pulse signal traveling from the transmitter to receiver units and the amplitude of the reflected pulses.
5) The trigger box for starting the measurement.
6) Alkaline batteries (12.0 V) for supplying power to the GPR system
7) Antenna handles for fixing distance between the transmitter and receiver antennae
8) Fiber optic cable for sending signal between the control unit and the transmitter and the receiver unit

2.1.2 Software

1) MapInfo Professional Version 8 (MapInfo Corporation, 2005)
2) Gradix Version 1.08 (Interprex Limited,1997)
3) ReflexW Version 4.5 (Sandmeier, 2007)
4) Microsoft Excel 2003

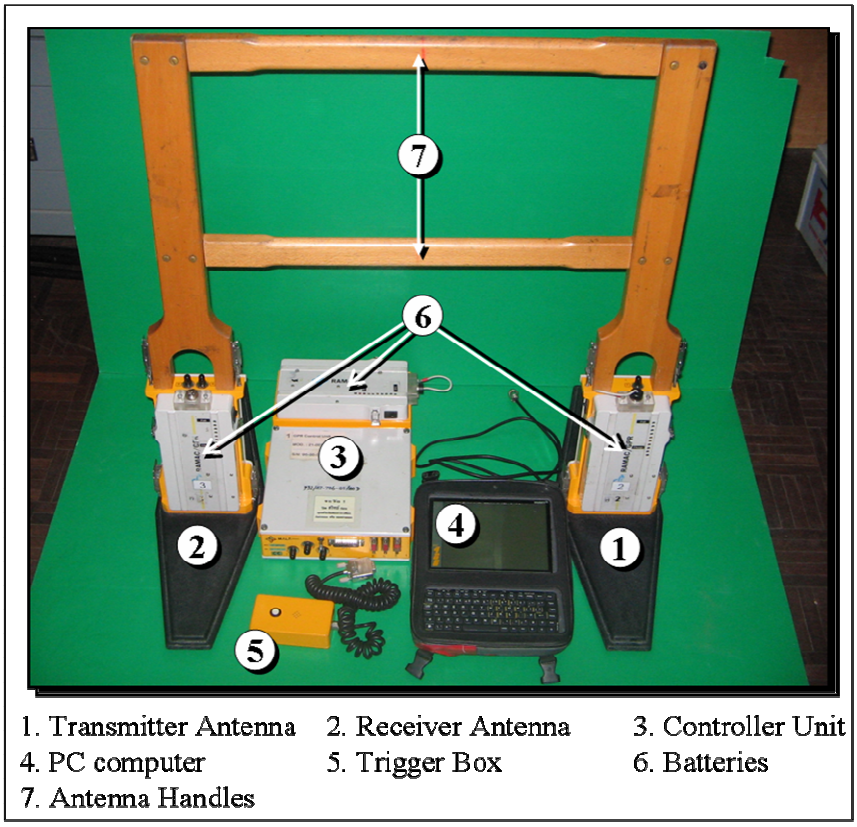

Figure 2.1 Malå System RAMAC/GPR.

2.1.3 Computer materials

1) Laptop
2) PC computer
3) CD Rom
4) USB

2.1.4 Field materials

1) Data recording paper
2) Distance measuring tape
3) Compass

2.2 Methodology

The research project was carried out both in the field and in the laboratory.

2.2.1 GPR measurement

The GPR acquisition was carried out at the Wat Mo Khlan archaeological site, Tha Sala District, Nakhon Si Thammarat Province, Southern Thailand, at $8°34'46.8''N$ and $99°55'48.8''E$ (Figure 1.2). The study area is located between the excavated Wat Mo Khlan archaeological site in the north and the Wat Mo Khlan School in the south (Figure 2.2).

Because the objective of this study was to construct 3D images of the subsurface feature, adequate field acquisition, which should be performed within a grid of GPR lines was required. Hence, the GPR data collection was carried out at a 20.0 m x 33.0 m squared area consisted of 101 parallel lines of measurement (Figure2.2).

Unaliased 3D GPR images of shallow subsurface require dense data measurement along closely spaced parallel profiles. Trace spacing has to be close enough to sample entire diffractions. The steep tails of diffraction hyperbola require trace spacing of a quarter wavelengths or less (Grasmueck and Weger, 2003). Measuring profile spacing should be less than one half the wavelengths of possible reflections returned from the smallest target to be mapped. With proper sampling, shallow subsurface features can be imaged in great detail.

In the measurement, the RAMAC/GPR system with unshielded antenna of 200 MHz central frequency with common offset configuration was employed with the following acquisition parameters; antennae spacing of 0.6 m, measuring line-spacing of 0.2 m, trace spacing of 0.1 m, sampling frequency of 1654.381779 MHz, 256 samples per scan, and recording time window of 154.74 ns.

During the field measurement, the sampling frequency was accidentally changed from the planed sampling frequency of 1654.381779 MHz to 3124.943360 MHz. The shift in sampling frequency that occurred in nearly half of the recording GPR data were recognized after the period of field acquisition. Therefore,

the RESAMPLING process was later applied to the GPR data in order to arrange the GPR data into the same sampling frequency (see section 2.2.2).

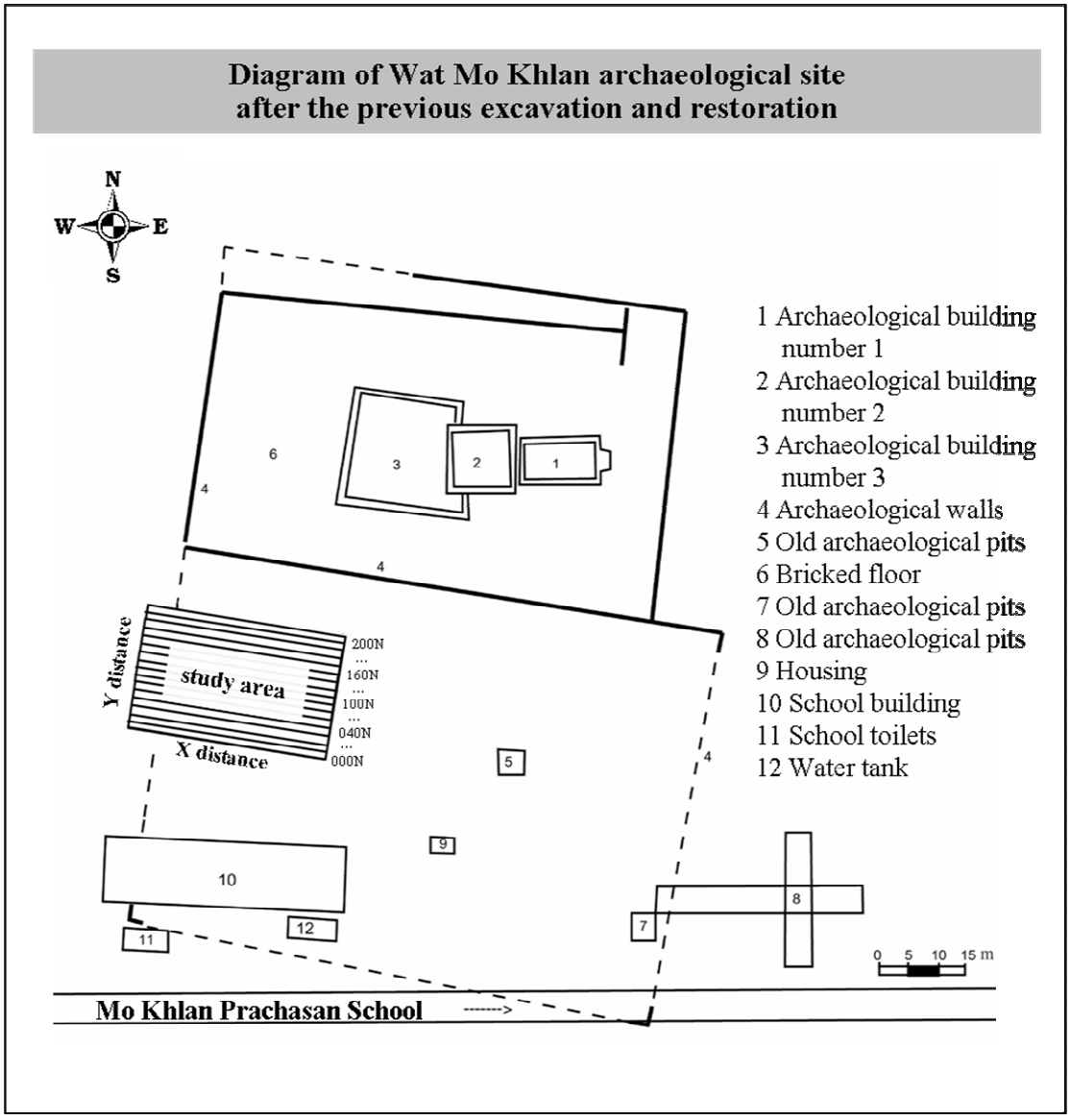

Figure 2.2 Map of study area and lines of measurement within the study area (modified from Fine Arts Department, 1993).

Figure 2.3 GPR measurement at Wat Mo Khlan archaeological site.

2.2.2 GPR processing and analysis

The quality of the original data required an appropriate processing for an accurate interpretation. The following processing steps as shown in Figure 2.4 were applied to the GPR data so that anomalies could be clearly observed on GPR sections. Detail of each processing step was described below:

2.2.2.1 RESAMPLING

Since 3D imaging requires equal sampling time interval, therefore GPR data of different profiles acquired with different sampling time intervals, as mentioned in section 2.2.1., should be resampled into the same sampling time interval. However, decreasing the original sampling time interval does not mean increasing of the vertical resolution.

2.2.2.2 TRACE EDIT

Since in the present study, trace shifts in recording data probably caused by field equipment and resulted in sawtooth GPR time sections were observed (Figure 2.5a), trace editing process was then conducted in order to shift all traces to the same starting time (Figure 2.5b).

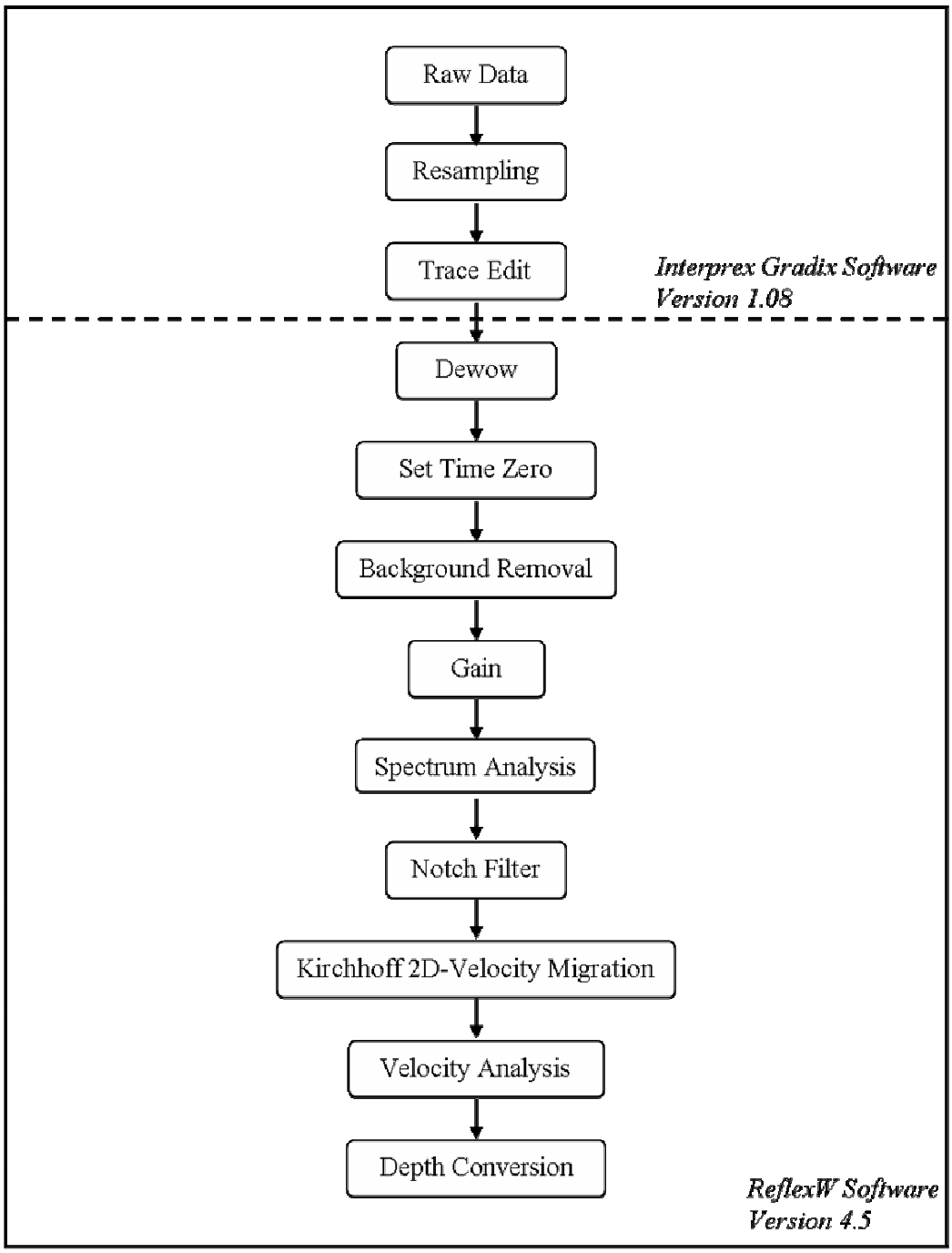

Figure 2.4 Processing steps applied to the GPR data.

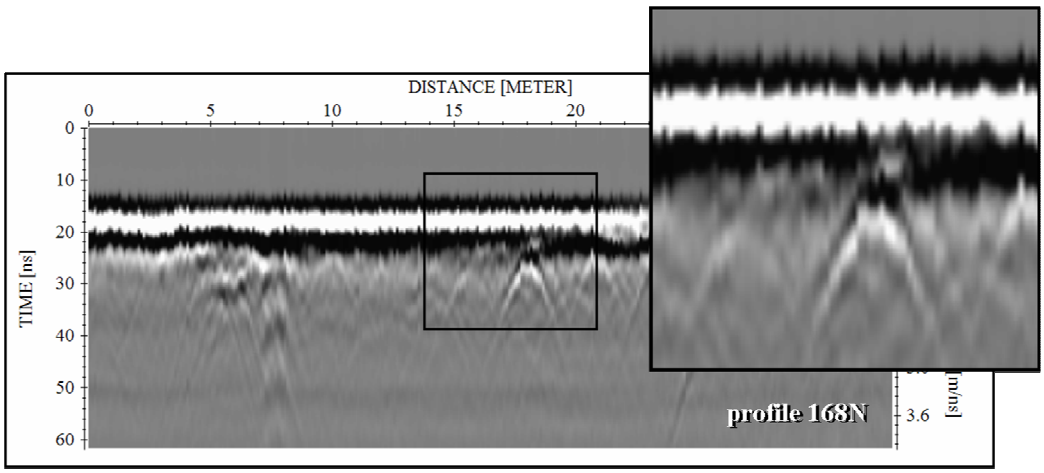

(a)

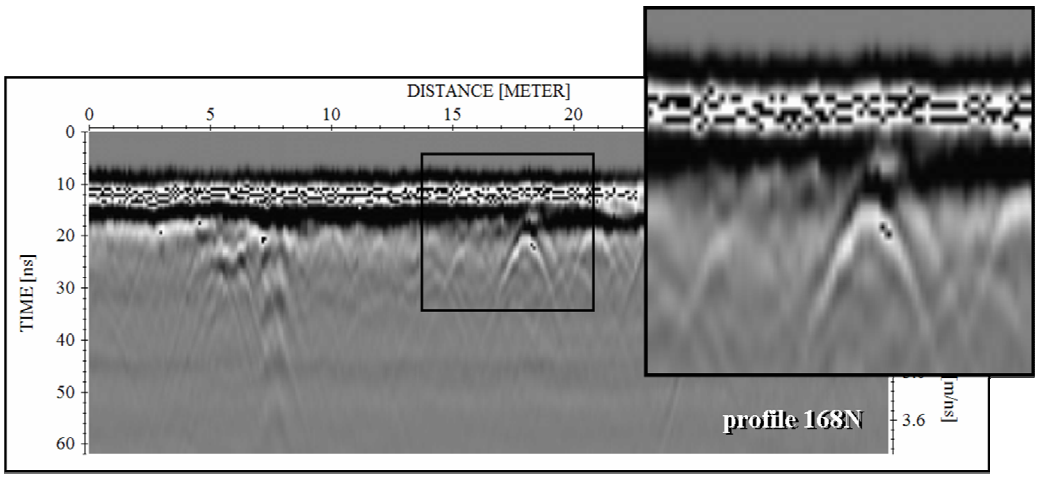

(b)

Figure 2.5 GPR section of the profile 168N (a) before and (b) after applying the trace edit process.

2.2.2.3 DEWOW

This filter was used for eliminating a possible low frequency part of the recording signal that may be caused by the equipments. The process was achieved by calculating a running mean value of each trace and subtracting this value from the central point. After applying this process to the GPR data, low frequency part of the recording signal was filtered out (Figure 2.6a and 2.6b).

2.2.2.4 SET TIME ZERO

This processing step is a static correction, a time-independent correction, for each trace in time direction. In this processing step, the first arrival

time of radar pulse at receiver was set to 0 ns (Figure 2.7c). It is reasonable to employ this filter in order to invert a possible time delay.

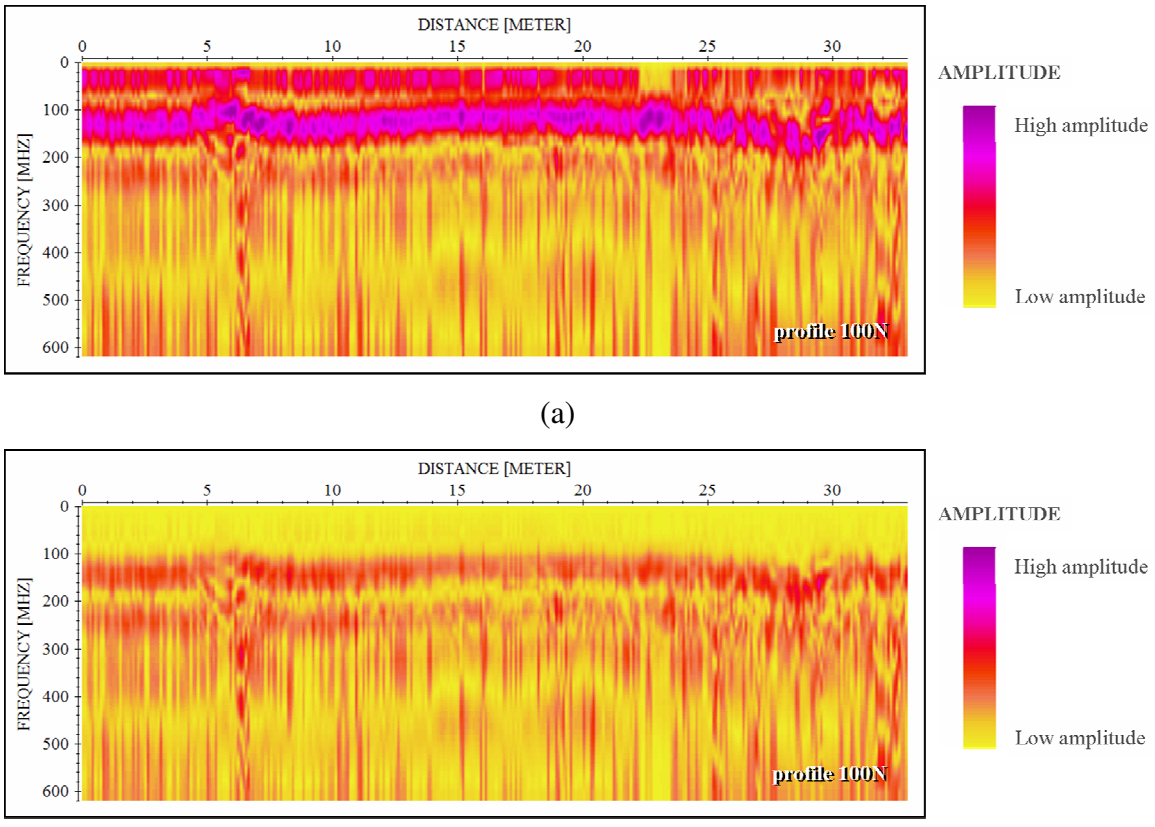

Figure 2.6 Trace spectrum of GPR section related to the profile 100N (a) before and (b) after applying the dewow process.

2.2.2.5 BACKGROUND REMOVAL

This processing step was applied to the GPR data in order to eliminate the temporally consistent noise from the whole profile which previously masked the signals (Figure 2.8d). This filter performs by constructing a reference trace by averaging all trace amplitude recording at the same time in the profile and subtracting this reference trace from the data set.

2.2.2.6 GAIN

The selected time-dependent manual gain performs by defining a digitized gain curve in y-direction (normally time axis) and applies this gain curve on

each trace of recording data in order to enhance the amplitude of the recording signals so that the deeper signals will appear more clearly (Figure 2.8e).

2.2.2.7 SPECTRUM ANALYSIS

In this process, all frequency information of the recording signals was calculated and displayed (Figure 2.10), so that suitable frequency filter will be chosen for reducing noise and enhancing significant signal.

2.2.2.8 NOTCH FILTER

Apart from hyperbolic-shape reflections from the finite subsurface objects, strips of alternating band of 100 to 200 MHz were observed on radar sections (Figure 2.10). Removing these bands from radar sections will enhance some of the hyperbolic-shape reflections, which are the main targets of this study.

The notch filter was applied to GPR data for suppressing nearly mono-frequency noise. The filter parameters are specified by four frequency values; namely, the low frequency plateau (lower plateau), the low-cut frequency, the high cut frequency and the beginning of the high frequency plateau (upper plateau). The filter is represented by a cosine-window between the end of the low/high frequency plateau and the low-cut/high-cut frequency. In this study, notch filters of 200 and 100 MHz (Figure 2.8f and 2.9g) were applied to recording traces and clear hyperbolic patterns were observed in radar sections.

2.2.2.9 KIRCHHOFF 2D-VELOCITY MIGRATION

A time migration of a 2D profile on the basis of a 2D-velocity distribution is performed in the x-t section. In this present study, the 2D-velocity functions that used in the migration were obtained from the velocity analysis with diffraction hyperbola method; one specific velocity function was used for the migration on each GPR profile. The goal of the migration is to trace the reflection and diffraction energy back to their source positions. In case of diffractions, the migration will contract diffractions to their corresponding apexes. This will be useful for constructing time-slices map. After the migration, the positions of the subsurface objects will appear at the correct positions in the GPR section (Figure 2.9h).

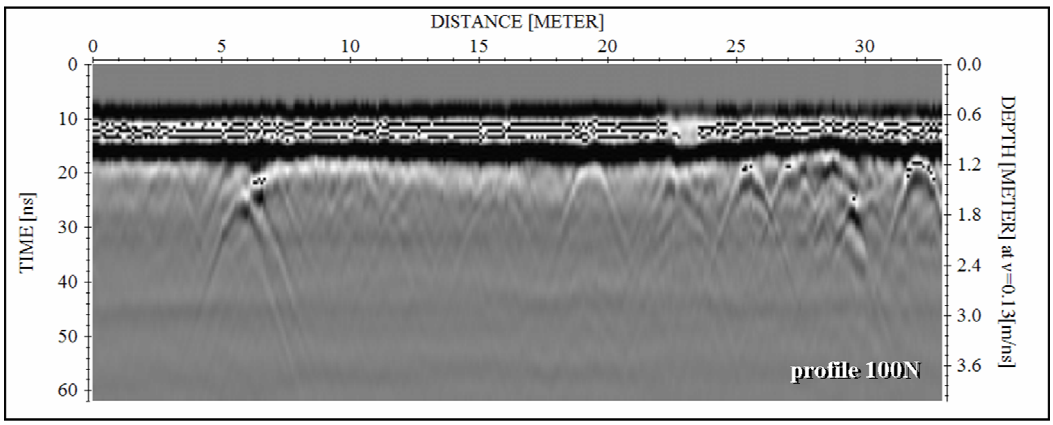

(a)

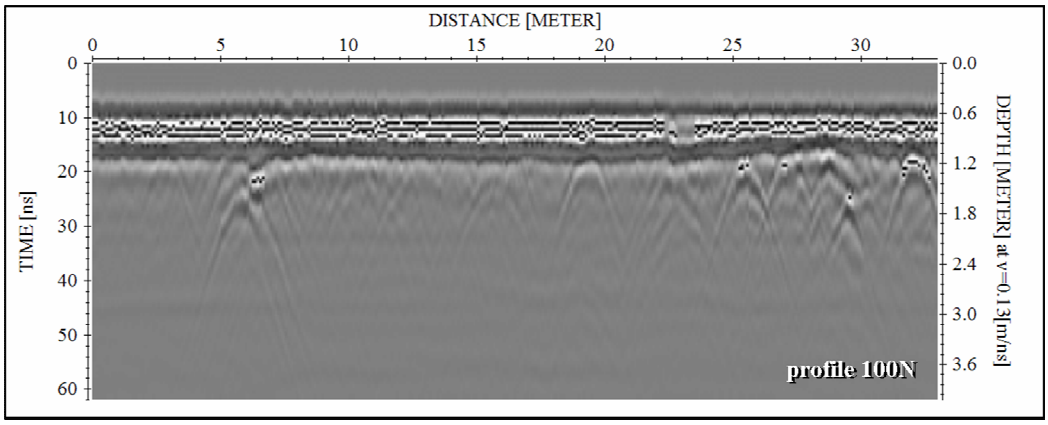

(b)

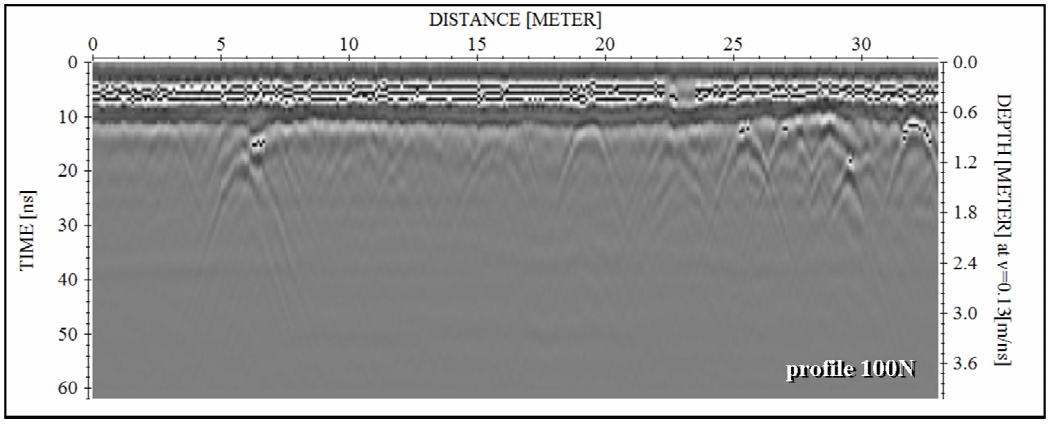

(c)

Figure 2.7 GPR data processing applied on the profile 100N, (a) raw data; (b) dewow and (c) set time zero.

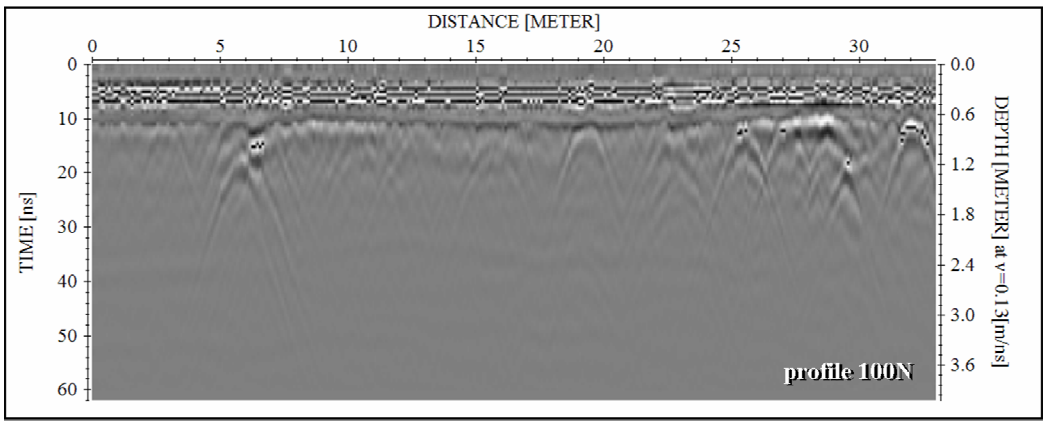

(d)

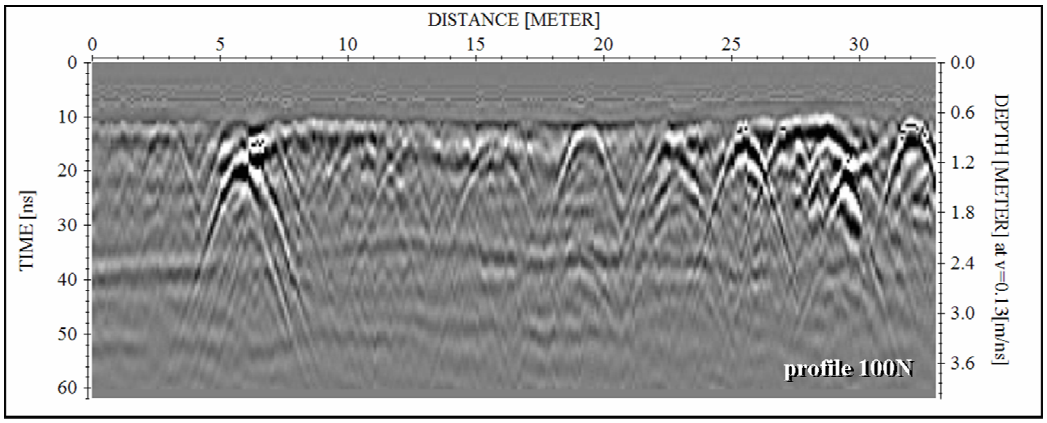

(e)

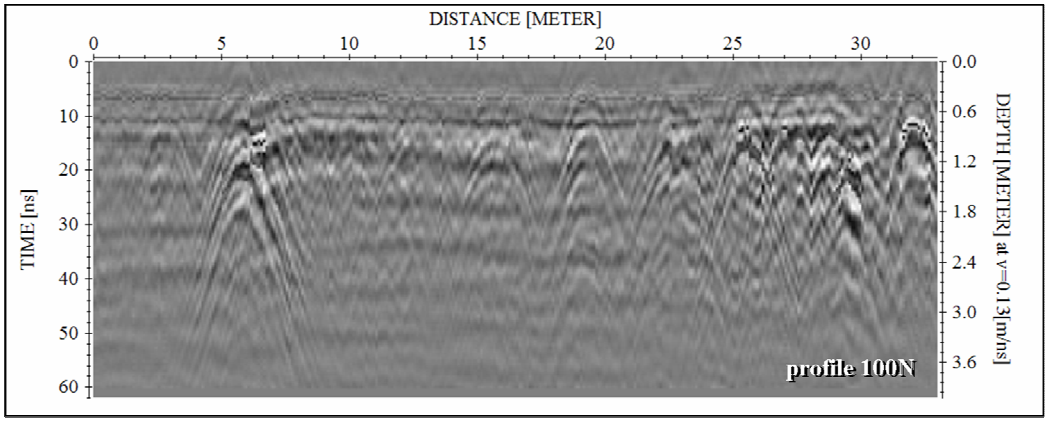

(f)

Figure 2.8 GPR data processing applied on the profile 100N, (d) background removal; (e) gain and (f) notch filter at 200 MHz.

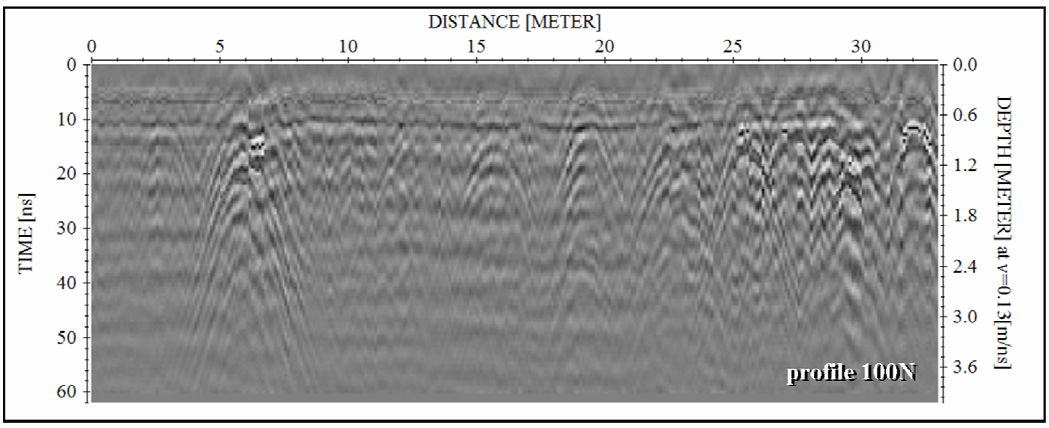

(g)

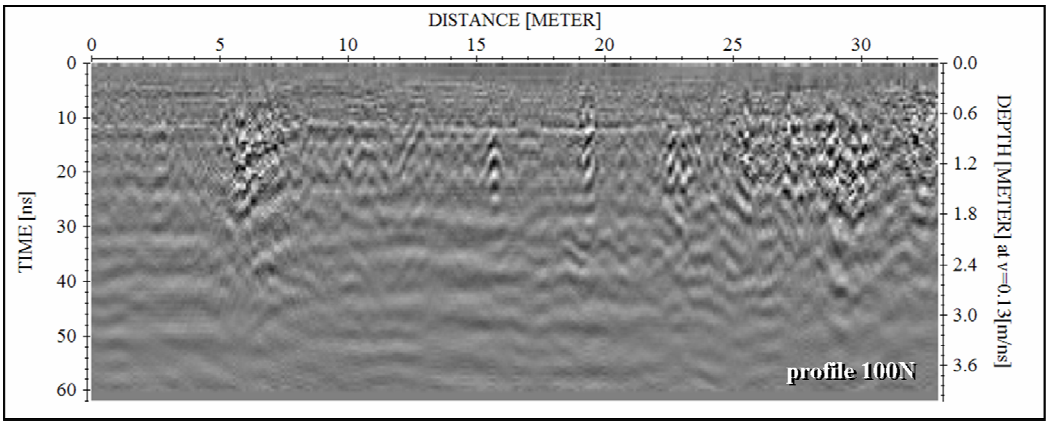

(h)

Figure 2.9 GPR data processing applied on the profile 100N, (g) notch filter at 100 MHz and (h) migration.

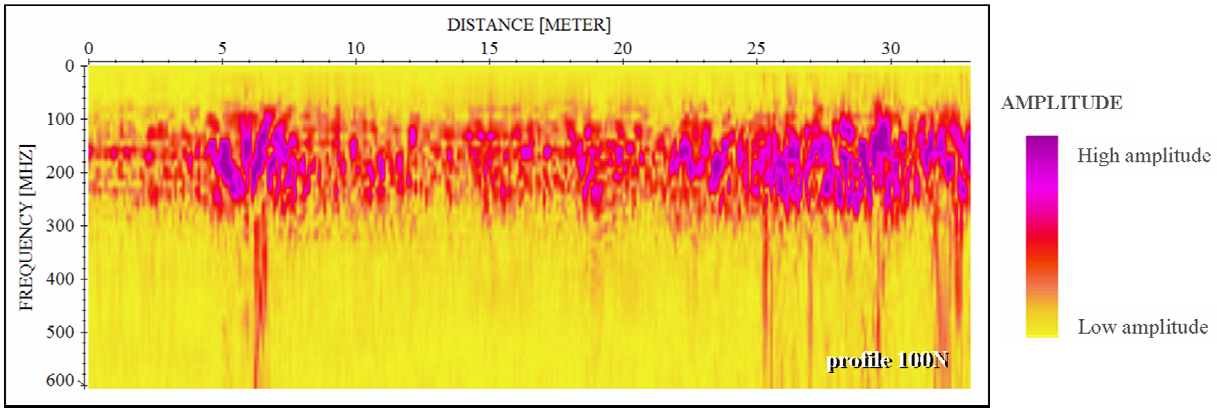

Figure 2.10 Trace-spectrum of the profile 100N.

2.2.2.10 VELOCITY ANALYSIS

Diffraction hyperbola analysis method, a common method for the radar wave velocity estimation, was used for determining the propagation velocity of radar pulse in the medium of the study area at any two-way time. This method is based on the phenomenon that a small object, of which dimension is less than the wavelength of the radar signal introduced in the ground, reflects the radar signal in every direction.

In order to convert GPR time section into depth section, the velocity of radar pulse propagates through the ground of the study area should be known. Since the reflections of small objects in the ground, such as boulders or artefacts, normally appear as hyperbolic-shape reflections or diffraction hyperbolas in radar sections, velocity of radar pulse in the ground can be quickly determined from these hyperbolic-shapes. This method is supported by common radar software packages but it should be applied only in case that the diffraction hyperbolas appear on at least 20 radar scans (Ranalli et al, 2004).

Several hyperbolic reflections on GPR section were observed in the present study. An example of velocity analysis with the diffraction hyperbola method is shown in Figure 2.11. In the present study, the average velocity of radar pulse is about 0.13 m/ns and it was applied for time to depth conversion of radar section. It also indicated that the study area characterized by poorly electromagnetic energy dissipating materials.

2.2.2.11 DEPTH CONVERSION

This process converts the time-section of GPR data into its corresponding depth-section with known velocity obtained from the velocity analyses step.

It should be noted that all processing steps described above utilized the ReflexW® software, version 4.5, except the RESAMPLING and the TRACE EDIT which were carried out by using the Gradix® software, version 1.08.

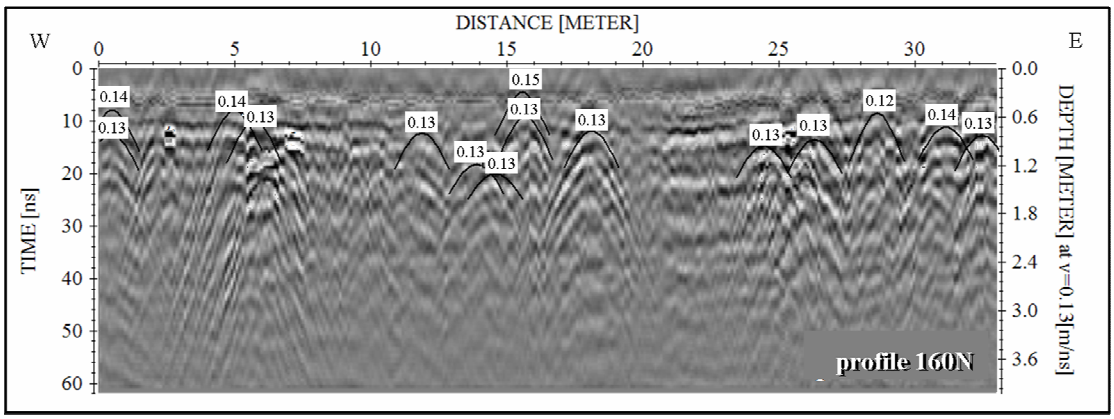

Figure 2.11 Velocity analyses with the diffraction hyperbola method on the profile 160N. Labeled numbers are their corresponding velocities in m/ns.

2.2.3 3D GPR visualization

3D visualization of GPR images was attempted in the present study in order to map the horizontally and vertically continuation of anomalies observed in the study area. Two methods were employed in the present study, the horizontal time-slices map and the iso-amplitude surfaces map.

2.2.3.1 Horizontal time-slices map

The horizontal time-slices map is a map showing the amplitude distribution of reflected radar pulse at a particular depth of interest. In order to compute horizontal amplitude time slices, amplitude variations of recorded traces acquired from a gridded area within a specific time window were determined. Both positive and negative reflections amplitudes are then compared to the norm of all amplitudes within that window without differentiation between positive or negative amplitudes. Sometimes the trace envelope is used instead of a particular complex-trace attribute. Being a measure for the reflectivity strength, it helps to show high reflection amplitude anomalies. Spatial averaging is also useful to reduce small-scale heterogeneity noise. Finally, data are interpolated and gridded on a regular mesh (Conyers, 2001).

2.2.3.2 Iso-amplitude surfaces map

Another method of 3D image visualization is the 3D iso-amplitude surfaces map where the reflection amplitude of GPR data are defined in the 3D cube represented the subsurface below the surveyed area.

After an appropriate processing of radar data, a 3D image of the sought diffractive or reflective objects could be obtained by the following steps:

- The grid data were converted to the reflection strength or amplitude envelope by a Hilbert transformation.
- A threshold value was set and all reflection amplitudes greater than or equal to this value are considered per definition.
- 3D contouring by means of iso-amplitude surface.

With this 3D visualization technique, various threshold values of the reflection amplitude can be assigned in order to show the reflective subsurface object in 3D location (Leucci and Negri, 2006).

CHAPTER 3

RESULTS

3.1 2D GPR image interpretation and anomaly characterization

The processed GPR data along measured profiles in the study area are displayed as normal-incidence time sections. In the sections, the signal voltages were plotted versus two-way traveling time with the downward vertical axis representing the two-way time and the horizontal axis representing distance along the measuring profile. In the present study, these time sections were converted into their corresponding depth sections with the average propagation velocity of 0.13 m/ns. In a depth section, horizontal axis also represents distance along the measuring profile and the downward vertical axis represents the depth. The letters in the time or depth sections denote the interpreted GPR anomalies.

After the appropriate processing steps were applied to GPR data, distinctive anomalies can be observed as high amplitude areas in GPR sections. Three groups of anomalies can be distinguished based on reflection pattern characteristics in the radargrams (Figures 3.1 to 3.7) as followings;

3.1.1 Strong reflection anomaly

Strong reflections are groups of high amplitude anomalies appeared clearly in the GPR sections. These strong reflection anomalies can be observed in the western part, named "WA", and the eastern part, named "EA", of the study area.

The strong anomaly in the western part of the study area, “WA”, was observed at distances of 4.0 to 8.0 m and two-way time of 6 to 34 ns or depth of about 0.39 to 2.21 m. The continuation of this anomaly into adjacent profiles was clearly observed.

The second group of strong anomaly in the eastern part of the study area, “EA”, was observed at distances of 23.0 to 33.0 m and two-way time of 6 to 30

ns or depth of 0.39 to 1.95 m. The continuation of this anomaly into the adjacent profiles was also observed.

The shapes and alignments of these anomalies suggested that they are likely caused by archaeological structures such as buried ancient walls or remains of ancient buildings.

3.1.2 Weak reflection anomaly

Weak reflection anomalies named “CA” were observed in the central part of the study area. Most of these anomalies appear at the distances of 15.0 to 20.0 m and at the two-way time of 6 to 28 ns or at depths of about 0.39 to 1.82 m. These weak anomalies were observed in the central portions of many profiles. According to their characteristics, these anomalies were probably caused by the presence of small-sized archaeological structures or parts of the collapsed ancient walls or buildings in the subsurface.

The hyperbolic-shape anomalies in radargrams as shown in Figure 2.9 (g) were mostly caused by small objects in the ground. By applying migration processing, hyperbolic-branches will be collapsed into their corresponding apexes and appeared as small groups of high amplitude anomaly as shown in Figure 2.9 (h). Such small anomalies of weakly amplitude were also observed in the central part of the study area. In the present study, this type of anomaly was interpreted as the small subsurface features, such as boulders, ancient bricks or roots of the surrounding trees.

3.1.3 Horizontally linear reflection event

Moreover, a horizontally linear reflection event labeled “I” was observed in most profiles at the two-way time of about 10 to 14 ns, or depth of about 0.65 to 0.91 m. This reflection event was interpreted as an interface between the present soil and the underlying ancient soil.

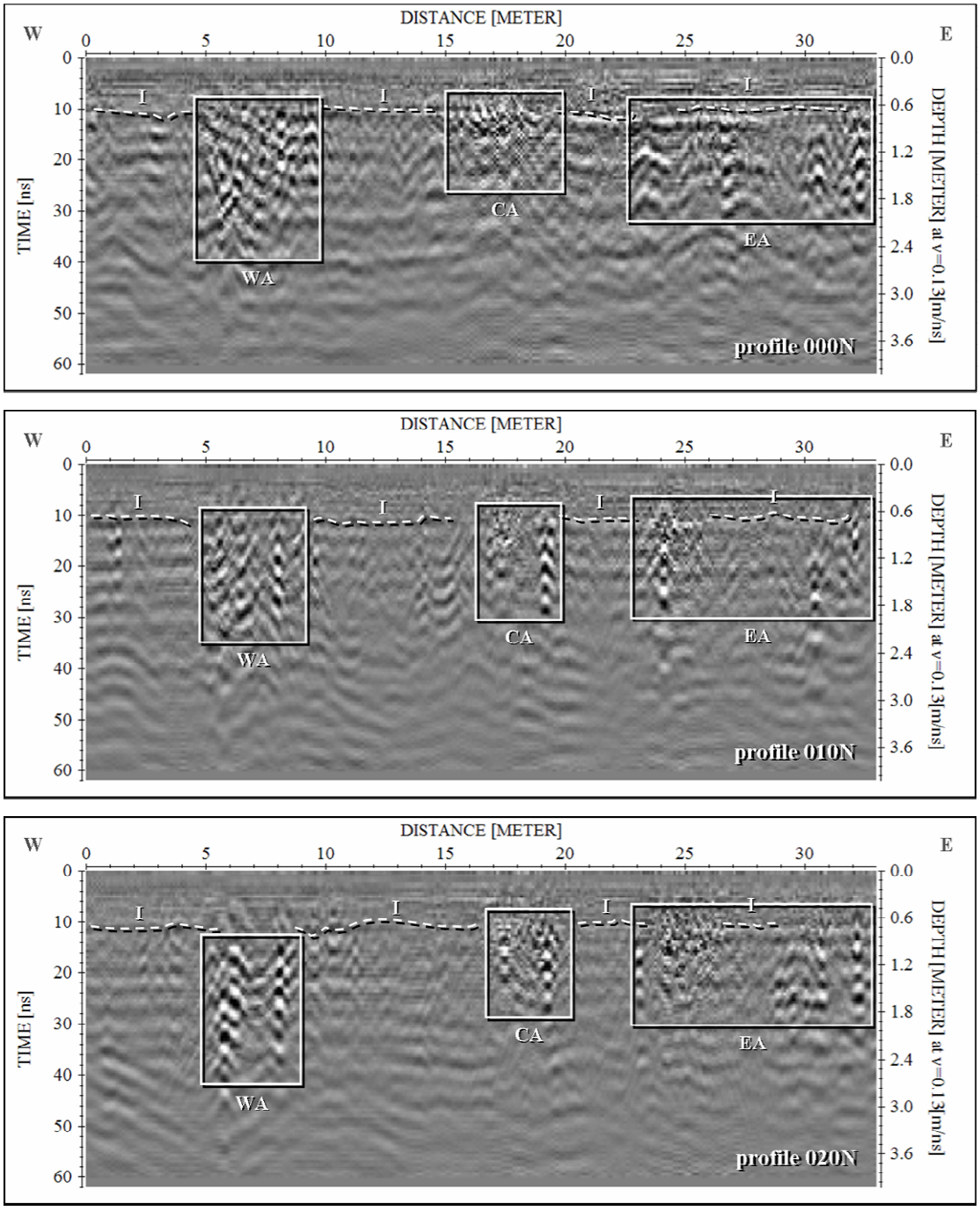

Figure 3.1 2D images of processed GPR data on profile 000N, 010N, and 020N (see explanation in text).

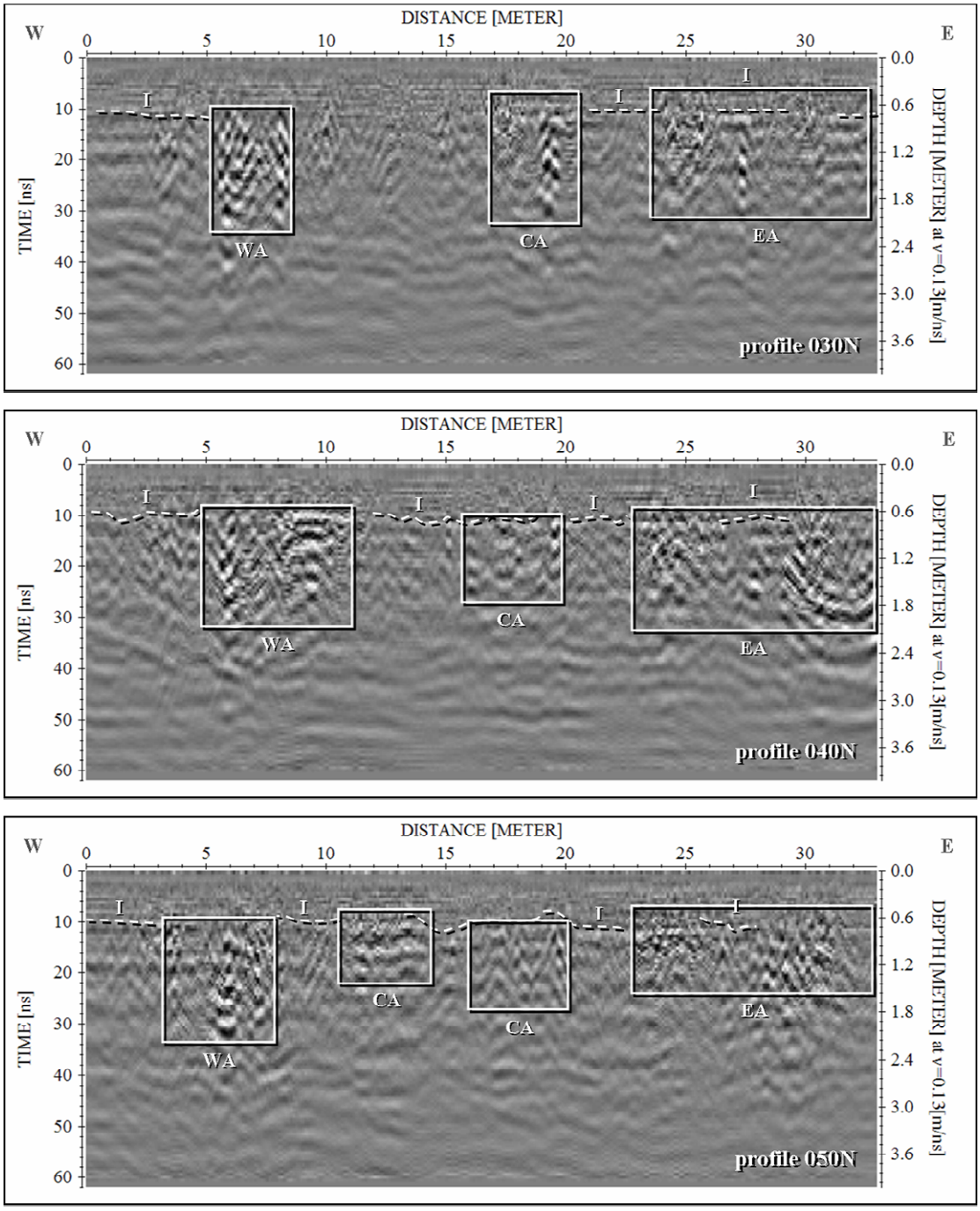

Figure 3.2 2D images of the processed GPR data on profiles 030N, 040N, and 050N (see explanation in text).

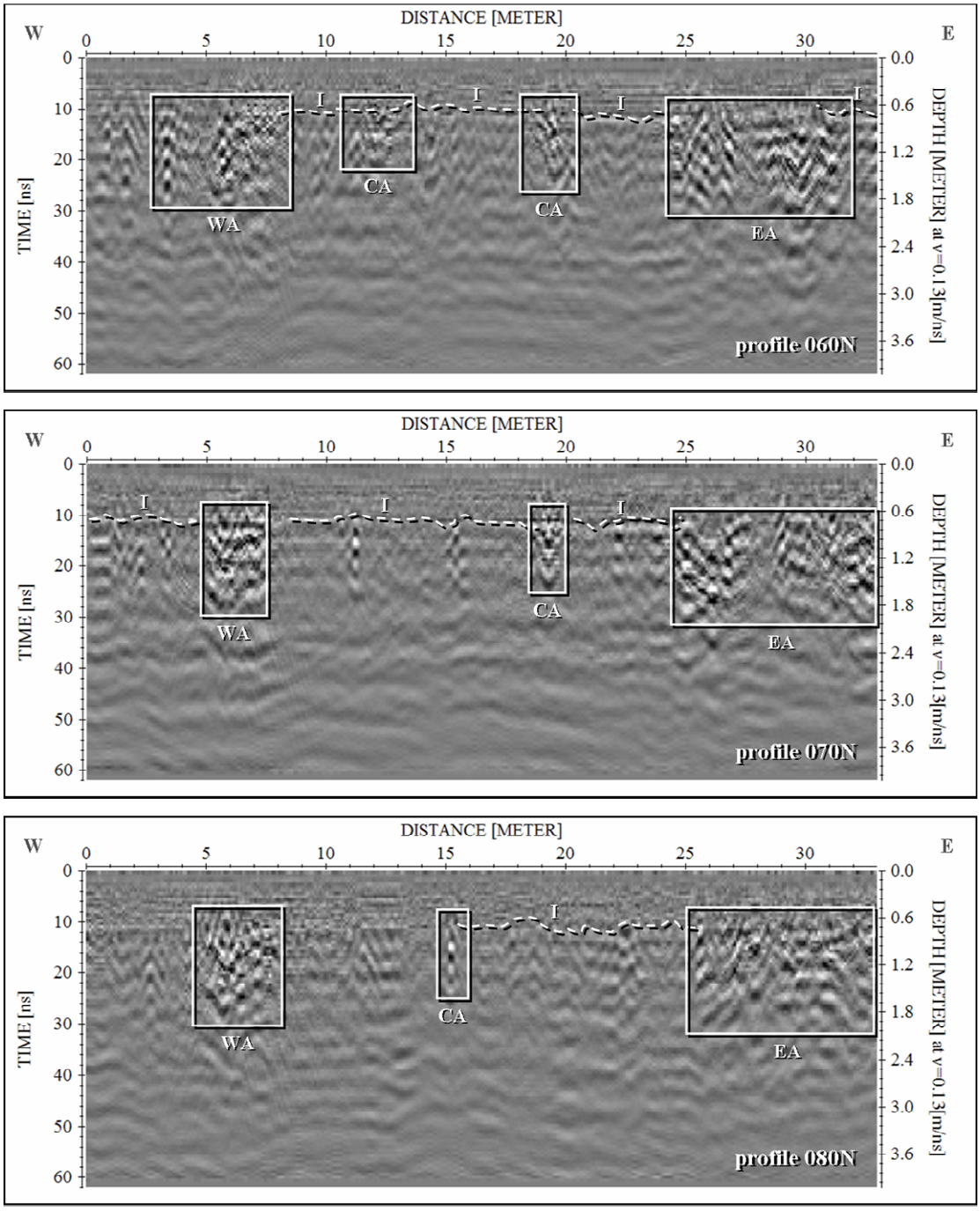

Figure 3.3 2D images of the processed GPR data on profiles 060N, 070N, and 080N (see explanation in text).

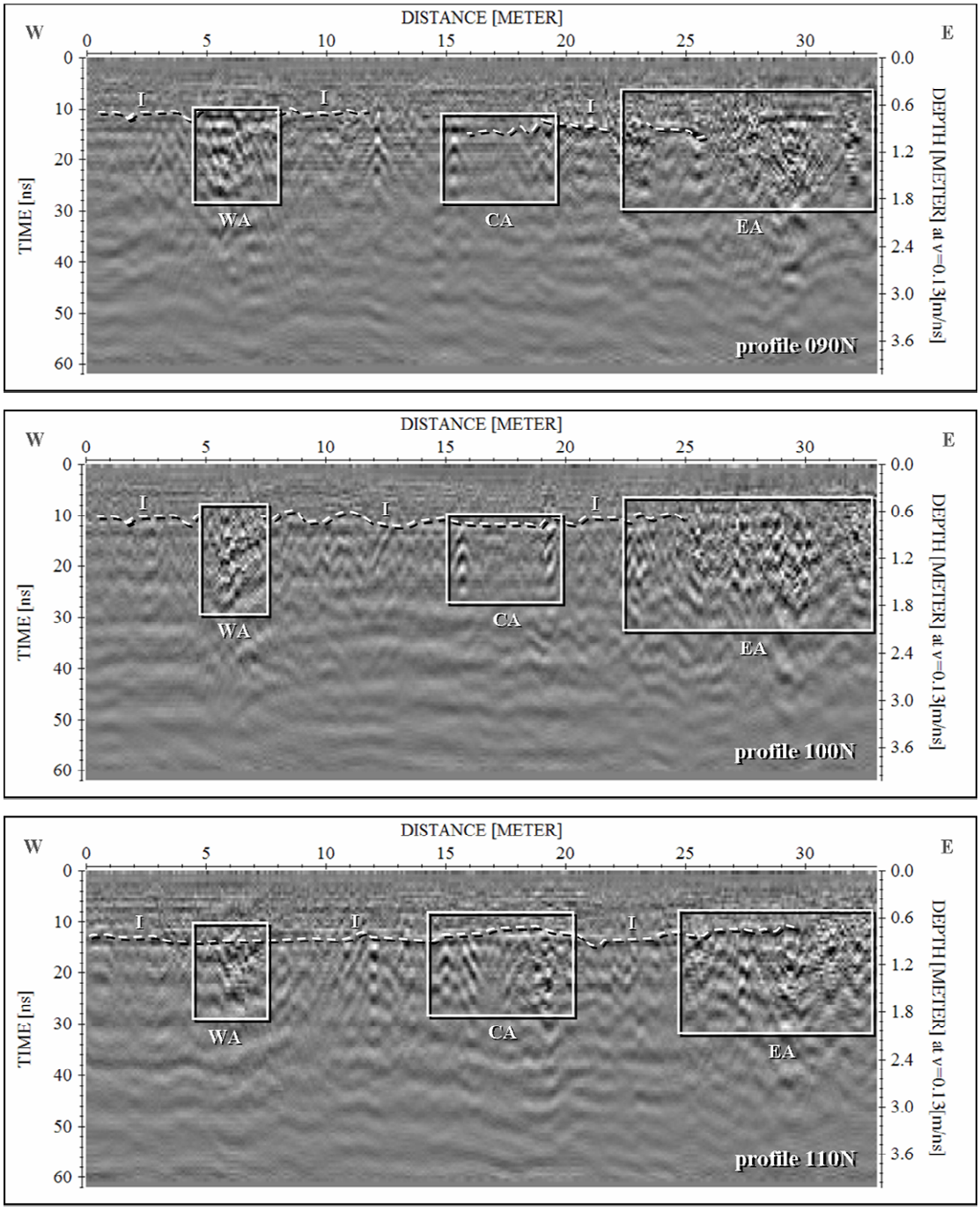

Figure 3.4 2D images of the processed GPR data on profiles 090N, 100N, and 110N (see explanation in text).

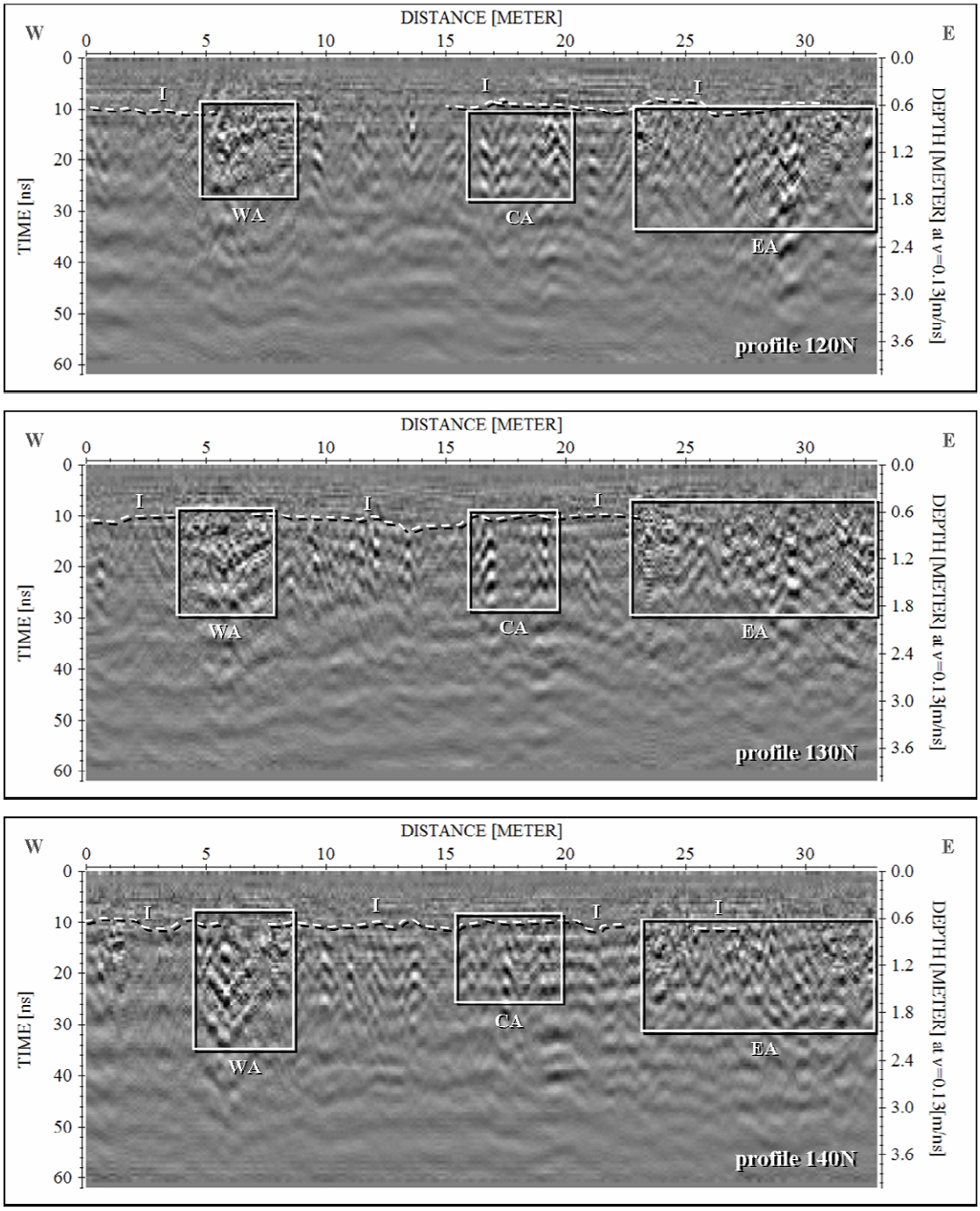

Figure 3.5 2D images of the processed GPR data on profiles 120N, 130N, and 140N (see explanation in text).

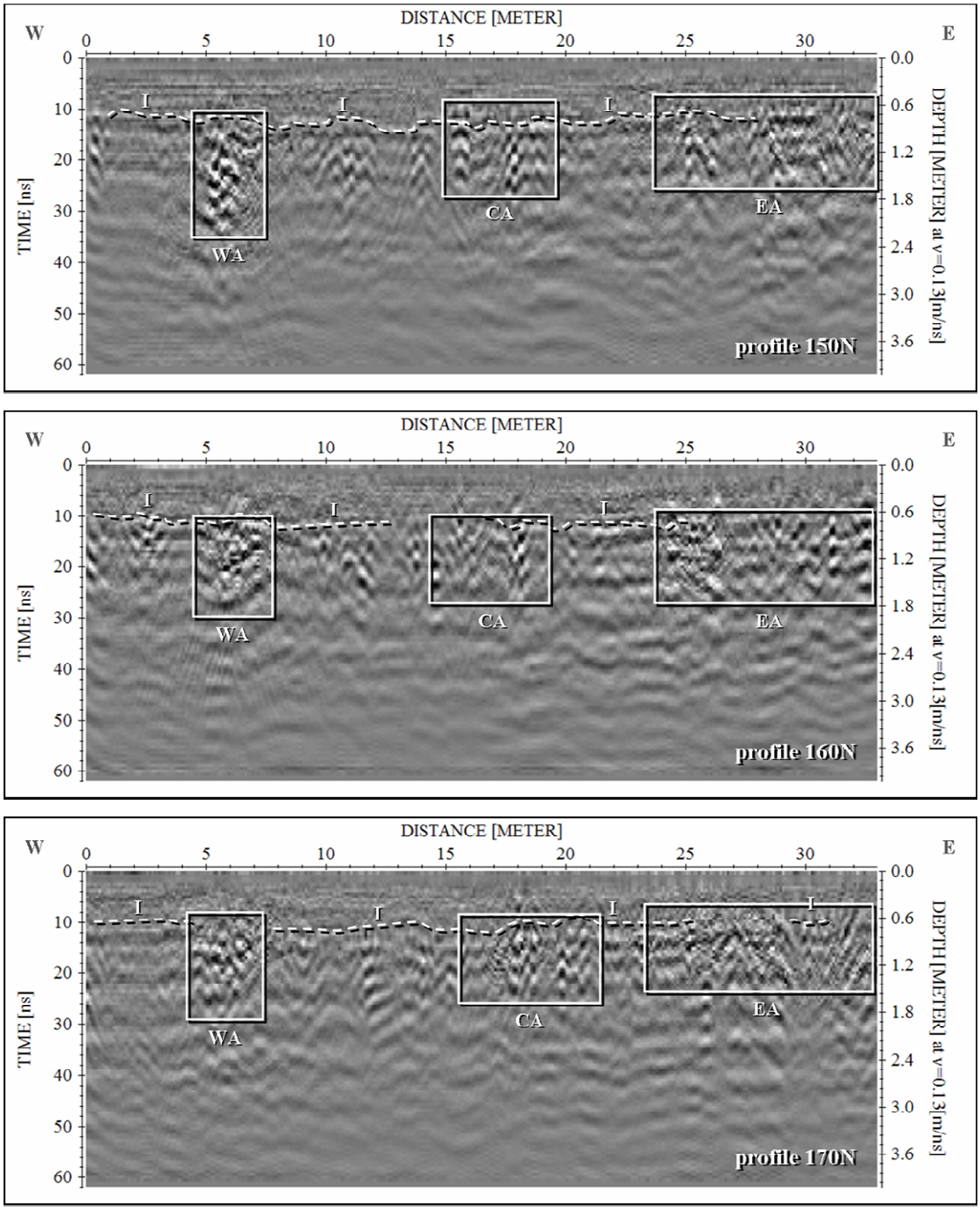

Figure 3.6 2D images of the processed GPR data on profiles 150N, 160N, and 170N (see explanation in text).

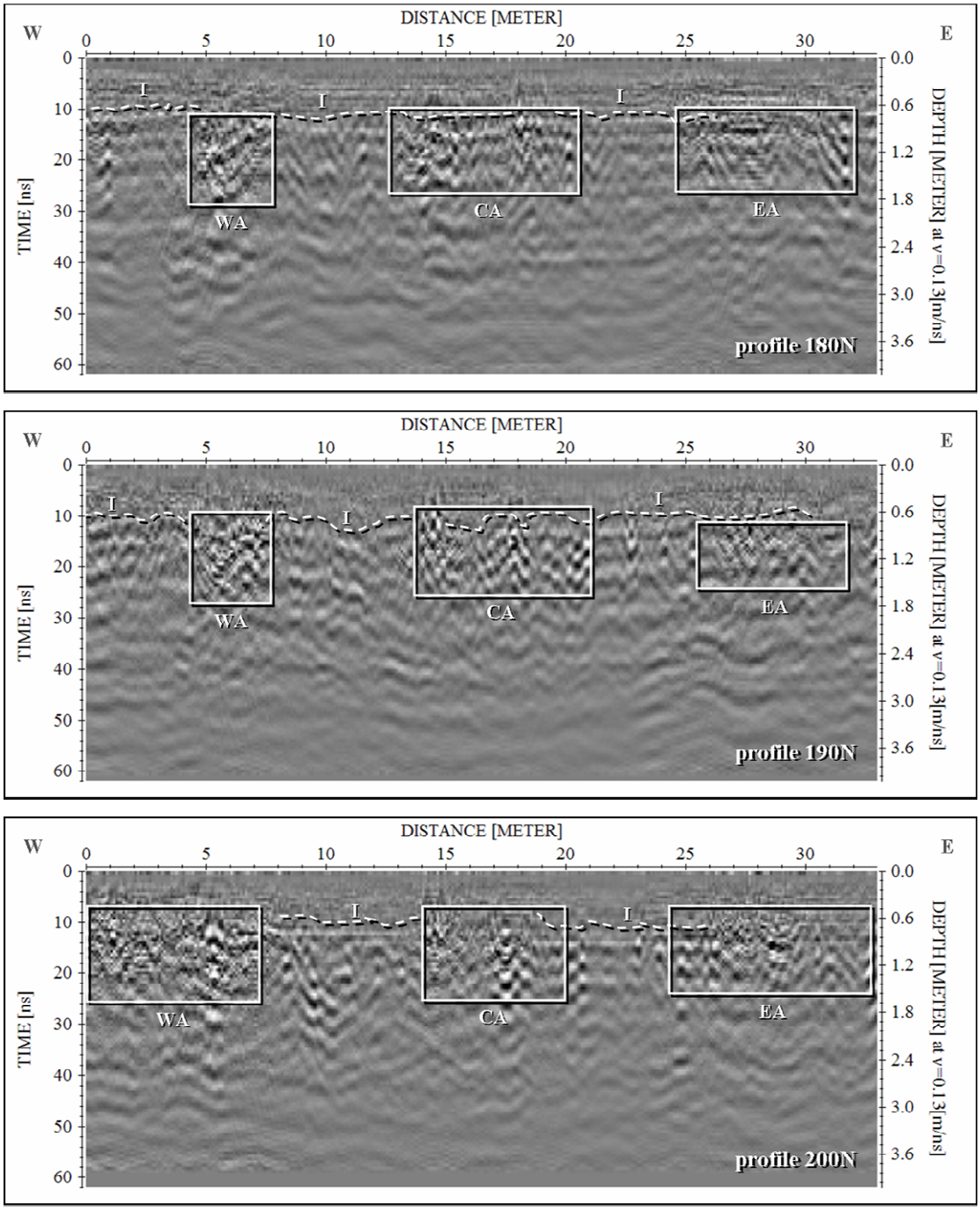

Figure 3.7 2D images of the processed GPR data on profiles 180N, 190N, and 200N (see explanation in text).

3.2 3D GPR visualizations

3D visualization of GPR images was attempted in the present study in order to map the continuation of the GPR anomalies both vertically and horizontally. Two methods employed in the present study were the time-slices map and the iso-amplitude surfaces map.

3.2.1 Horizontal time-slices maps

The time-slices map is a map showing the reflected wave amplitudes distribution of radar pulses at a particular depth of interest in the study area. The variations of amplitudes of the reflected pulses were used as indicators of the subsurface changes in physical properties or lithologies across interfaces. In any slice, the low-amplitude corresponds with small changes in physical properties and high-amplitude indicates large changes in physical properties or the presences of buried features.

Due to gradually changes in radar velocity both horizontally and vertically, which may be encountered in any study area, horizontal time slices should be consider only as approximate depth slices. However, the depth-slices map produced with an average velocity are generally sufficient for most applications. In the present study, the time-slices technique was used to display the amplitude variations within consecutive soil layer of approximately 0.25 m thick between 0 and 2.5 m depth.

The depth-slices map constructed from the processed GPR data of the study area is shown in Figure 3.8. Continuations of several anomalies identified by 2D GPR images, namely, “WA”, “CA”, and “EA” in the western, the central and the eastern parts of the study area respectively, are clearly observed in this depth-slices map. No amplitude variation in the soil layer from 0.0 to 0.5 m indicates that the soil layer of this depth characterized by the fairly homogenous material. High amplitude variation indicating high subsurface changes and in many cases related to archaeological remains at the depth range from 0.75 to 2.25 m correspond very well with the identified anomalies “WA” and “EA”. Another amplitude variation associated with “CA” at depth from 0.75 to 1.5 m suggests the presence of slightly

changes in properties of the subsurface material, which might related to the small objects in the ground, for examples; boulders, tree roots, or small archaeological features.

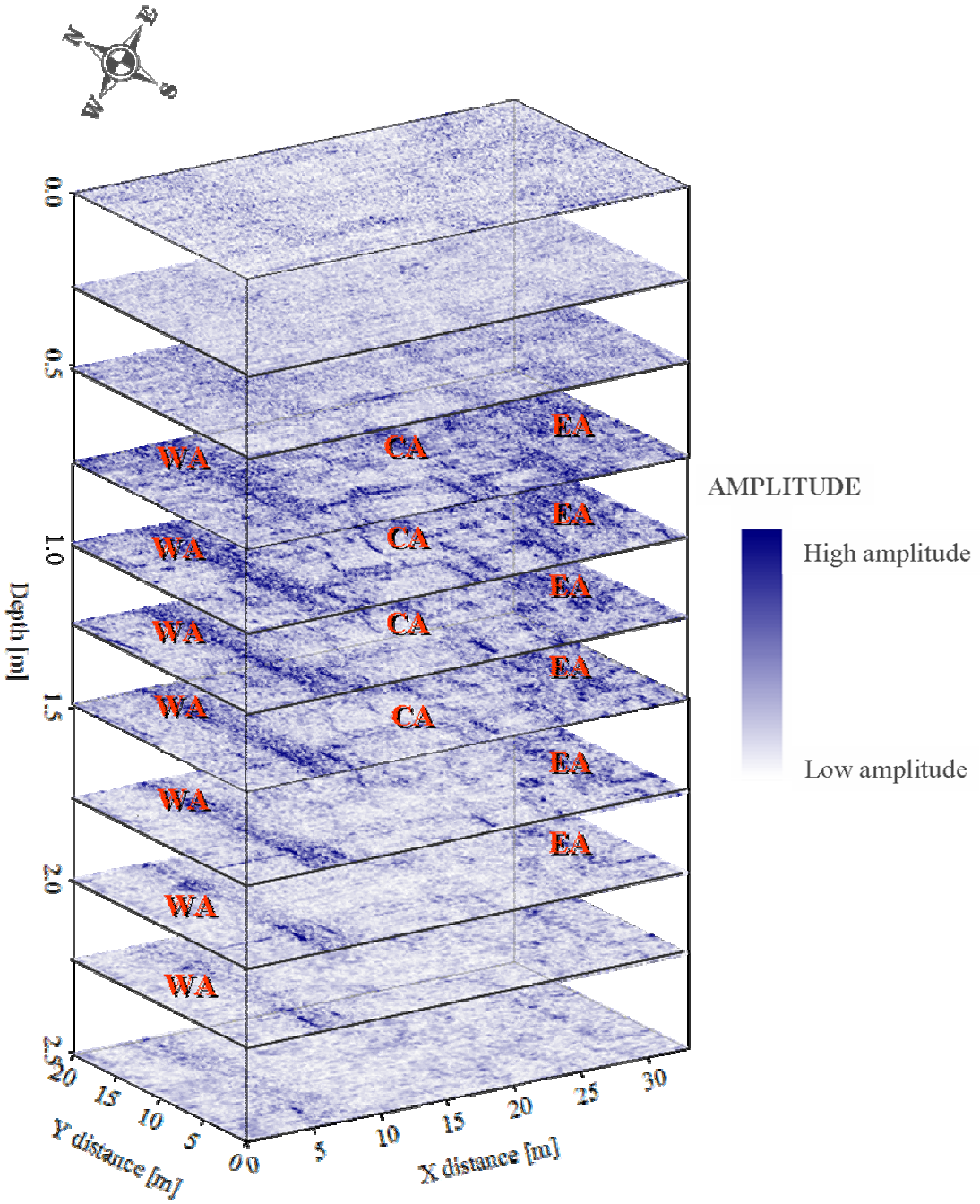

Figure 3.8 GPR depth-slices map of the study area.

3.2.2 Iso-amplitude surfaces maps

GPR results can also be displayed as the iso-amplitude surfaces map, which allows the reflective bodies be clearly observed in the 3D volume below the study area. The same GPR data set was employed in the iso-amplitude surfaces map of various threshold values; 60%, 70%, 80% and 90% of the maximum complex trace amplitude; as shown in Figure 3.9. Small and large anomalous objects are clearly visible in maps of low threshold values, but only large anomalous objects are visible in maps of high threshold values. Therefore, the threshold values of 80% and 90% are chosen in the present study because the continuations of the anomalies "WA", "EA", and "CA" are clearly distinguished from the surrounding ground.

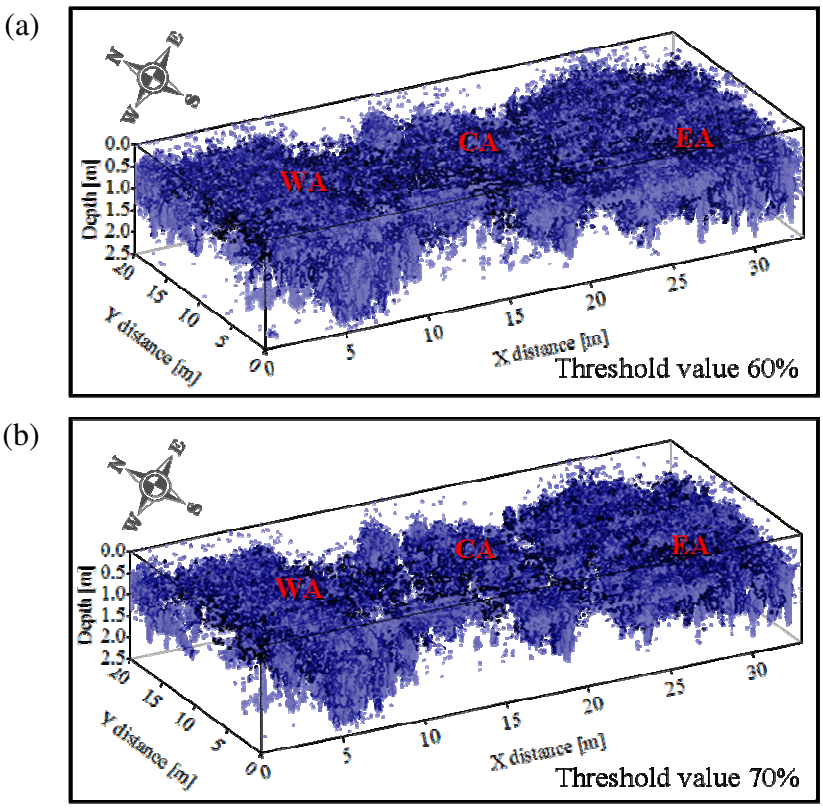

Figure 3.9 3D visualization with iso-amplitude surfaces maps of different threshold values; (a) 60% and (b) 70%.

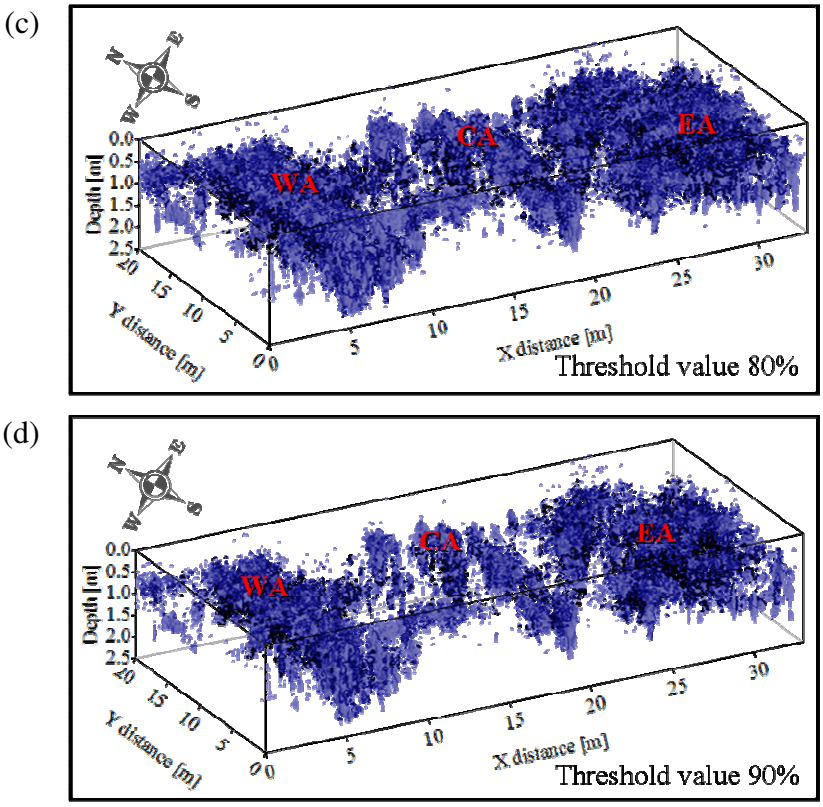

Figure 3.10 3D visualization with iso-amplitude surfaces maps of different threshold values; (c) 80%, and (d) 90%.

The combination visualization of side-view (x-z plane) and the top-view (x-y plane) of the iso-amplitude surfaces map at the threshold value of 80%, as shown in Figure 3.10, display the vertical and horizontal continuation of anomalies; “WA”, “EA”, “CA”, and “I”; in the study area. It should be noticed that the alignment of WA anomaly in the western part of the study area corresponds very well with the western wall of the previous excavated area (Figure 3.11).

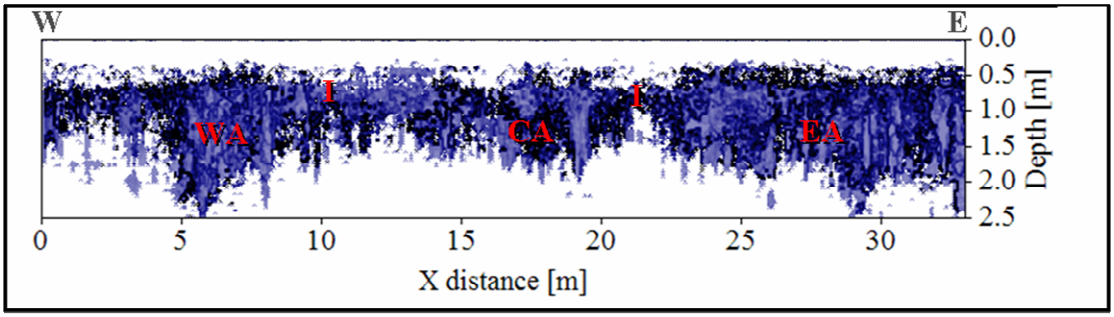

(a)

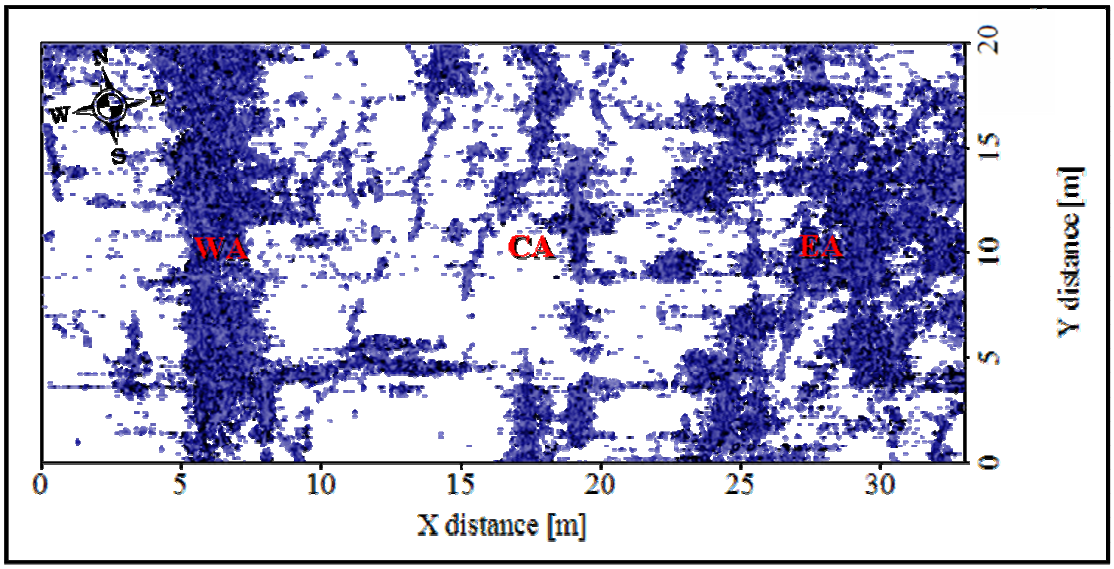

(b)

Figure 3.11 The iso-amplitude surfaces map of the GPR data with a threshold value of 80%; (a) side-view (x-z plan) and (b) top-view (x-y plan). Note that maps show the result at depth from 0.0-2.5 m.

Figure 3.12 The iso-amplitude surfaces map of the GPR data with a threshold value of 80% superimposed on the map of the previous excavated area at Wat Mo Khlan archaeological site.

3.3 Archaeological tested pits

Archaeological tested pits were planned and conducted in the study area in order to verify the interpreted GPR anomalies in the present study. The locations of ten tested pits were shown in Figure 3.12. In general, good correlation between GPR anomalies and archaeological targets were observed.

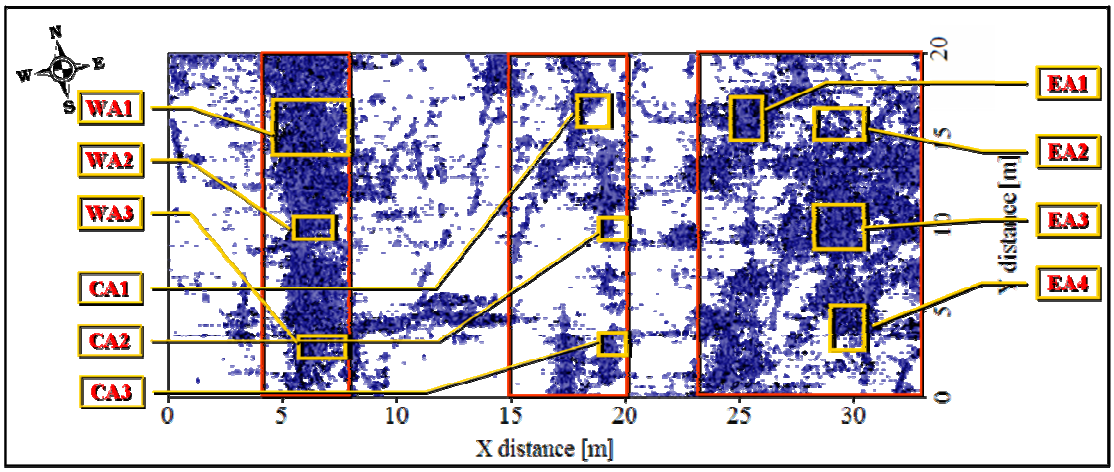

Figure 3.13 Locations of ten tested pits and GPR anomalies in the study area.

The followings are the results obtained from all tested pits. The result of each tested pit will be shown by four photographs of 4 different view directions, namely, northward, eastward, westward, and southward.

The archaeological pitting of the tested pits labeled “WA1”, “WA2”, and “WA3” (Figures 3.14-3.16) were conducted in order to verify the high amplitude radar anomalies, “WA”, in the western part of the study area. The anomalies were at the distance of about 4.0 to 8.0 m or in the western red rectangle in Figure 3.12.

Figure 3.14 Archeological remains in the "WA1" tested pit.

Figure 3.15 Archaeological remains in the "WA2" tested pit.

Figure 3.16 Archaeological remains in the“WA3” tested pit.

Excavation results of the "WA1", "WA2", and "WA3" tested pits are the remains of the western archaeological wall buried at the estimated depth of about 0.3 to 0.5 m. Most of the wall was in good condition, even though some parts of it collapsed into the surrounding ground. The wall is about 1.0 m wide and it was made of well arranged bricks. The alignment of the wall in N10E direction was clearly observed from the photographs looking northward in these three tested pits, as shown in Figure 3.17. Moreover, the alignment of the buried wall was in the same direction as the surface restored archaeological wall in the north (wall no. 4 in Figure 3.12). The shallower was the buried wall, the better wall condition was observed.

Figure 3.17 Alignment of archaeological remains in the tested pits labeled “WA1”, “WA2”, and “WA3”.

The archaeological pitting of the tested pits labeled "EA1", "EA2", "EA3", and "EA4" were carried out to verify high amplitude anomalies labeled as “EA” in the eastern part of the study area. These tested pits were at the distance of about 23.0 to 33.0 m or in the eastern red rectangle (Figure 3.13).

In the tested pit labeled “EA1”, a row of ancient bricks interrupted by roots of trees at about 0.4 m deep was observed (Figure 3.18). High amplitude radar anomalies in this area might associate with these buried features.

In the “EA2” tested pit, scattering ancient remains were found at about 0.3 m depth (Figure 3.19). The findings agreed with the top-view of iso-amplitude

surfaces map that showed the dispersed anomalies (yellow rectangle labeled as “EA2” in Figure 3.13).

Figure 3.18 Archaeological remains in the “EA1” tested pit.

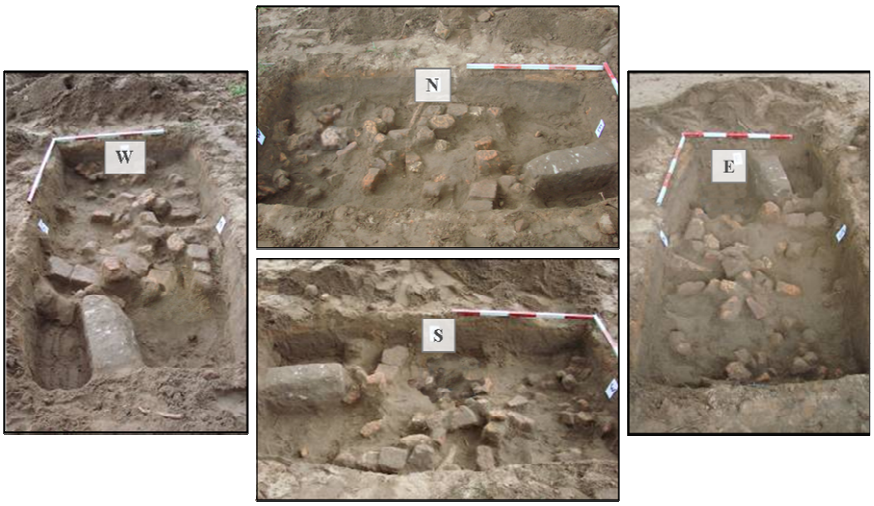

Figure 3.19 Archaeological remains in the “EA2” tested pit.

The tested pit labeled “EA3” was excavated to check the strong radar anomalies in the middle of the eastern anomalies labeled as “EA” (yellow rectangle labeled “EA3” in Figure 3.13). In this pit, the buried features can be clearly divided into western half and eastern half features (Figure 3.20). Archaeological remains in

good condition were found in the eastern half of the pit whereas the collapsed archaeological structures interrupted by roots of trees were observed in the western half of the pit. Most of the buried structures were at depth ranging from 0.3 to 0.4 m.

Figure 3.20 Archaeological remains in the "EA3" tested pit.

Figure 3.21 Archaeological remains in the "EA4" tested pit.

Most of the buried structures found in the "EA4" tested pit were still in very good condition as shown in Figure 3.21. These buried structures were at the depth of about 0.3 to 0.5 m. Moreover, the boundaries of the buried structures in this

pit correspond very well with the boundary of the radar anomaly in this area (yellow rectangle labeled “EA4” in Figure 3.13).

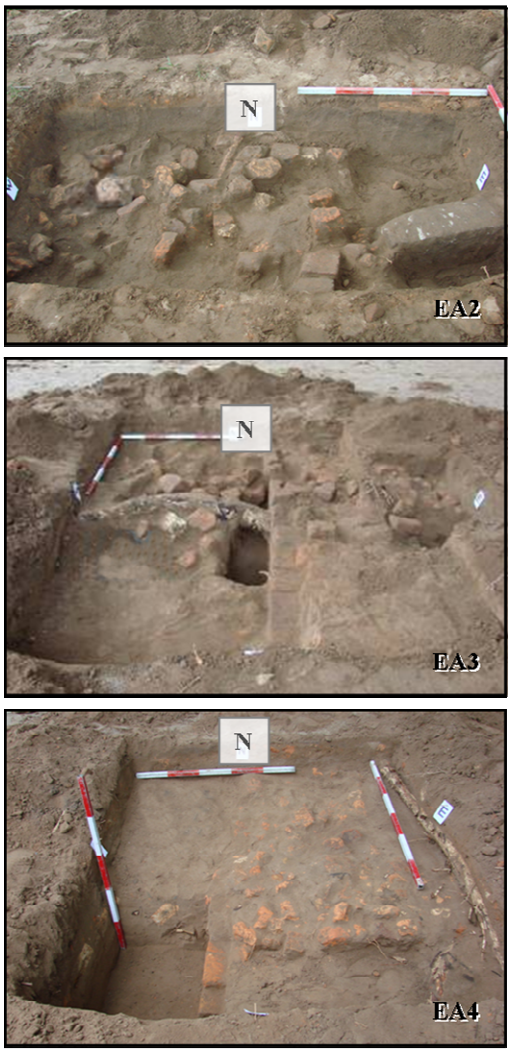

Figure 3.22 Alignment of archaeological remains in the tested pits labeled as “EA1”, “EA2”, and “EA3”.

Weak reflection GPR anomalies associated with the anomalies labeled “CA” in central part of the study area were verified with the archaeological tested pits labeled “CA1”, CA2”, and “CA3”. Locations of these anomalies were at the distance of about 15.0 to 20.0 m or the central red rectangle in Figure 3.13.

The excavation results of these three tested pits showed that the weak and small radar anomalies in the central part of the study area correspond with the

buried boulders, ancient bricks, parts of collapsed ancient structures, and roots of trees at the estimated depth of about 0.3 to 0.5 m (Figures 3.23 to 3.25).

In addition, the horizontal linear reflection event labeled as "I" corresponded with the interface between present topsoil and an ancient ground layer of about 0.3 m thick which composes of sand and small pieces of ancient brick at the depth ranging from 0.2 to 0.4 m (Figures 3.23 to 3.25).

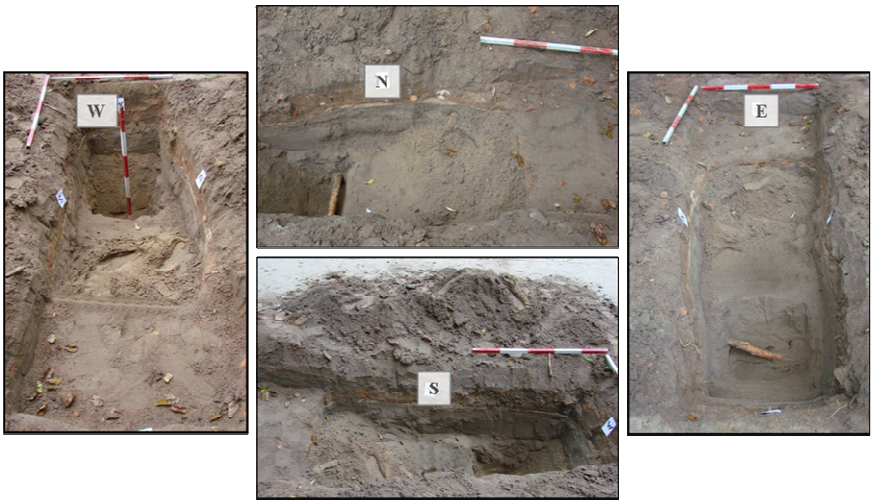

Figure 3.23 Archaeological remains in the "CA1" tested pit.

Figure 3.24 Archaeological remains in the "CA2" tested pit.

Figure 3.25 Archaeological remains in the "CA3" tested pit.

It should be noted that there is a discrepancy between the interpreted depth of burial determined from the present GPR measurement and that of the excavation results. Accidental changes in sampling frequency and sawtooth characteristics in the recording signals encountered during data recording probably caused this discrepancy.

RESAMPLING and TRACE EDIT processes were carried out in the pre-processing steps in order to have GPR data in the same sampling time interval and to eliminate undesigned sawtooth characteristics in the data, respectively. Both processes were conducted in the Gradix® software and the GPR data results were later exported for main processing steps with the ReflexW® software. Bad radar signals at the two-way time of about 0 to 6 ns, or depth shallower than 0.39 m, was observed in the exported radargram. Therefore, subsurface information shallower than 0.39 m could not be identified in the present study.

CHAPTER 4

DISCUSSION AND CONCLUSION

In this study, 3D GPR visualization techniques were applied for locating buried archaeological structures in a selected area of the Wat Mo Klan archaeological site in Nakhon Si Thammarat Province. The data collection was carried out on 101 parallel lines of measurement, 33.0 m in length on each line, with line spacing of 0.2 m and trace spacing of 0.1 m covering an area of 20 m x 33 m.

Three types of reflection events in various locations of the study area were obtained from the analysis of 2D GPR images. The first type were strong reflections appeared as groups of high amplitude anomalies, which composed of two groups; WA and EA respectively. The "WA" anomalies appeared in the western part of the study area at distances of 4.0 to 8.0 m and depths of 0.39 m to 2.21 m, whereas the "EA" appeared in the eastern part of the study area at distances of 23.0 to 33.0 m and depths of 0.39 to 1.95 m. Continuation of these strong reflection anomalies into adjacent profiles was clearly observed and their causative bodies were interpreted as buried ancient walls or remains of ancient buildings. The second type of reflection events was the weak reflection anomalies, named "CA", observed in the central part of the study area at the distances of 15.0 to 20.0 m and depths of 0.39 m to 1.82 m. Their causatives bodies were interpreted as small buried archaeological structures, parts of the collapsed ancient walls or buildings, boulders, bricks or tree roots. The third type of reflection event observed in the present study, named "I", was the horizontally linear reflection event observed in several profiles at depths of 0.65 to 0.91 m. Its causative body was interpreted as an interface between the present soil and the underlain ancient soil.

The vertical and horizontal continuation of the GPR anomalies were clearly observed with 3D visualization techniques, namely, time-slices map and iso-amplitude surfaces map. The time-slices map showed the amplitude variations of the reflected radar waves and was used as indicators of the subsurface changes in physical properties and lithologies across interfaces at a particular depth of interest in the study

area. Whereas the Iso-amplitude surfaces map, or the 3D contouring of reflective anomalies, with suitable amplitude threshold values, displays the reflective subsurface objects in 3D location.

Ten archaeological tested pits were excavated in the study area in order to verify the GPR anomalies and good correlations between GPR anomalies and archaeological remains were observed. The “WA” anomalies in the western part of the study area corresponded with a well arranged bricks wall of about 1.0 m in width buried at the estimated depth of about 0.3 m to 0.5 m. The buried western wall was in good conditions and aligned in the same direction as the restored archaeological wall in the north (archaeological wall number 4). The “EA” anomalies associated with ancient building remains and bricked structures at the depth of 0.3 to 0.5 m. The remains are likely to be the ancient building of similar pattern as the surface archaeological structure in the north (archaeological wall number 3). The weak reflection anomalies, “CA”, correlated with the buried boulders, ancient bricks, parts of collapsed ancient structures, and roots at the estimated depth of about 0.3 to 0.5 m. In addition, the horizontally linear reflection event “I” corresponded with the interface between present and the ancient topsoils at the depth of 0.2 to 0.4 m. In general, the findings obtained from this case study suggested that the denser the high amplitude anomalies were (appearance in top-view of iso-amplitude surfaces map), the more intact of the archaeological remains.

REFERENCES

Acqua, A. D., Sarti, A., Tubaro S. and Zanzi, L. 2004. Detection of linear objects in GPR data. Signal Processing. Vol. 84: 785-799.

Arlsan, E., Biella, G., Boniolo, G., Caporusso, D., Franco, R., Lozej, A. and Veronese, L. 1999. Geophysical investigations of the Olonium Roman site Northern Como Lake. Journal of Applied Geophysics. Vol. 41: 169-188.

Avila-Olivera, J. A. and Garduño-Monroy, V. H. 2008. GPR study of subsidence-creep-fault processes in Morelia, Michoacán, Mexico. Engineering Geology. Vol. 100: 69-81.

Basile, V., Carrozzo, M.T., Negri, S., Nuzzo, L., Quarta, T. and Villani, A.V. 2000. A ground-penetrating radarsurvey for archaeological investigations in an urban area (Lecce, Italy). Journal of Applied Geophysics. Vol. 44: 15-32.

Brancaccio, A., Pierri, R., Leone G. and Soldovieri, F. 2004. Measurements and material characterization for masonry imaging. Proceeding of 10th International Conference on Ground Penetrating Radar. Delft, The Netherlands, June 21st-24th, 2004. pp 383-386.

Cezar, G.S., Rocha, P., Buarque, A. and Costa, A. 2001. Two Brazilian archaeological sites investigated by GPR: Serrano and Morro Grande. Journal of Applied Geophysics. Vol. 47: 227-240.

Conyers, L. B. 2001. Ground-penetrating radar. In: Encyclopedia of Imaging Science and Technology. Hornak, J.P., Ed. John Wiley and Sons, New York. pp 463-476.

Conyers, L.B. 2006. Ground-penetrating Radar. In: Remote Sensing in archaeology. Johnson, J. K., Ed. The University of Alabama Press, Tuscaloosa, Alabama. pp 131-160.

Conyers, L.B. 2007. Ground-penetrating Radar for Archaeological Mapping. In Remote Sensing in Archaeology. Wiseman, J. and Baz, F., Ed. Springer, New York. pp 329-344.

Conyers, L.B. 2006. Ground-Penetrating Radar Techniques to Discover and Map Historic Graves. Historical Archaeology. Vol. 40(3): 64-73.

Davis, J.L., and Annan, A.P., 1989. Ground Penetrating Radar for high-resolution mapping of soil and rock stratigraphy. Geophysical Prospecting. Vol. 37: 531-551.

Fine Arts Department, 1993. Wat Mo Khlan Archaeological Sites in Tha Sala District, Nakhon Si Thammarat Province. Nakhon Si Thammarat: 8th Regional Office of Fine Arts Department (in Thai).

Fine Arts Department, 1998. Master Plan for the Early History Archaeological Sites in Nakhon Si Thammarat Project. Nakhon Si Thammarat: 14th Regional Office of Fine Arts Department. 137 p (in Thai).

Gracia, V.P., Canas, J.A., Pujades, L.G., Clapes, J., Caselles, O., Garcia, F. and Osorio, R. 2000. GPR survey to confirm the location of ancient structures under the Valencian Cathedral Spain. Journal of Applied Geophysics. Vol. 43: 167-174.

Grasmueck, M. and Weger, R. 2003. How dense is dense enough for a ‘real’ 3D GPR Survey? SEG Technical Program Expanded Abstracts. pp 1180-1183.

Grasmueck, M., Weger, R. and Horstmeyer, H. 2005. Full-resolution 3D GPR imaging. Geophysics. Vol. 70: K12-K19.

Hayee-uma, A. 2003. A Study of Pah-O Ancient Kilns with Geophysical Methods, Hat Yai. Master of Science Thesis in Physics, Prince of Songkla University, Thailand (in Thai).

Heincke, B., Green, A.G., Kruk, J. and Horstmeyer, H. 2005. Acquisition and processing strategies for 3D georadar surveying a region characterized by rugged topography. Geophysics. Vol. 70: K53-K61.

Hruska, J. and Fuchs, G. 1999. GPR prospection in ancient Ephesos. Journal of Applied Geophysics. Vol. 41: 293-312.

Interprex Ltd. 1997. Gradix Radar Processing System, v.1.08. Golden, Co., 1997.

Leucci, G. and Negri, S. 2006. Use of ground penetrating radar to map subsurface archaeological features in an urban area. Journal of Archaeological Science. Vol. 33: 502-512.

Lohawijarn, W. 2005. Geophysical Investigation at Some Archaeological Sites of Nakhon Si Thammarat Province in Peninsular Thailand. Proceeding of the Seminar on Thailand-Malaysia: Malay Penninsula Archaeology Programme. Nakhon Si Thammarat, September 4-10th, 2004. pp 125-132.

Negri, S. and Leucci, G. 2006. Geophysical investigation of the Temple of Apollo (Hierapolis, Turkey). Journal of Archaeological Science. Vol. 33: 1505-1513.

Olhoeft, G.R. 2006. Ground Penetrating Radar. Proceedings of the 11th International Conference on Ground Penetrating Radar. Columbus, Ohio, USA, June 19th-22nd, 2006.

Parasnis, D.S., 1997. Principle of Applied Geophysics. Chapman & Hall, London Press, UK.

Phattanaviriyaphisarn, A. 2002. A study of Archaeology Morphology with High Frequency Electromagnetic wave. Master of Science Thesis in Physics, Prince of Songkla University, Thailand (in Thai).

Ranalli, D., Scozzafava, M. and Tallini, M. 2004. Ground penetrating radar investigations for the restoration of historic buildings: the case study of the Collemaggio Basilica (L'Aquila, Italy). Journal of Cultural Heritage. Vol. 5: 91-99.

Reynolds, J.M. 1997. An Introduction to Applied and Environmental Geophysics. North Wales, UK.

Sambuelli, L., Socco, L.V. and Brecciaroli, L. 1999. Acquisition and processing of electric, magnetic and GPR data on a Roman site Victimulae, Salussola, Biella. Journal of Applied Geophysics. Vol. 41: 189-204.

Sandmeier, K.J. 2007. Reflexw 4.5 Manual, Sandmeier Software, Karlsruhe, Germany.

Shaaban, F.F. and Shaaban, F.A. 2001. Use of two-dimensional electric resistivity and ground penetrating radar for archaeological prospecting at the ancient capital of Egypt. Journal of African Earth Sciences. Vol. 33: 661-671.

Sampaongen, P. 2007. Archaeological Evidence in the Upper Malay Peninsular: Related to Religion and Belief [online]. Available from http:// www.fad14.go.th/article/overview.htm [26 February 2007]

Sigurdsson, T. and Overgaard, T. 1998. Application of GPR for 3-D visualization of geological and structural variation in a limestone formation. Journal of Applied Geophysics. Vol. 40: 29-36.

Singsoupho, S. 2008. Application of Geophysical Methods in Archaeological Investigation: A Case Study from Lao Pako, Vientiane Capital, Lao PDR. Master of Science Thesis in Geophysics, Prince of Songkla University, Thailand.

Thongjarienchaikit, C. 2008. Wat Mo Khlan Archaeological Site [online]. Available from: http://archaeology.thai-archaeology.info/index.php?option=com_content&task=view&id=289&Itemid=0 [2 January, 2009] (in Thai).

Wikipedia, 2008. Nakhon Si Thammarat [online]. Available from: http://en.wikipedia.org/wiki/Nakhon_Si_Thammarat [28 August, 2008].

Whiting, B.M., McFarland, D.P. and Hackenberger, S. 2001. Three-dimensional GPR study of a prehistoric site in Barbados, West Indies. Journal of Applied Geophysics. Vol. 47: 217-226.

APPENDICES

2D GPR images of processed GPR data in the study area

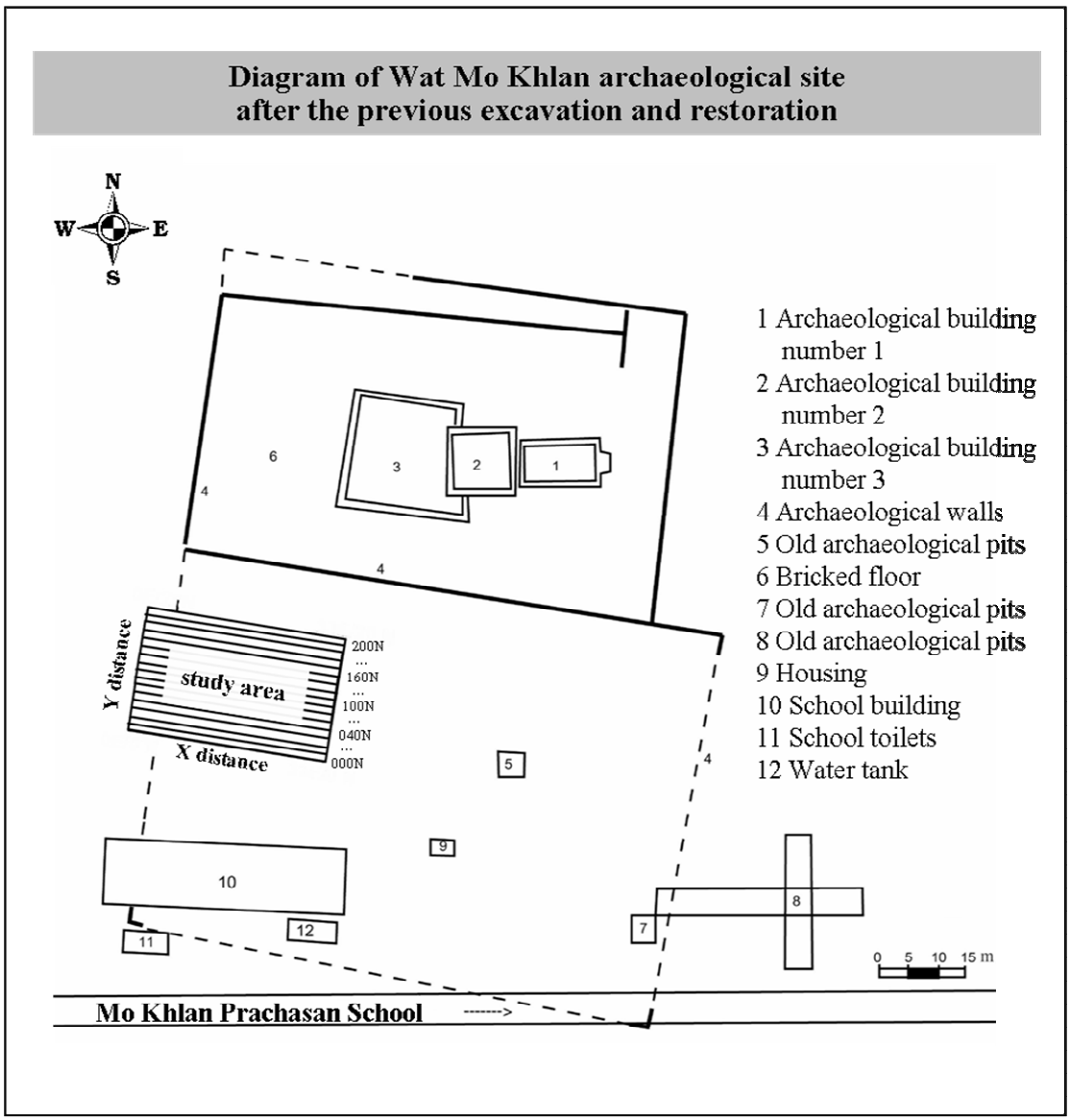

Figure A1 Map of study area and lines of measurement within the study area (modified from Fine Arts Department, 1993).

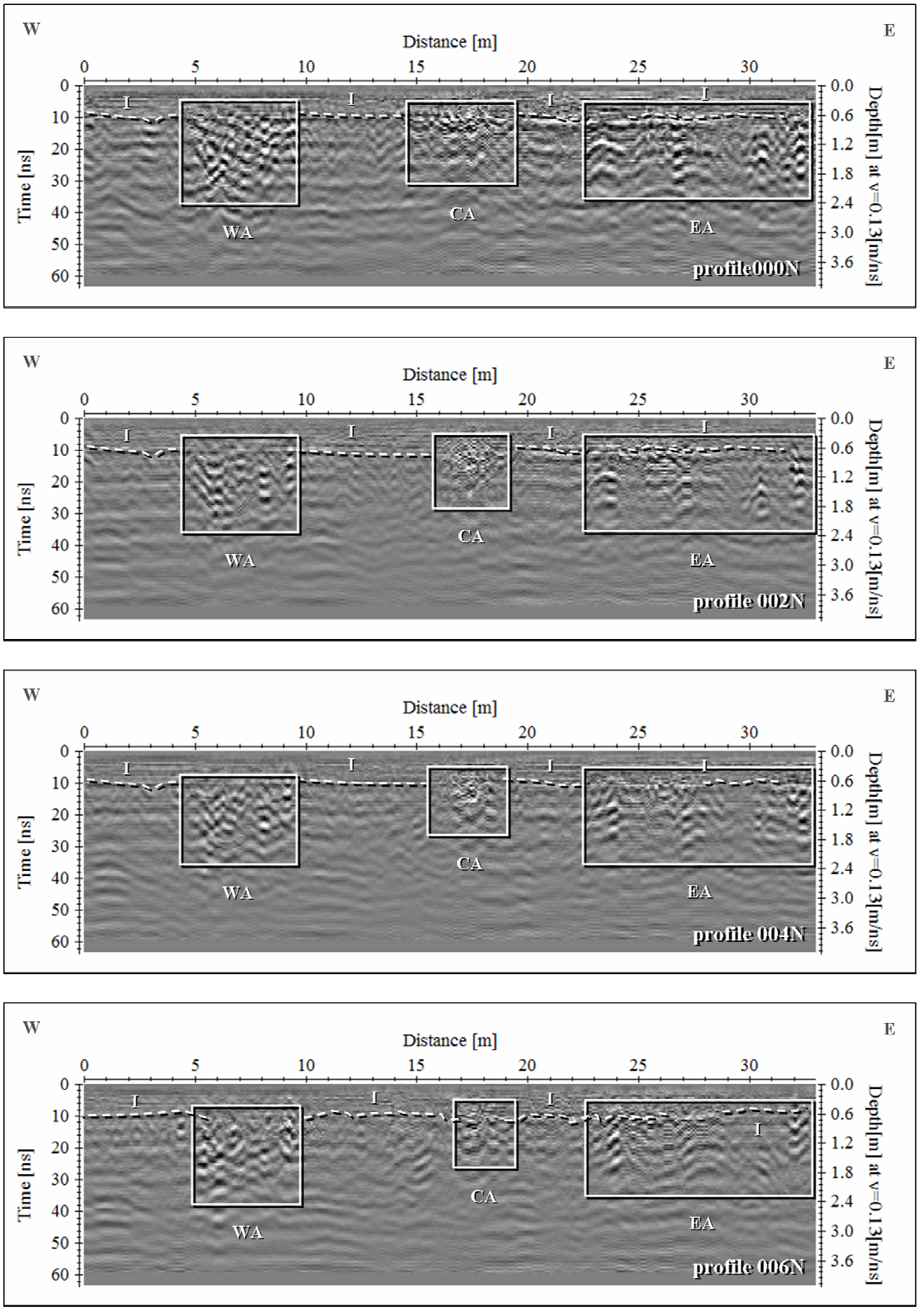

Figure A2 2D images of processed GPR data on profile 000N, 002N, 004N, and 006N.

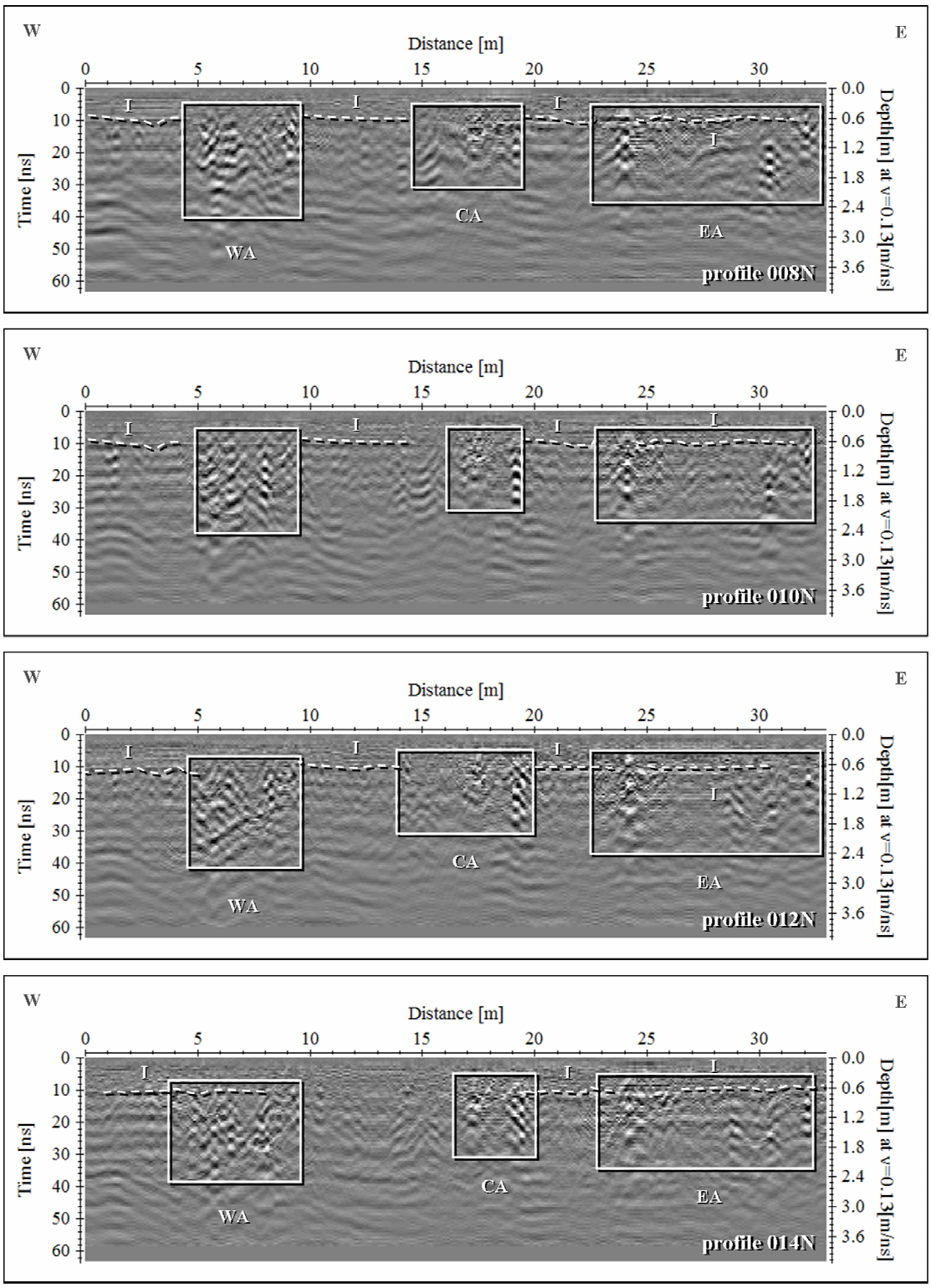

Figure A3 2D images of processed GPR data on profile 008N, 010N, 012N, and 014N.

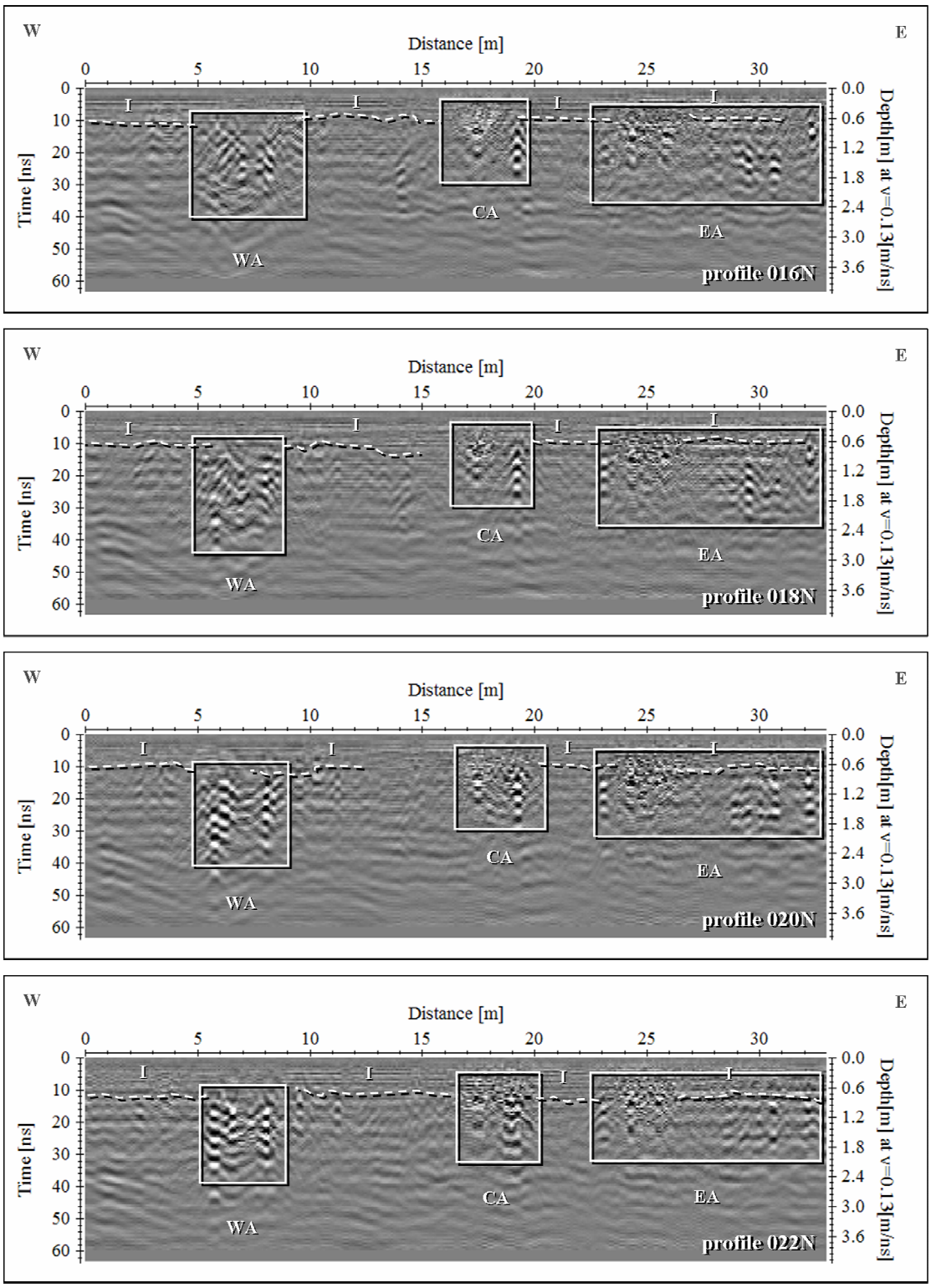

Figure A4 2D images of processed GPR data on profile 016N, 018N, 020N, and 022N.

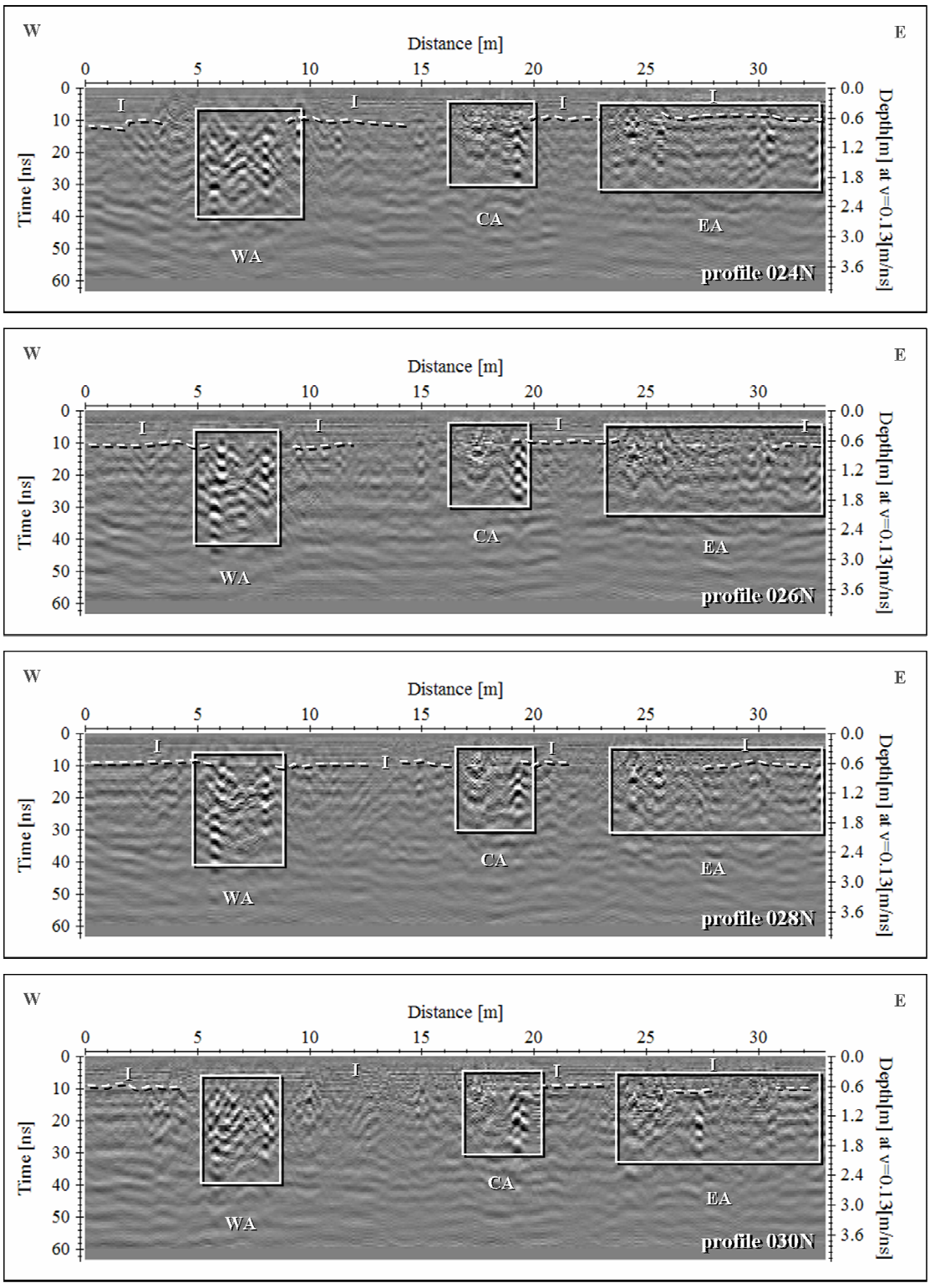

Figure A5 2D images of processed GPR data on profile 024N, 026N, 028N, and 030N.

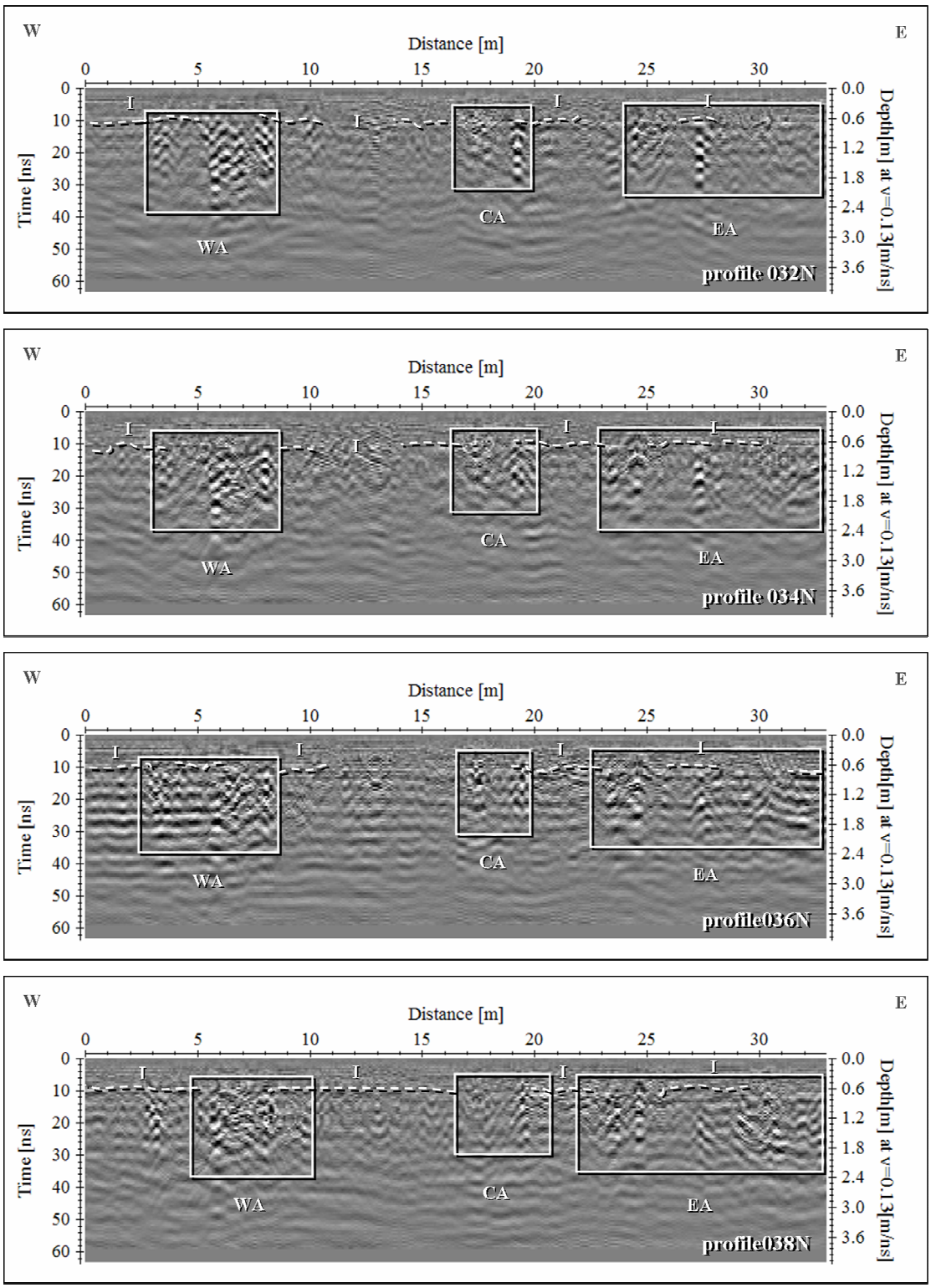

Figure A6 2D images of processed GPR data on profile 032N, 034N, 036N, and 038N.

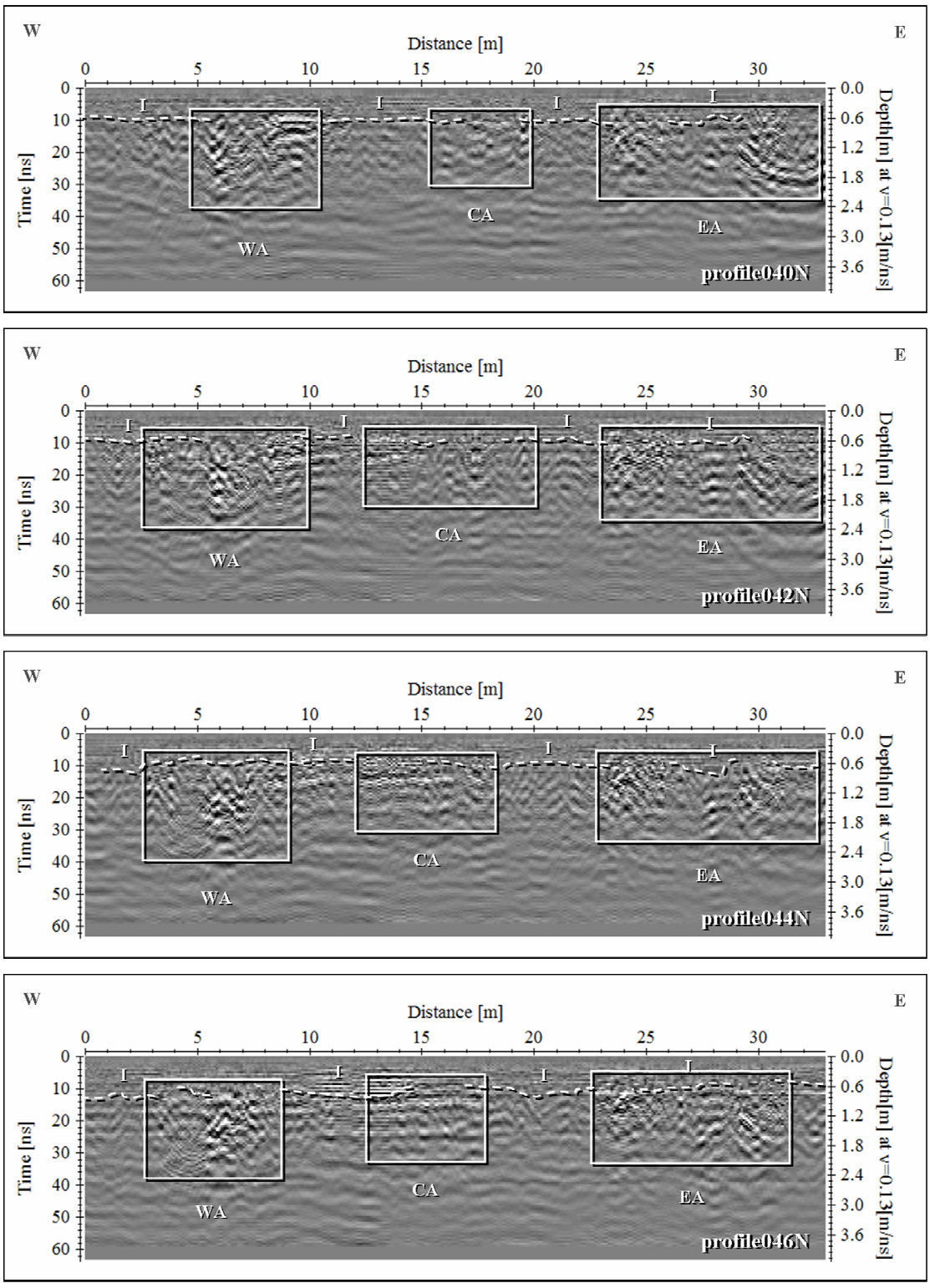

Figure A7 2D images of processed GPR data on profile 040N, 042N, 044N, and 046N.

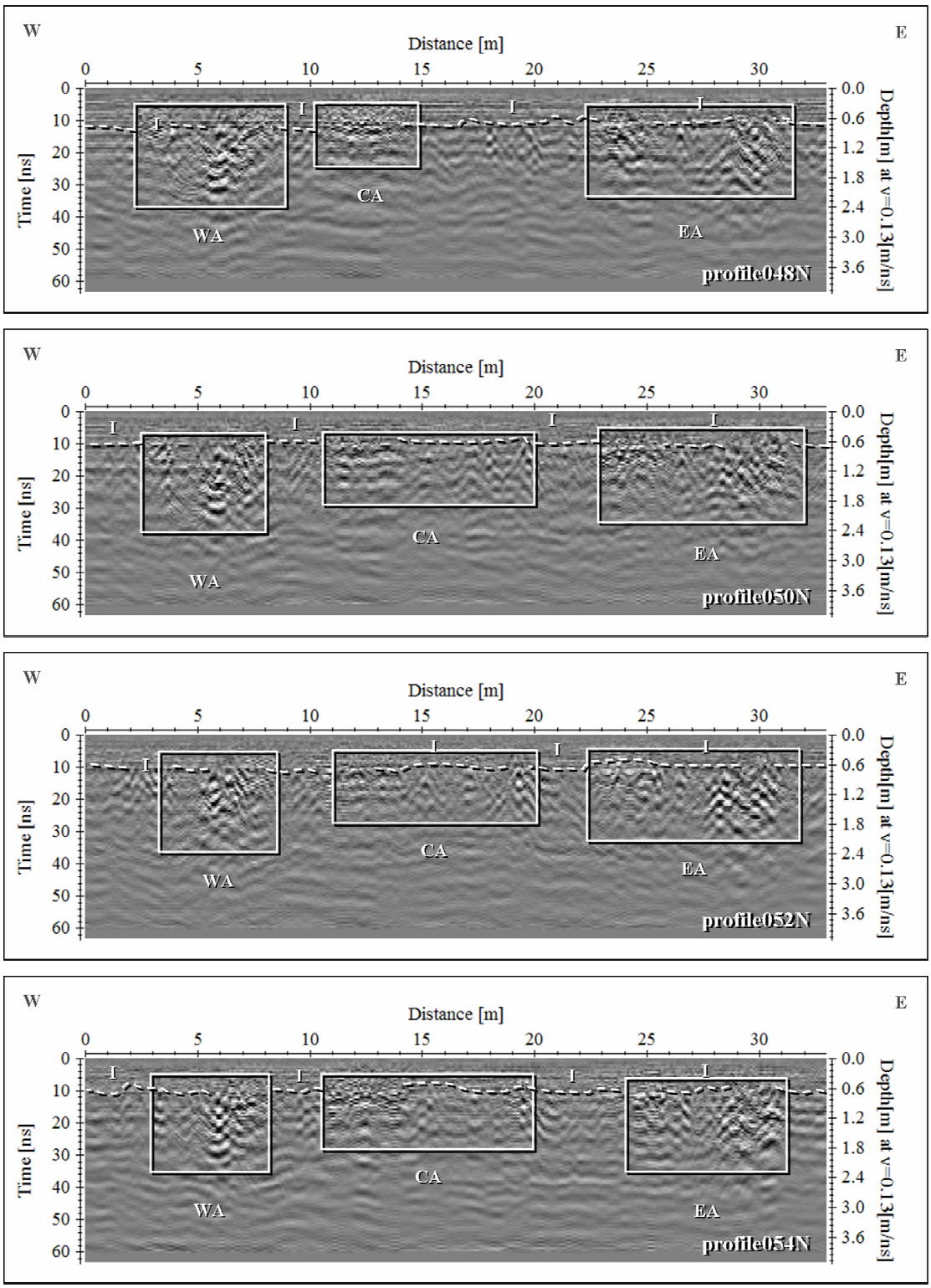

Figure A8 2D images of processed GPR data on profile 048N, 050N, 052N, and 054N.

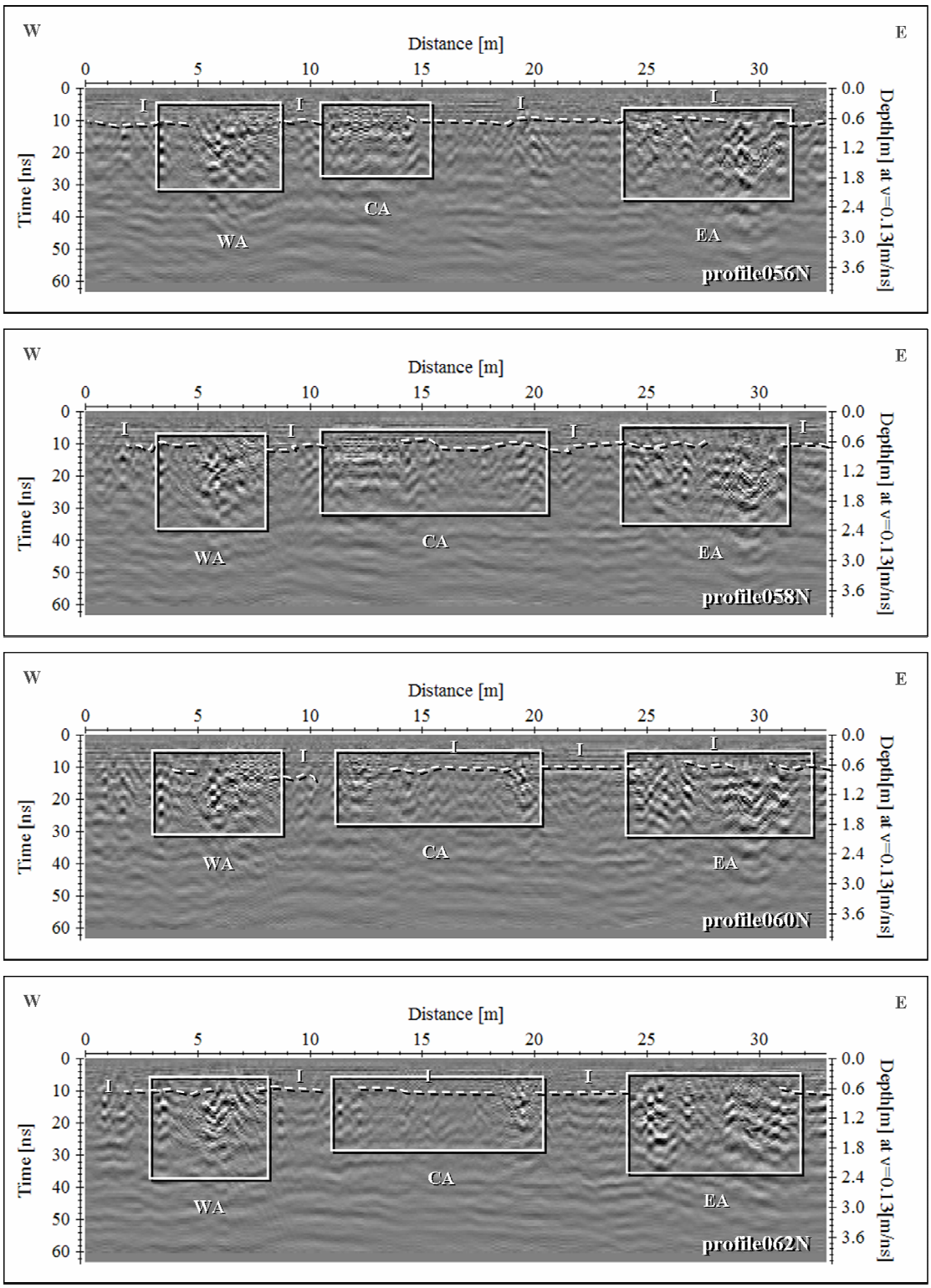

Figure A9 2D images of processed GPR data on profile 056N, 058N, 060N, and 062N.

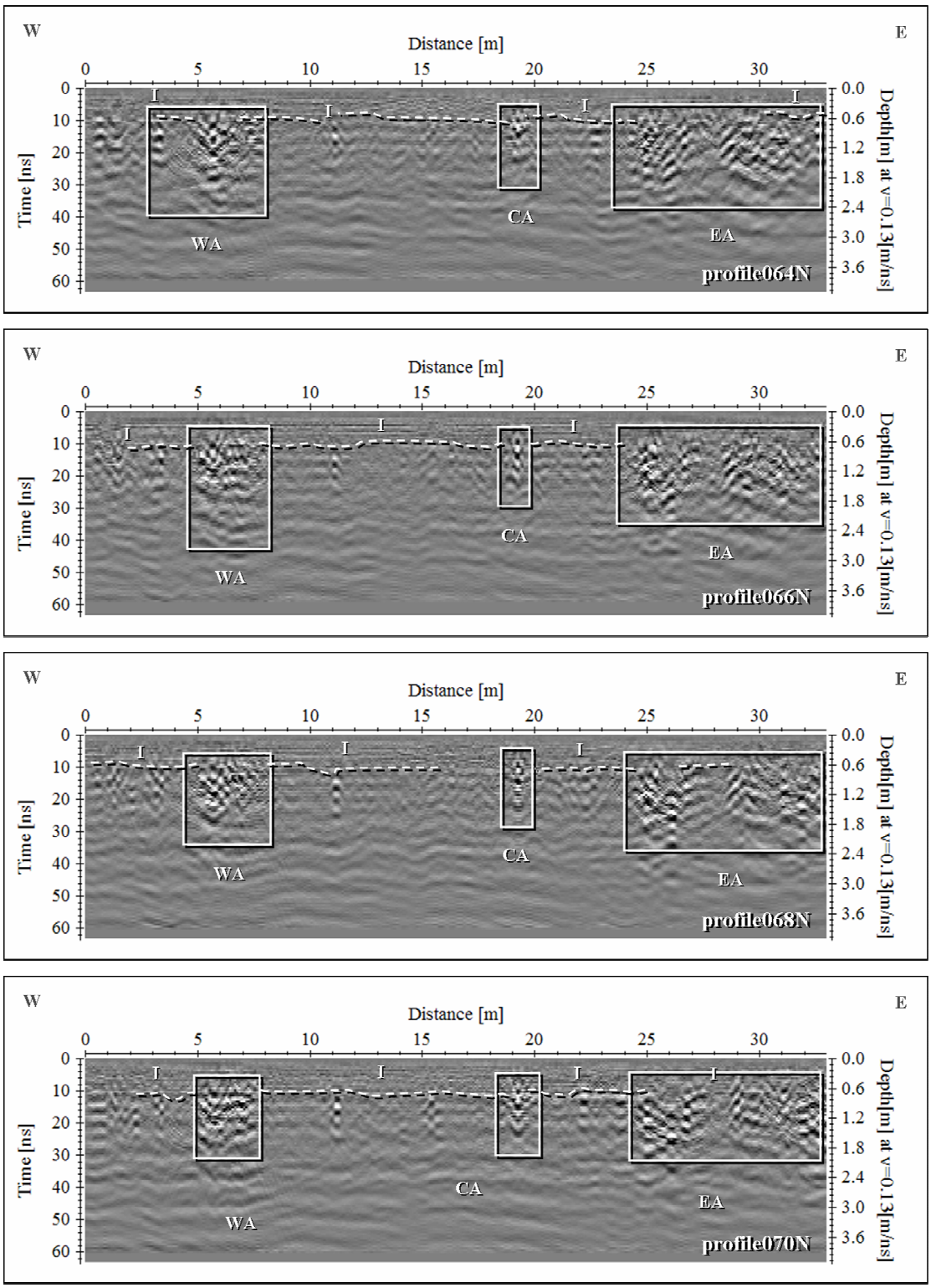

Figure A10 2D images of processed GPR data on profile 064N, 066N, 068N, and 070N.

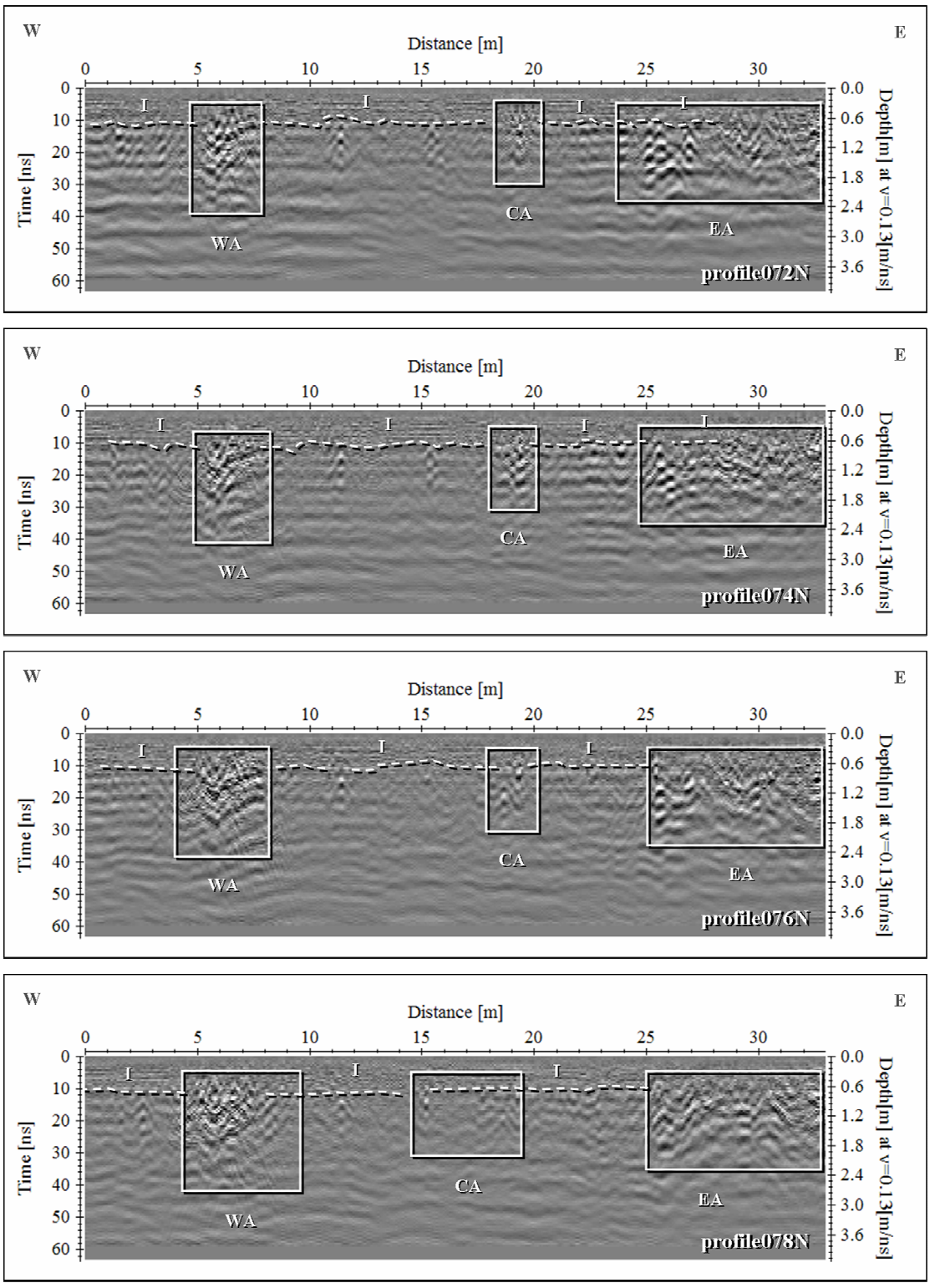

Figure A11 2D images of processed GPR data on profile 072N, 074N, 076N, and 078N.

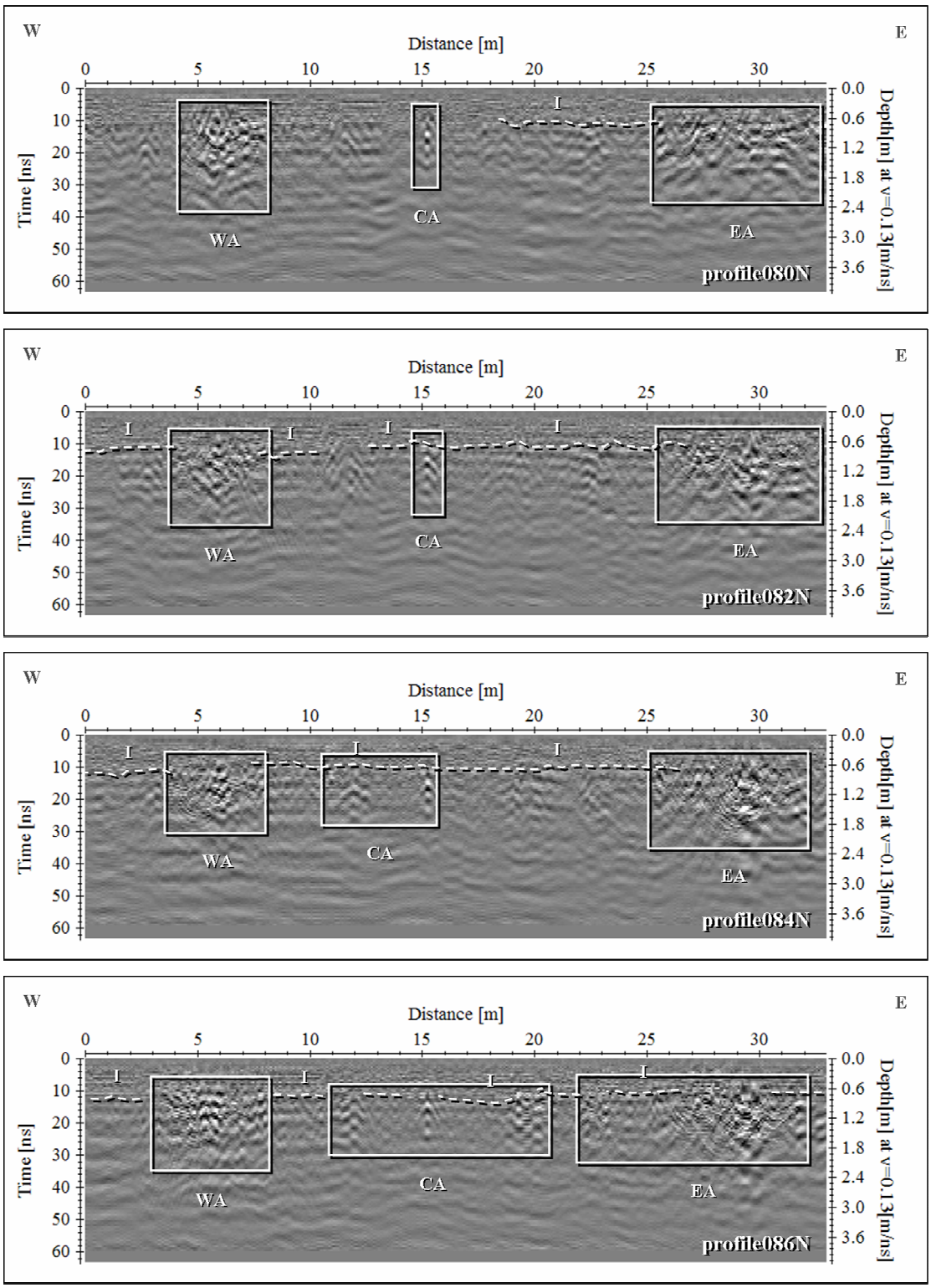

Figure A12 2D images of processed GPR data on profile 080N, 082N, 084N, and 086N.

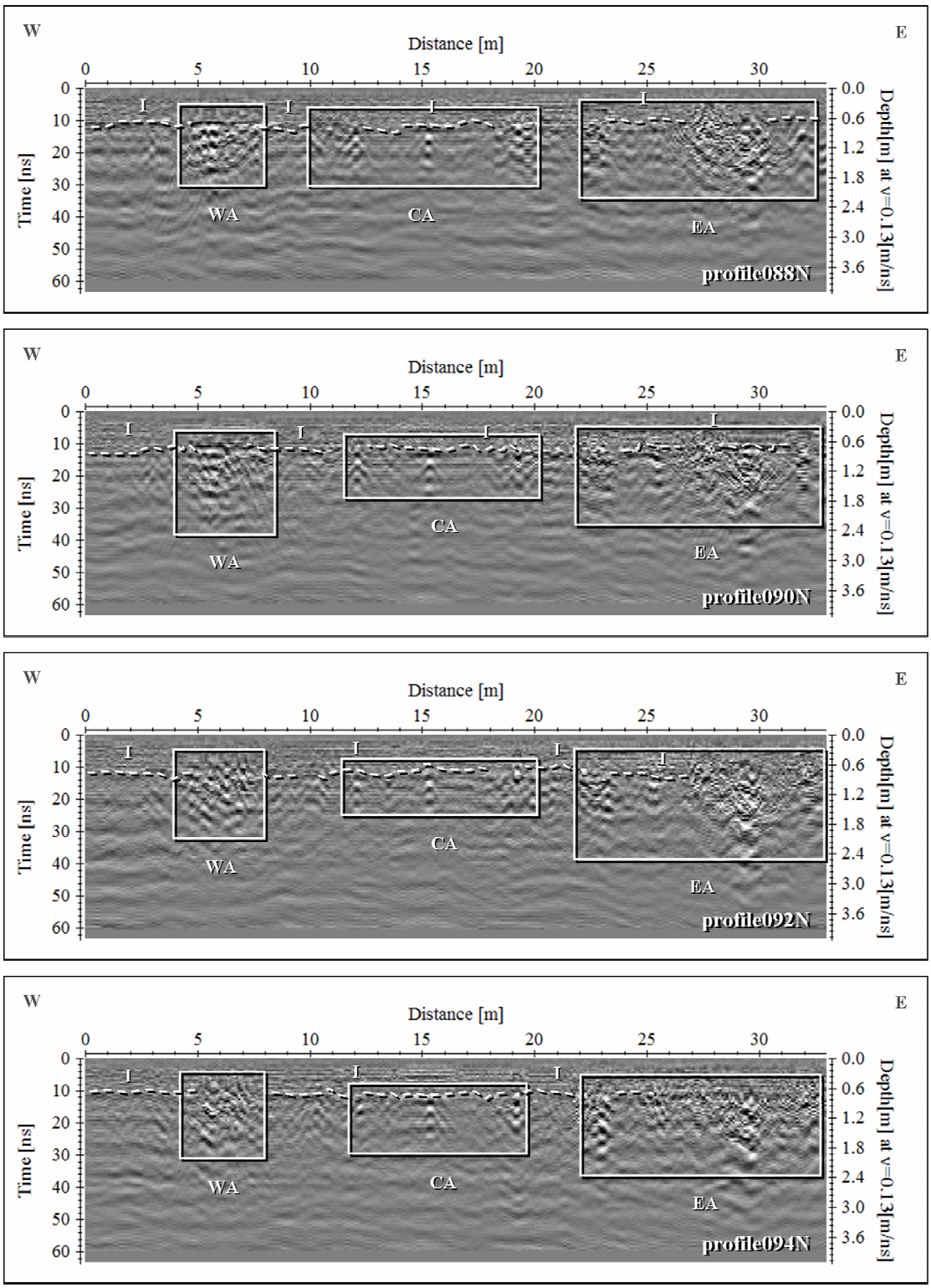

Figure A13 2D images of processed GPR data on profile 088N, 090N, 092N, and 094N.

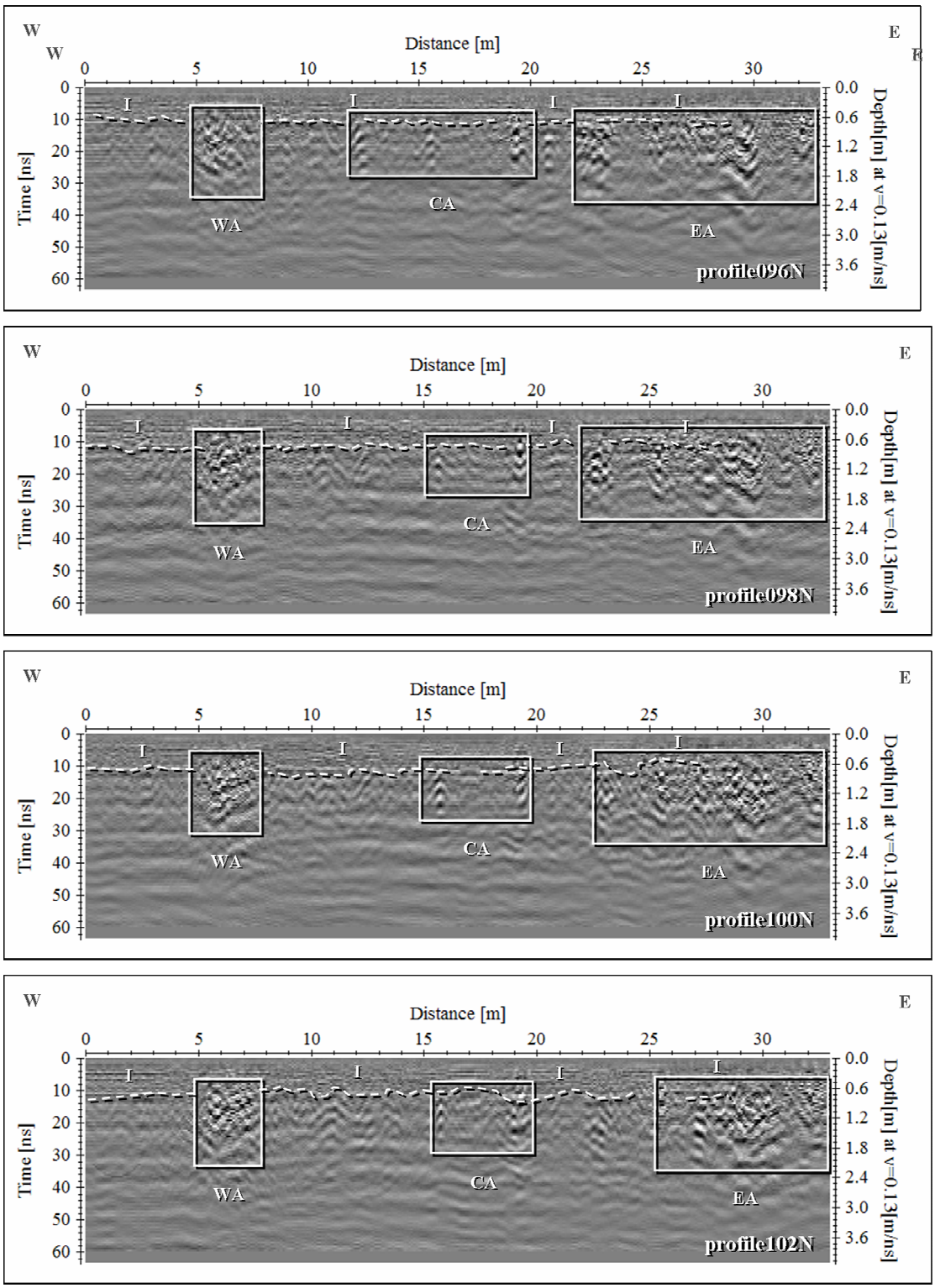

Figure A14 2D images of processed GPR data on profile 096N, 098N, 100N, and 102N.

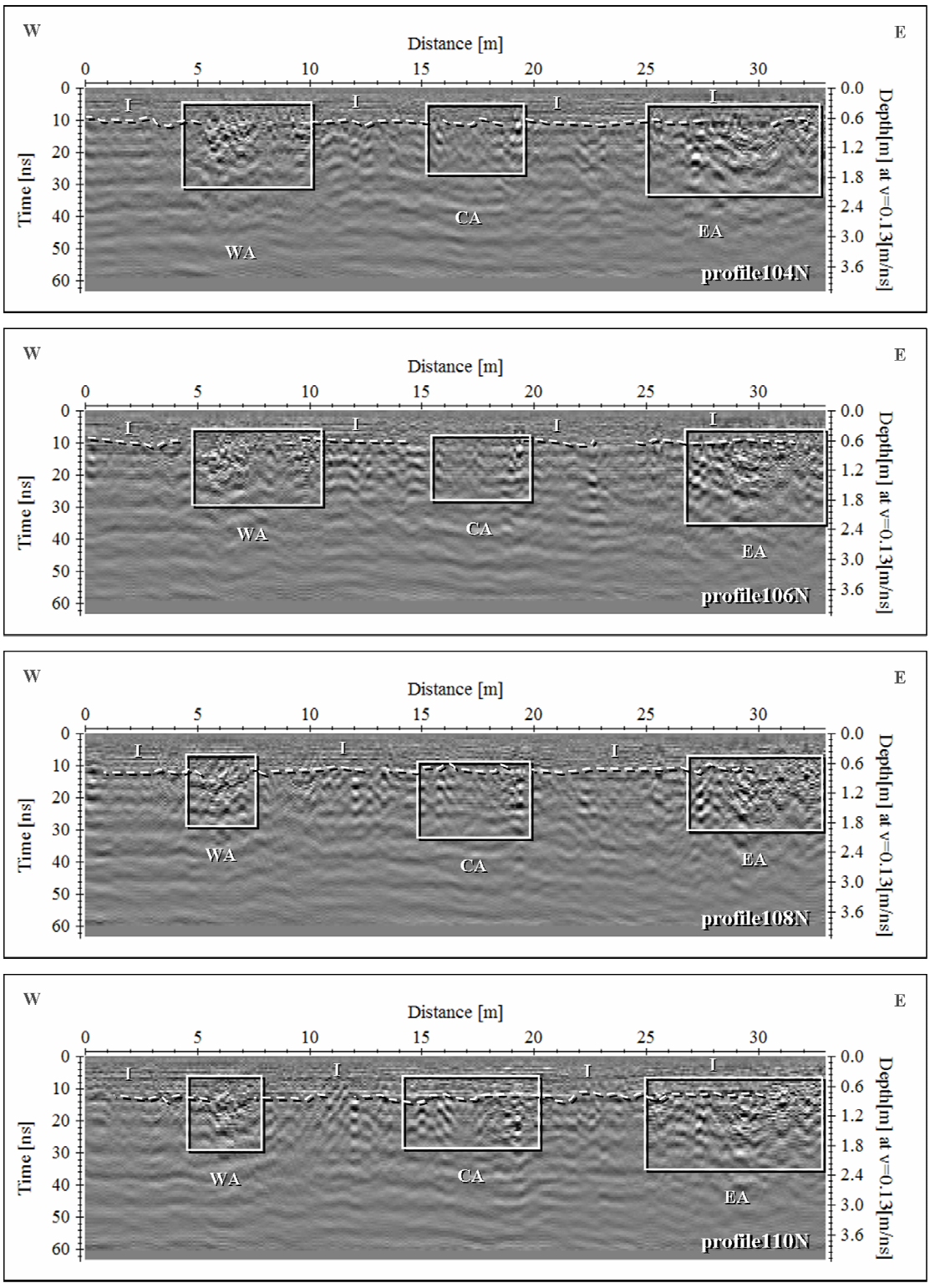

Figure A15 2D images of processed GPR data on profile 104N, 106N, 108N, and 110N.

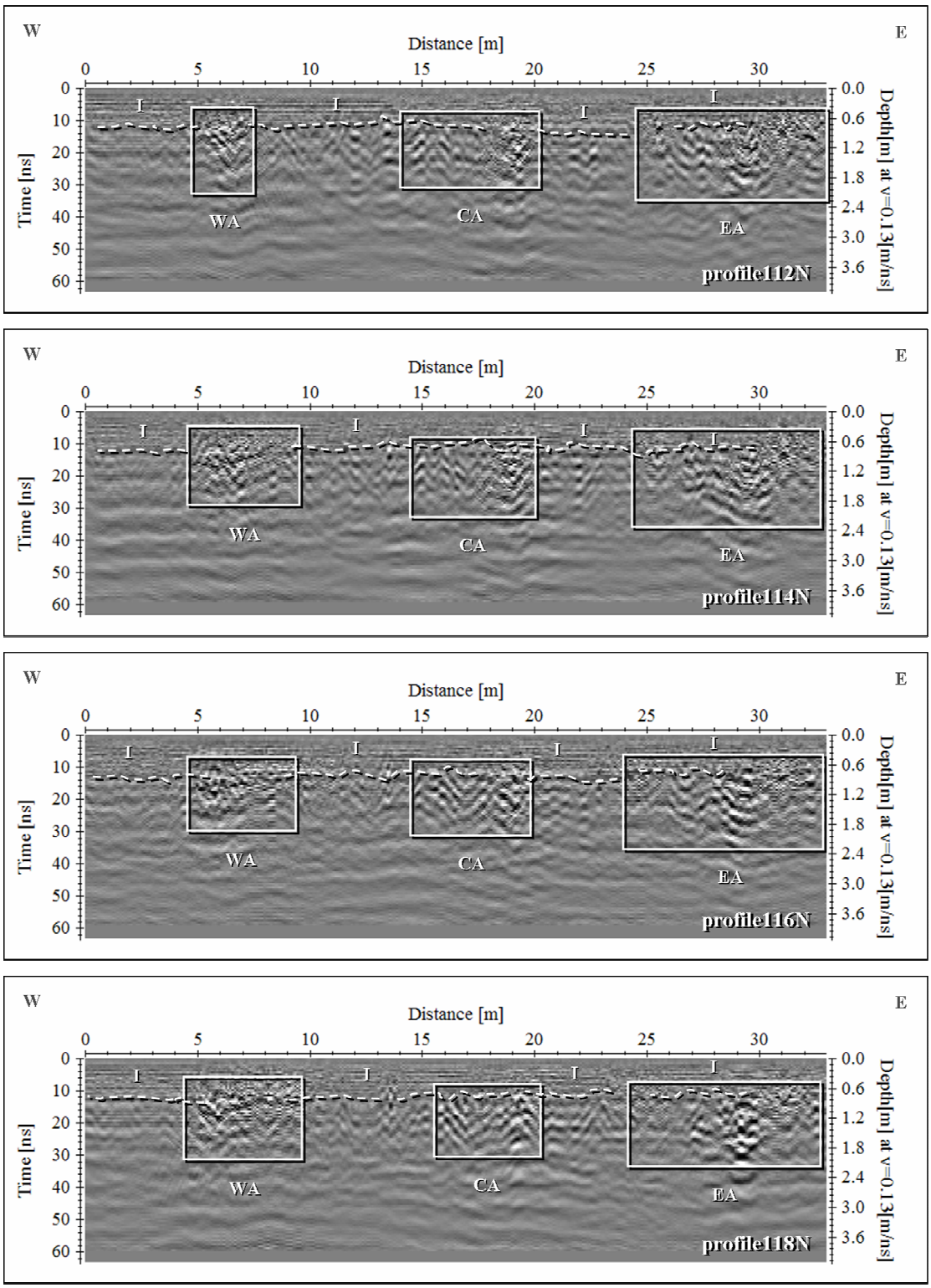

Figure A16 2D images of processed GPR data on profile 112N, 114N, 116N, and 118N.

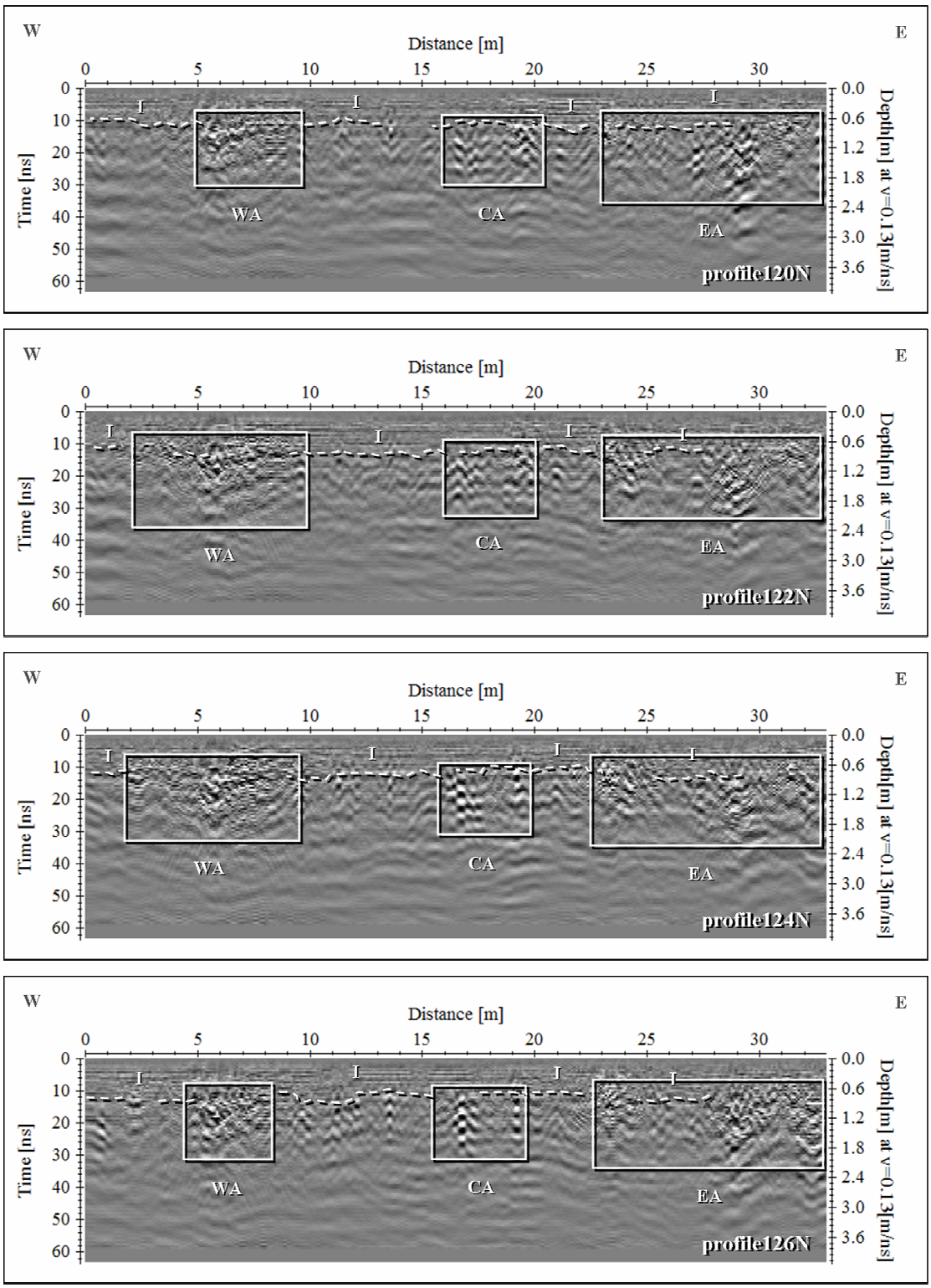

Figure A17 2D images of processed GPR data on profile 120N, 122N, 124N, and 126N.

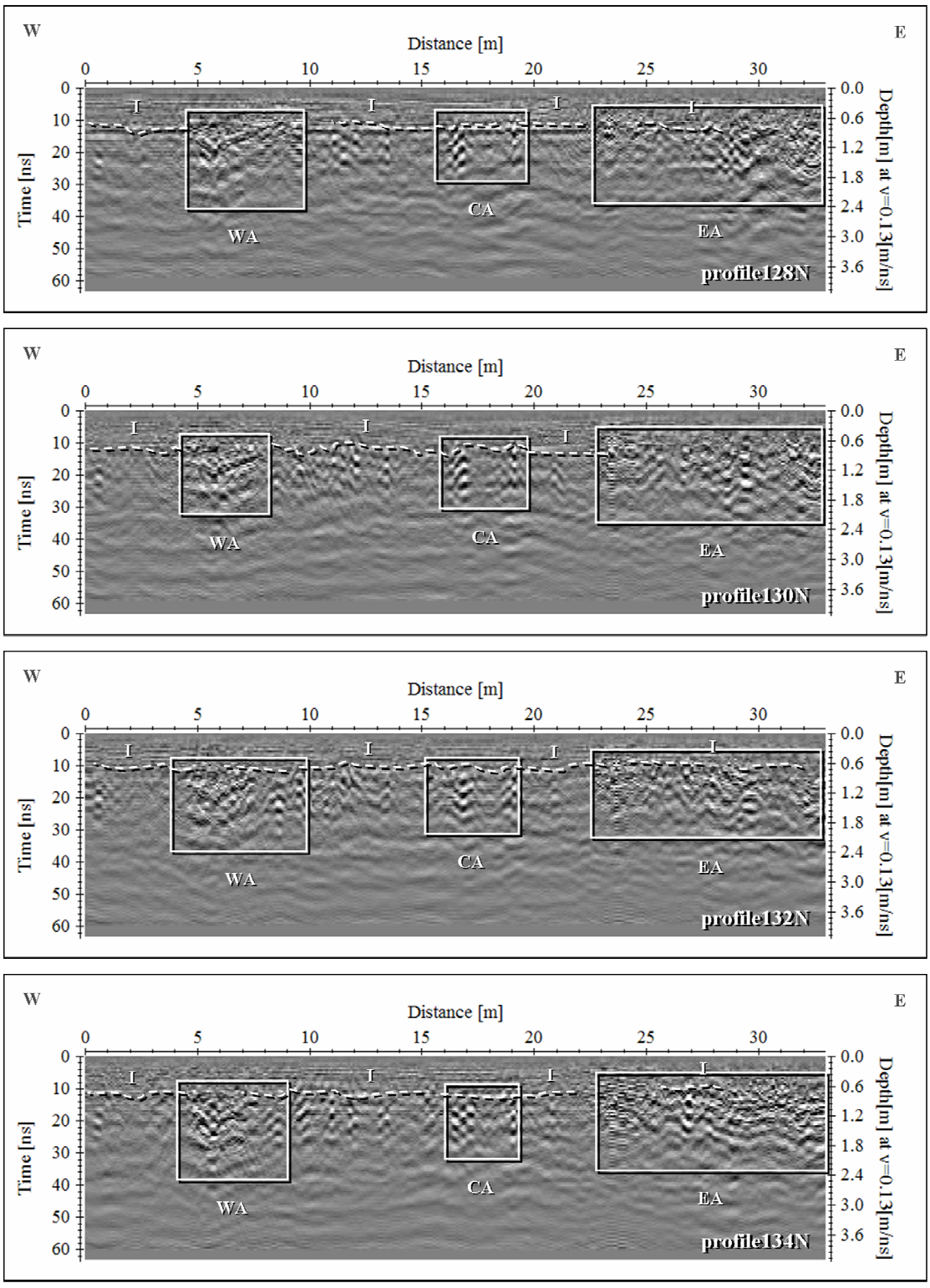

Figure A18 2D images of processed GPR data on profile 128N, 130N, 132N, and 134N.

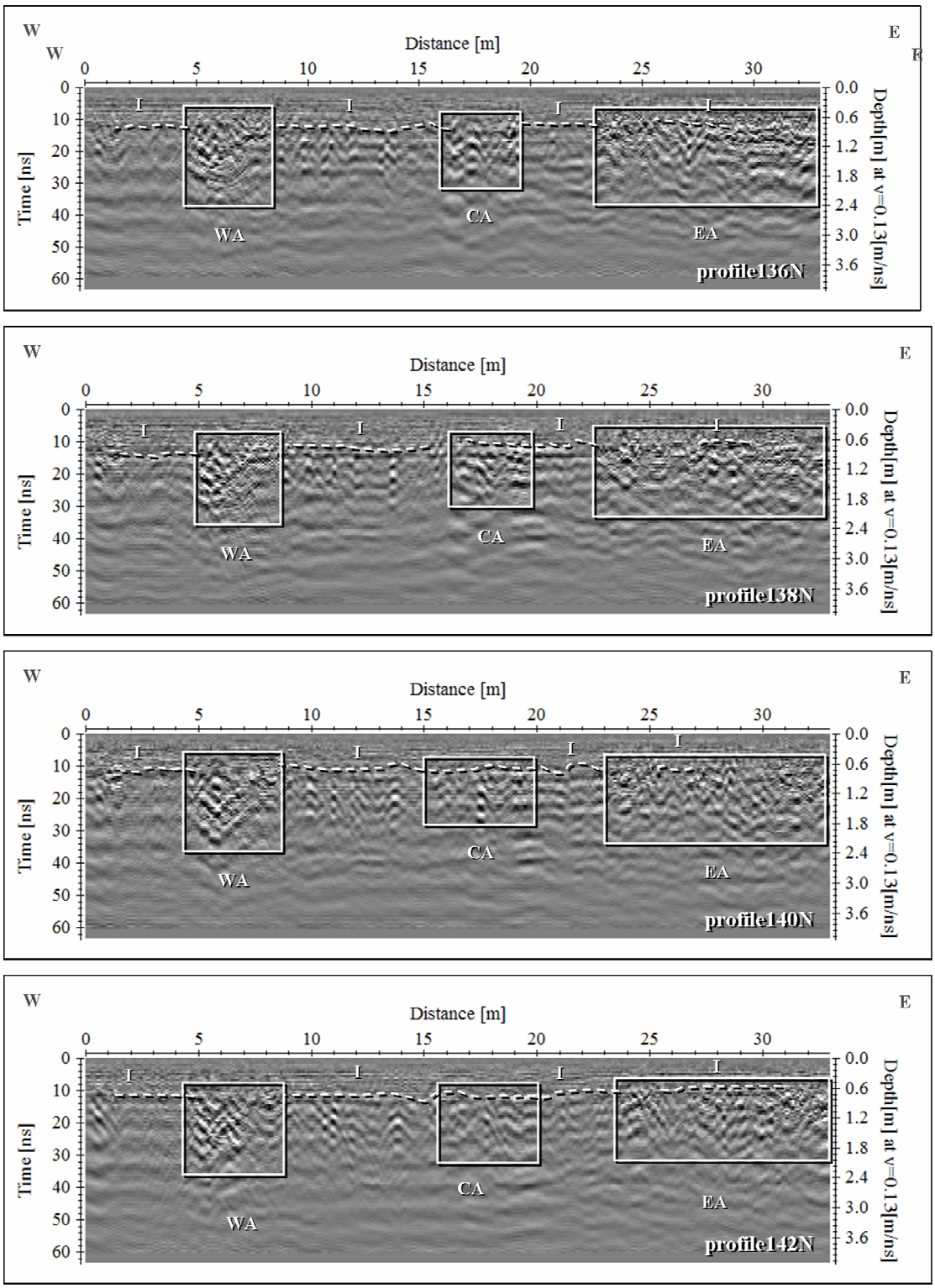

Figure A19 2D images of processed GPR data on profile 136N, 138N, 140N, and 142N.

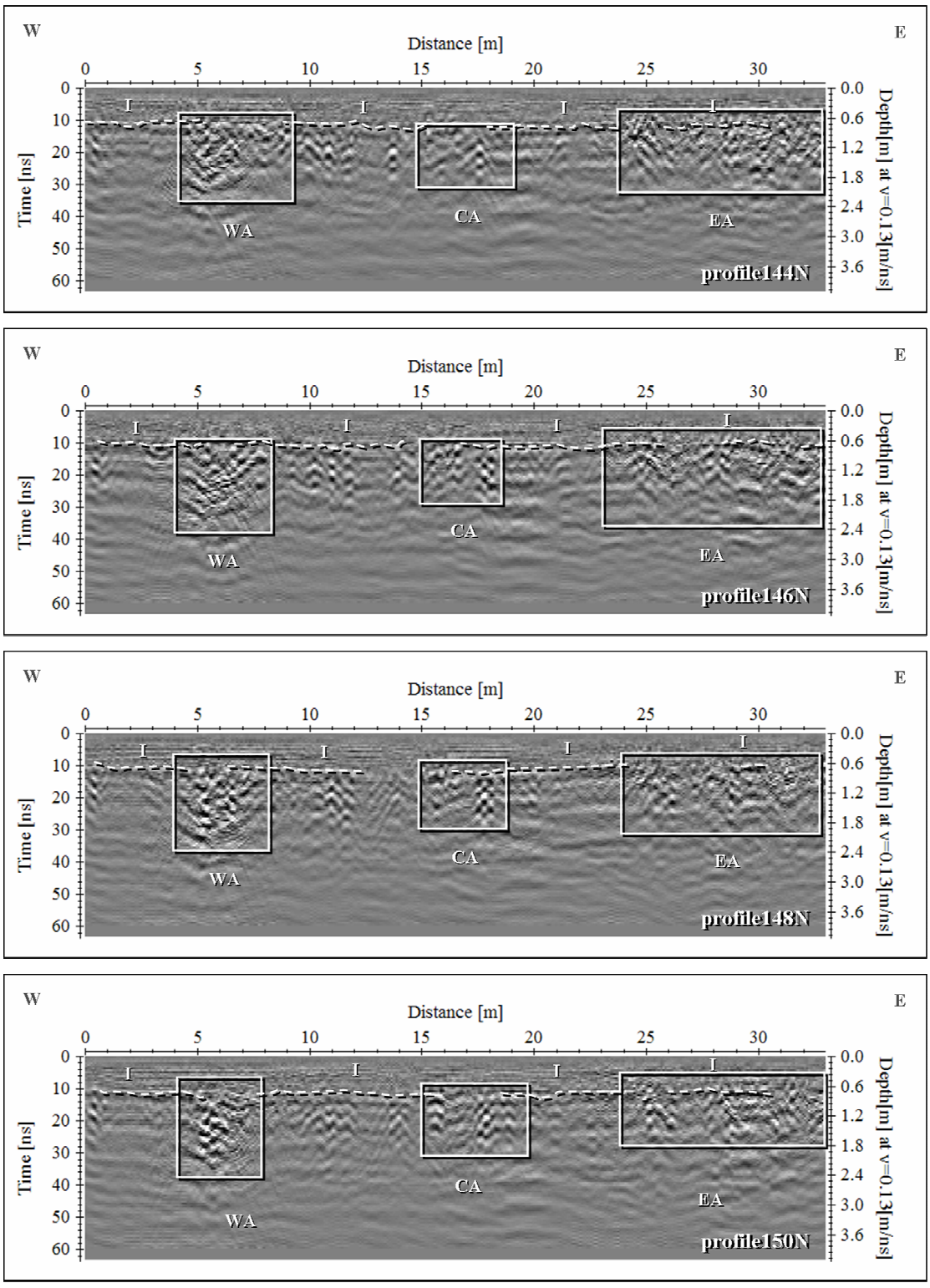

Figure A20 2D images of processed GPR data on profile 144N, 146N, 148N, and 150N.

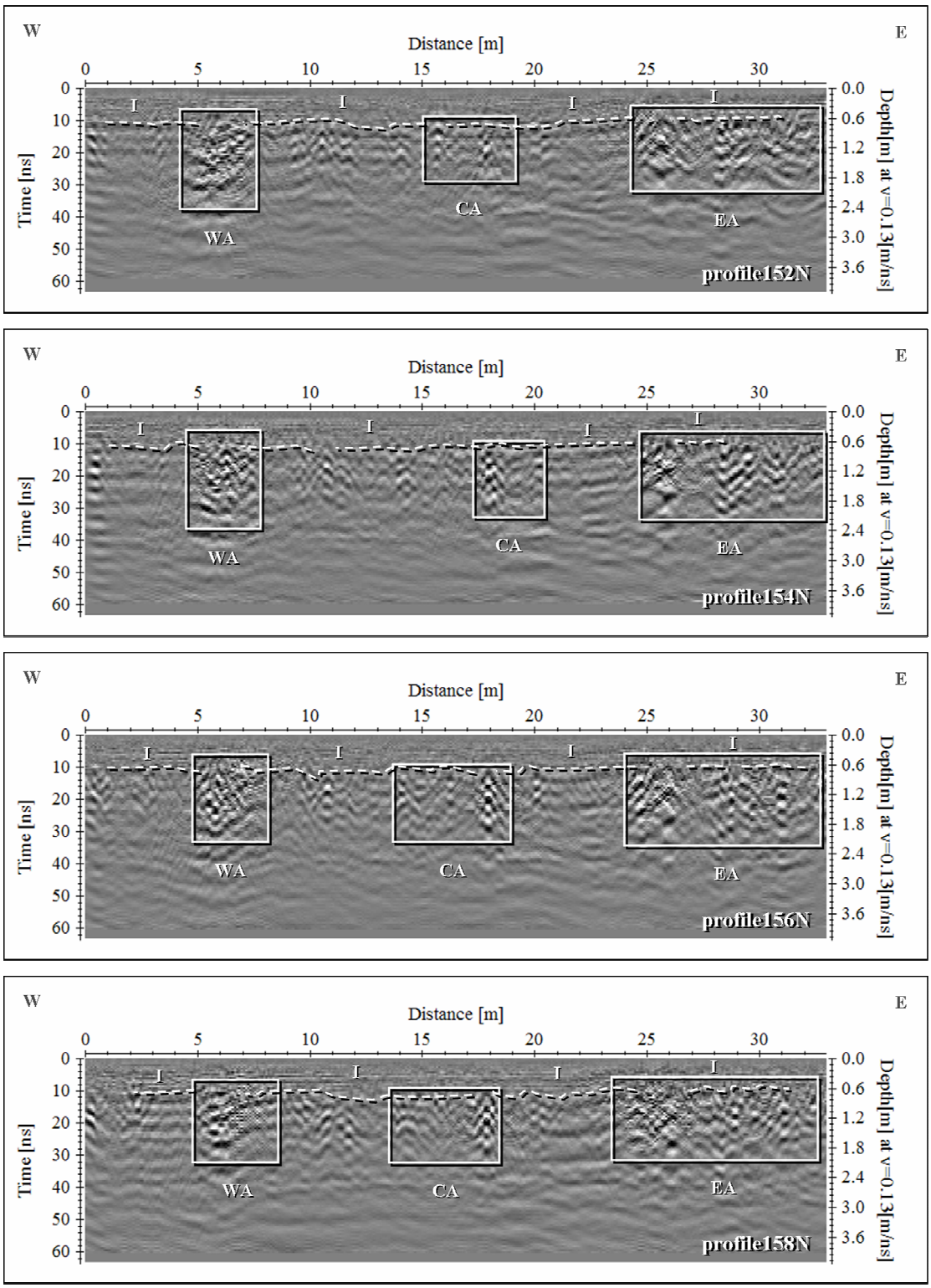

Figure A21 2D images of processed GPR data on profile 152N, 154N, 156N, and 158N.

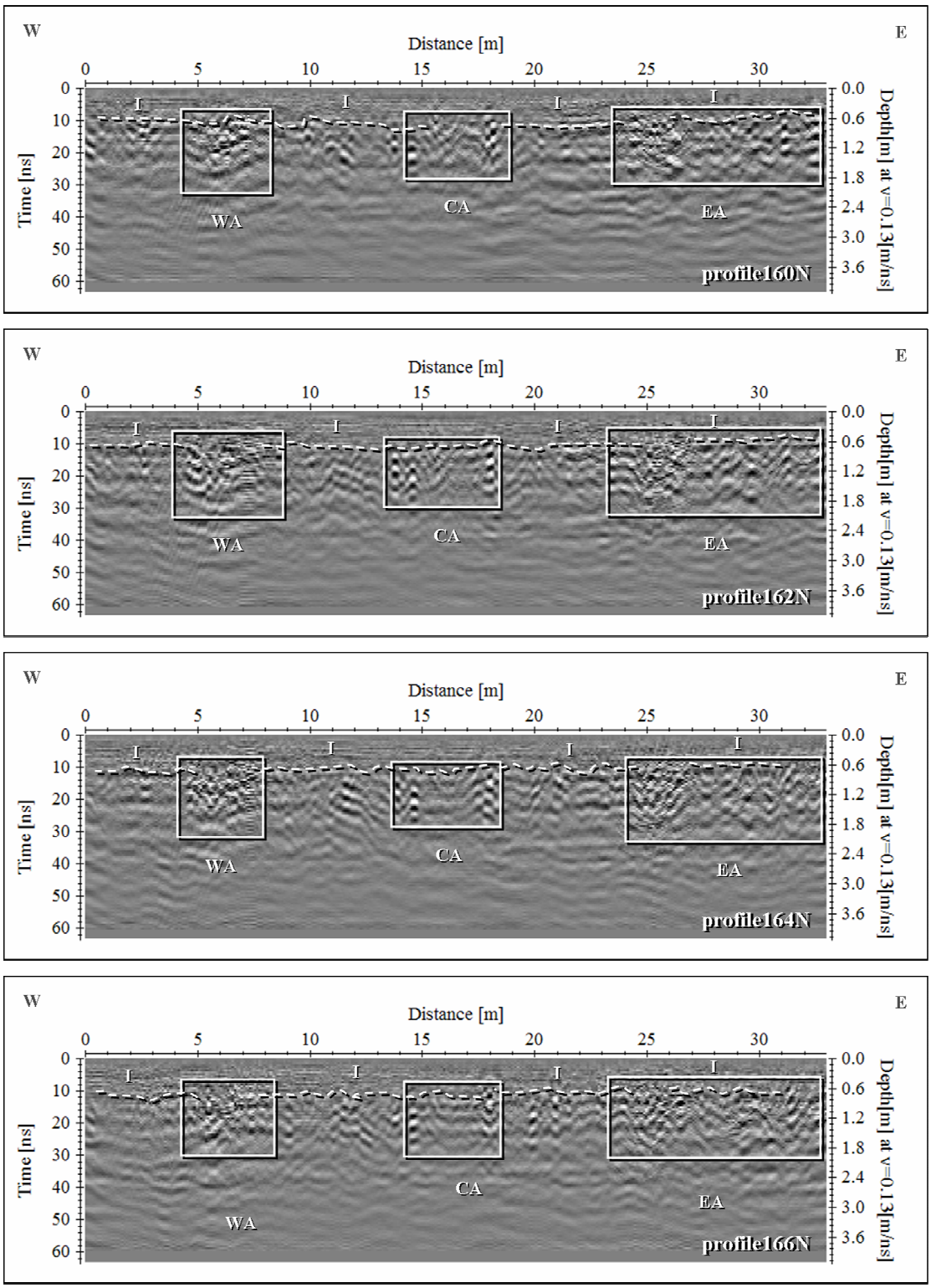

Figure A22 2D images of processed GPR data on profile 160N, 162N, 164N, and 166N.

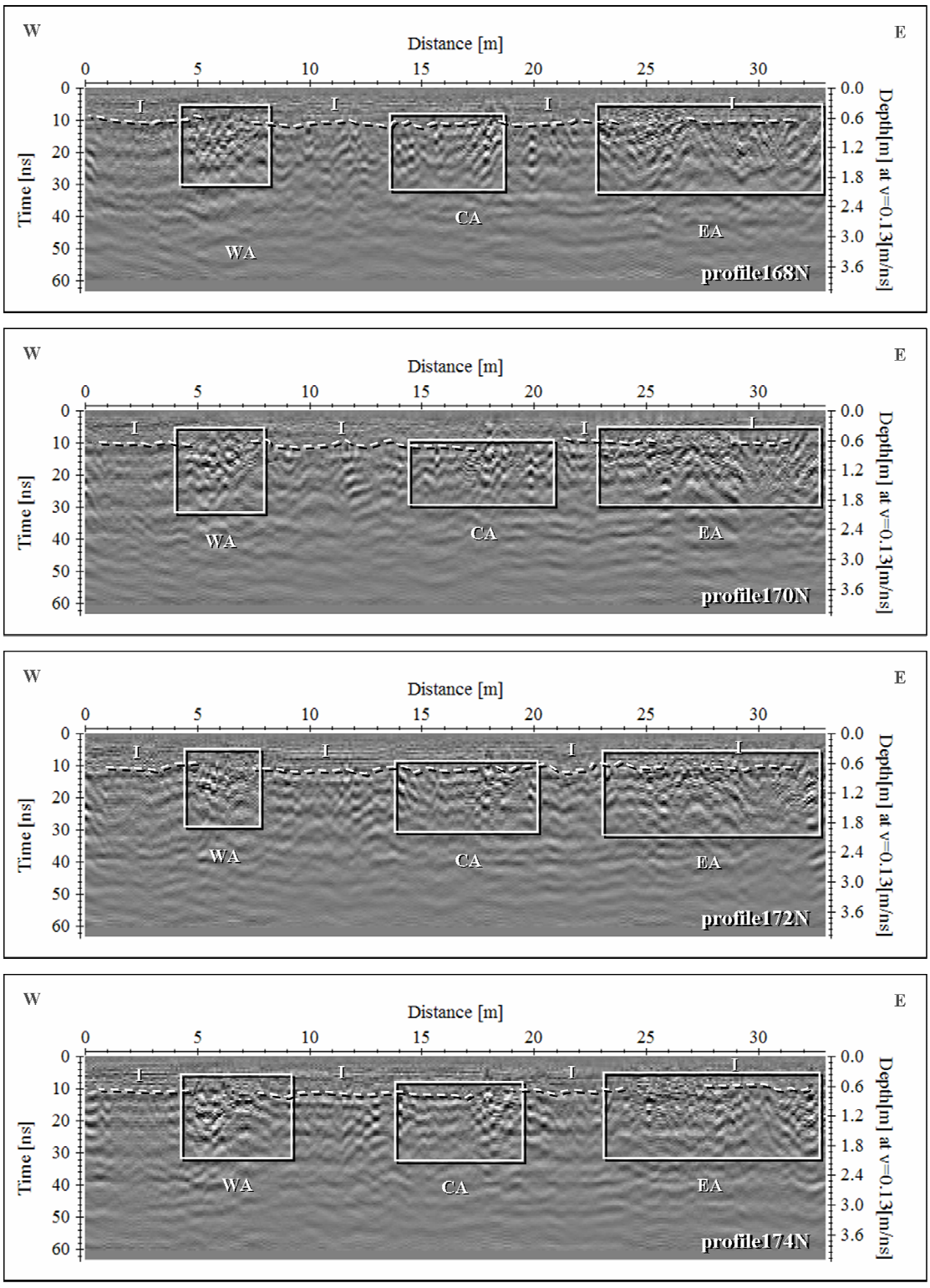

Figure A23 2D images of processed GPR data on profile 168N, 170N, 172N, and 174N.

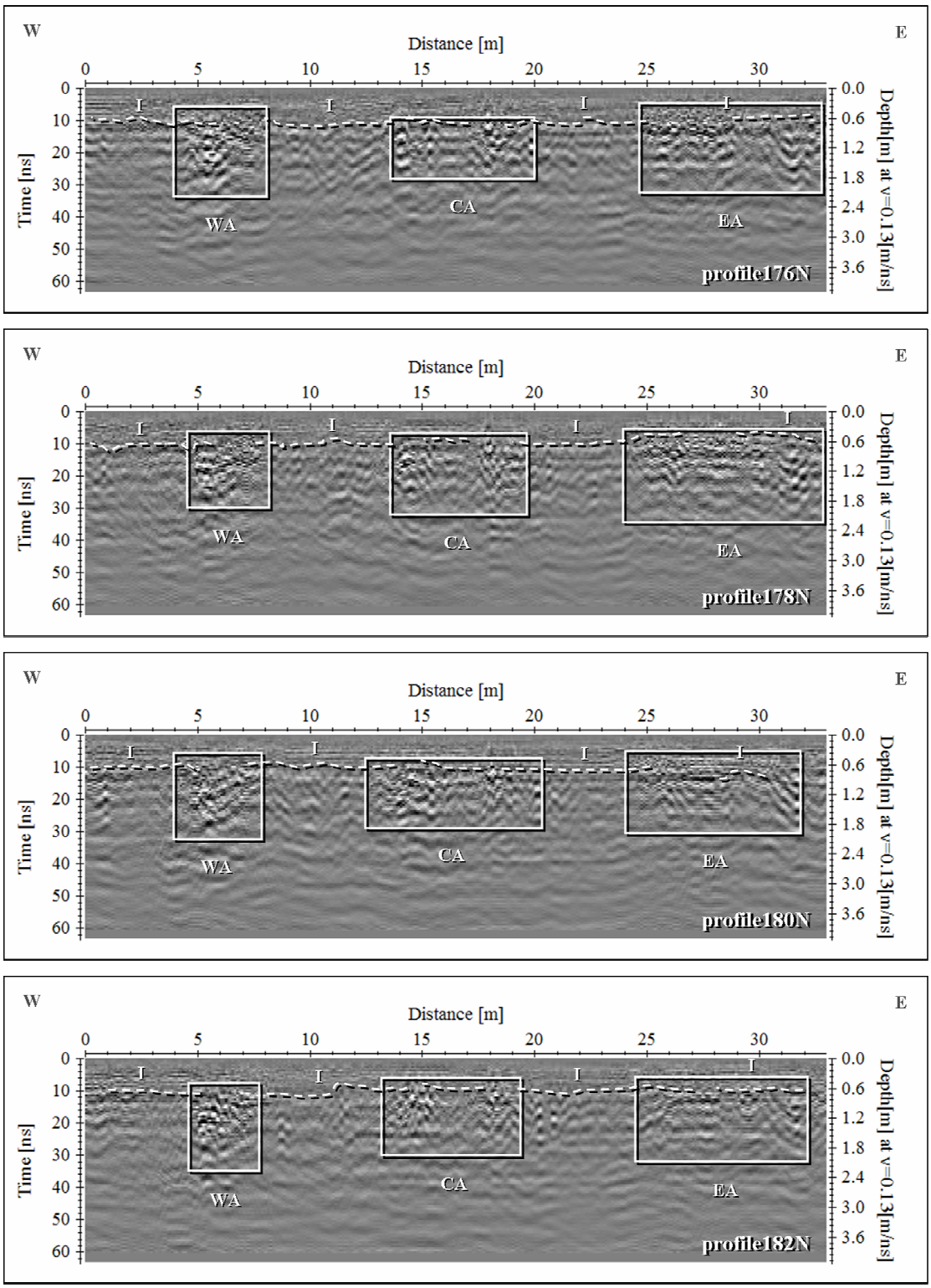

Figure A24 2D images of processed GPR data on profile 176N, 178N, 180N, and 182N.

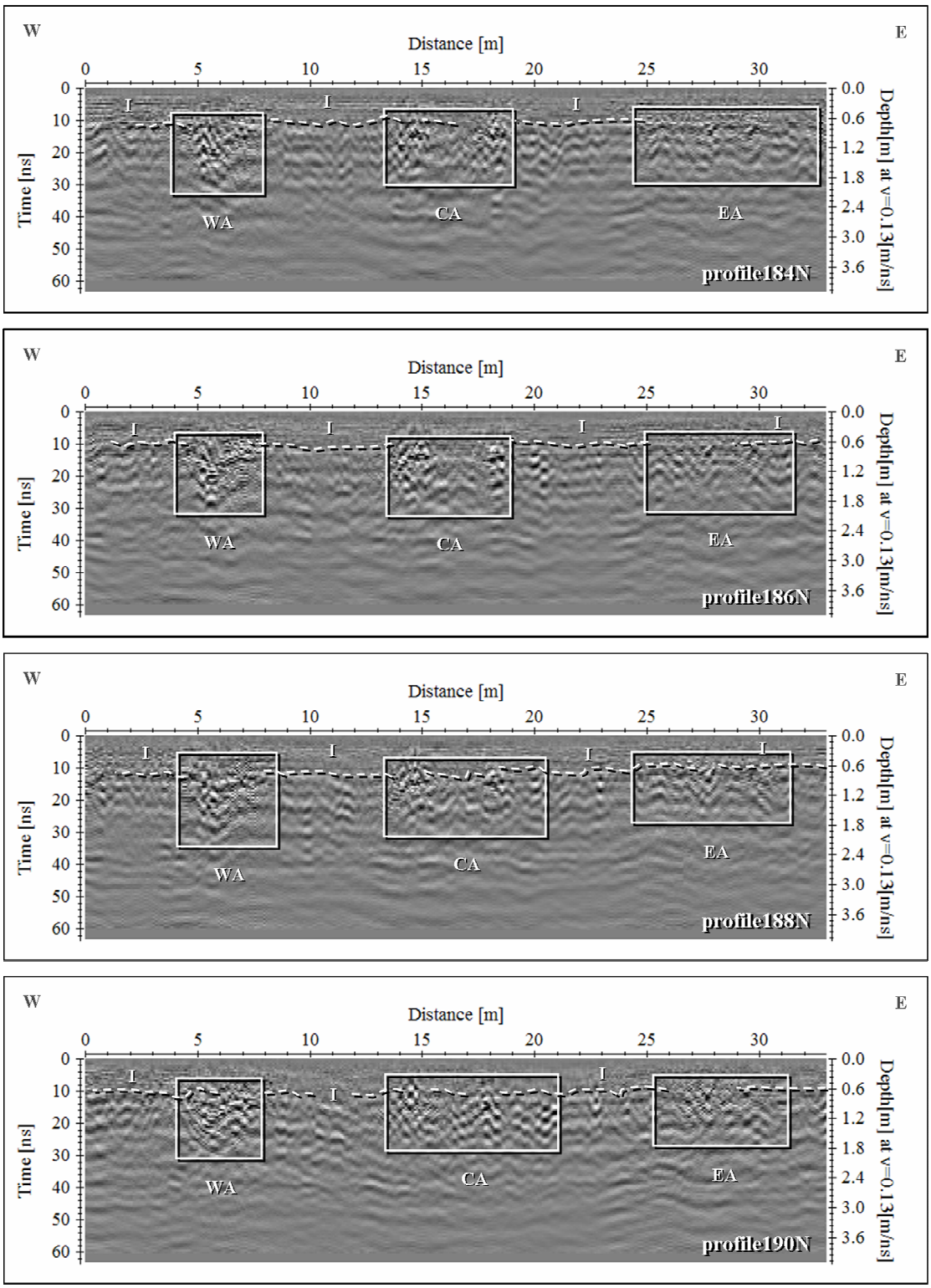

Figure A25 2D images of processed GPR data on profile 184N, 186N, 188N, and 190N.

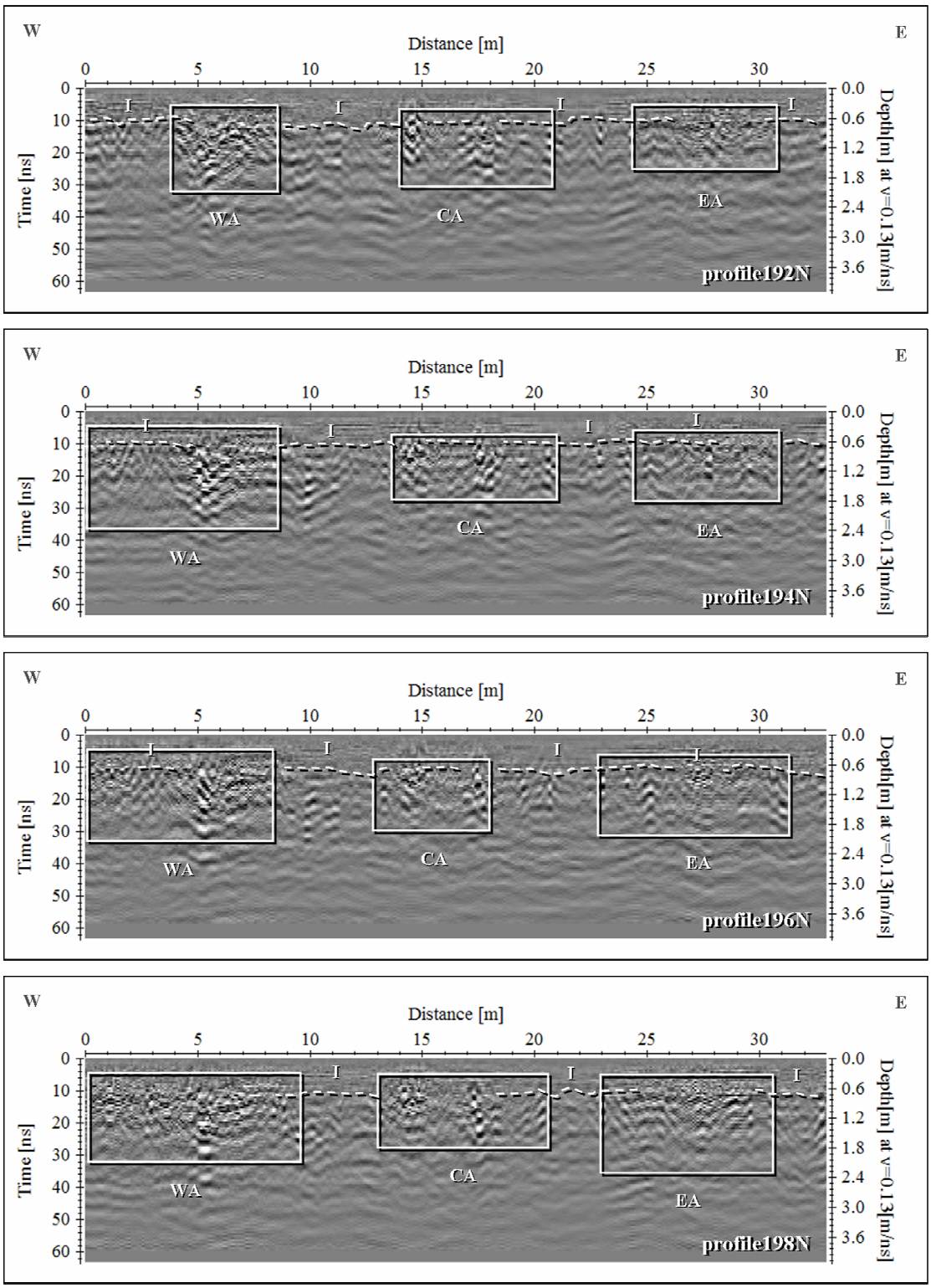

Figure A26 2D images of processed GPR data on profile 192N, 194N, 196N, and 198N.

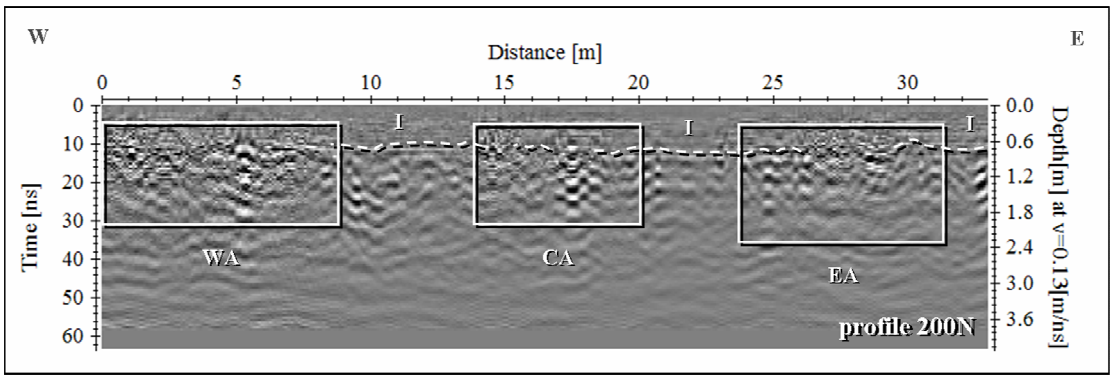

Figure A27 2D image of processed GPR data on profile 200N.

PUBLICATION

PROCEEDINGS
OF THE INTERNATIONAL CONFERENCE
ON
APPLIED GEOPHYSICS

Geophysics

NOVEMBER 12 – 13, 2008 CHIANG MAI, THAILAND

Editors

Mr. Sidney Rieb
Dr. Pisanu Wongpornchai
Dr. Siriporn Chaisri

Department of Mineral Fuels
MINISTRY OF ENERGY

ORGANIZED BY Chiang Mai University

IN COLLABORATION WITH Prince of Songkla University
Department of Mineral Resourceses
Department of Mineral Fuels

Fourth International Conference on Applied Geophysics 29
12 – 13 November 2008, Chiang Mai, Thailand

Application of Three-Dimensional Ground Penetrating Radar Imaging in Locating Wat Mo Khlan Archaeological Site in Nakhon Si Thammarat, Thailand

A. Chansane, W. Lohawijarn and B. Phongdara
Geophysics Laboratory, Department of Physics, Faculty of Science, Prince of Songkla University, Songkhla, 90112, Thailand

ABSTRACT

Three-dimensional ground penetrating radar imaging was used to map buried archaeological structures at the Wat Mo Klan archaeological site in Nakhon Si Thammarat Province. This ground penetrating radar survey used a 200-megaheartz central frequency antenna along 101 parallel lines in a 20-meter x 33-meter area. Time–slice maps and iso–amplitude surface maps revealed buried ancient walls, archaeological structural remains, and the interface between present and ancient surface soils. The presence of these features was confirmed by archaeological test pits.

KEYWORDS: Ground penetrating radar, archaeological application, three-dimensional image, time–slice map, iso–amplitude surface map

INTRODUCTION

Ground penetrating radar utilizes propagation and scattering of electromagnetic waves to image, locate, and quantitatively identify changes in electrical and magnetic properties in the ground. A pulse of radar energy is generated on a transmitting antenna dipole placed on the ground surface. This radar energy pulse propagates downward into the ground where a portion of it is reflected back to the surface at discontinuities created by changes in electrical properties of sediment or soil, variations in water content, lithologic changes, or changes in bulk density at stratigraphic interfaces. Reflection can also occur at the interface between anomalous archaeological features, buried pipes, and the surrounding soil or sediment. The greater the contrast in electrical properties between the two materials, the stronger the reflected signal.

The use of ground penetrating radar for archaeological investigations is increasing due to its non–destructive nature, fast operating time, and its high resolution images which allow buried features of relatively small size to be discovered. Another advantage is the possibility of processing data in the field so that the anomalies can be quickly identified. The ground penetrating radar method has been successfully used in archaeological prospecting for mapping shallow subsurface objects (Garcia and others, 2000; Hruska and Fuchs, 1999; Lohawijarn, 2005; Pattanaviriyapisan, 1999; Ranalli and others, 2004; and Sambuelli and others, 1999).

The goal of most ground penetrating radar surveys is to identify size, shape, depth, and location of buried remains and related stratigraphy. The straightforward way to accomplish this is by identifying and correlating important reflections within two-dimensional images where hyperbolic patterns reveal the presence of scattered buried objects. In standard two-dimensional profiles, the specific amplitudes within individual traces that contain important reflective information are usually difficult to visualize and interpret and may be sufficient only in case of simple buried features. Also, the interdependence between aligned views, not having been taken, increases the limitation of interpretation. To overcome this limitation, three-dimensional ground penetrating radar images have been recently applied on the data set of two-dimensional parallel profiles. The three-dimensional location of reflective anomalies can be derived from a computer analysis of all available two-dimensional profiles by correlating the reflections from profile to profile throughout a grid.

Three-dimensional visualization benefits the important information for archaeological applications by displaying complex data in an easily understandable fashion, thus improving the quality and efficiency of the archaeological interpretation. One of the sophisticated types of ground penetrating radar data manipulation is time–slice map analysis that creates maps of reflected wave amplitude differences within a grid. The arrangement of these amplitude slices in horizontal layers, representing real depths, is in a visual format familiar to archaeologists. These are analogous to excavation levels. Another way of three-dimensional image visualization is three-dimensional iso–amplitude surface maps where the reflection amplitude of ground penetrating radar data is defined in a three-dimensional cube representing the subsurface below the surveyed area. With this three-dimensional visualization technique, various threshold values of the reflection amplitude can be assigned in order to show the reflective subsurface object in a three-dimensional location. This makes understanding and interpretation easy.

Currently, three-dimensional ground penetrating radar imaging has been successfully employed in locating and detailed mapping in archaeological investigations (Arlsan and others, 1999; Leucci and Negri, 2006; Negri and Leucci, 2006; Shaaban and Shaaban, 2001; and Whiting and others, 2001). The same technique can be applied in shallow and small subsurface applications (Acqua and others, 2004) and for geological purposes (Beres and others, 1999; Grasmueck and others, 2005; Heincke and others, 2005; Sigurdsson and Overgaard, 1998; and Zeng and others, 2004).

In this work the ground penetrating radar survey was carried out at the Wat Mo Khlan archaeological site in Nakhon Si Thammarat, Thailand. The study aimed to apply ground penetrating radar measurements and display these as three-dimensional images by using three-dimensional ground penetrating radar imaging techniques. Doing this involved the use of time–slice, or depth–slice, maps and iso–amplitude surface maps to locate archaeological remains and structures in the subsurface. The findings of this study will be very helpful for archaeologists in later archaeological excavation.

SITE DESCRIPTION

The study area is located in the Wat Mo Khlan archaeological site, Tha Sala district, Nakhon Si Thammarat province, Thailand, at north latitude 8° 34' 46.8" and east longitude 99° 55' 48.8" (Figure 1).

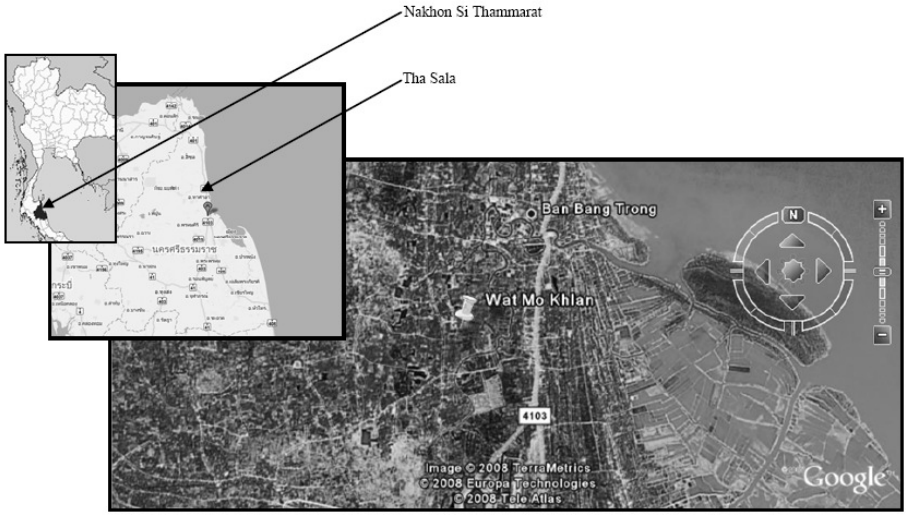

Figure 1. Wat Mo Khlan archaeological site in Tha Sala District, Nakhon Si Thammarat Province

The Wat Mo Khlan archeological site was registered as a national archaeological site in 1975. This site is one of the archaeological sites that are very important to the history and archaeology of Nakhon Si Thammarat province, where prehistoric humans settled about 6,500 years ago. There is much archaeological evidence of this settlement in this region.

The Wat Mo Khlan archaeological site was explored in 1992 and 1993 in order to do restoration (Figure 2). At that time, fractions of limestone and sandstone sculptural art, such as door frames, rectangular rocks, and pedestal pillars, were found. Other archaeological evidence found included metal earrings, obsolete coins, ancient pottery, ancient bricks, broken Siva–lingas, and broken Siva–linga pedestals. With this information and collateral evidence, archaeologists believed that there should be other ancient remains, such as walls and building structures, buried southwest of the excavated and restored Wat Mo Khlan archaeological site (Figure 2). Because this southwesterly area was quite extensive, archaeological excavation within it could be quite time consuming and expensive. Therefore, use of geophysical techniques could reduce the time and expense of locating archeological remains. A case study of this was in the abandoned Tumpung temple (Lohawijarn, 2005).

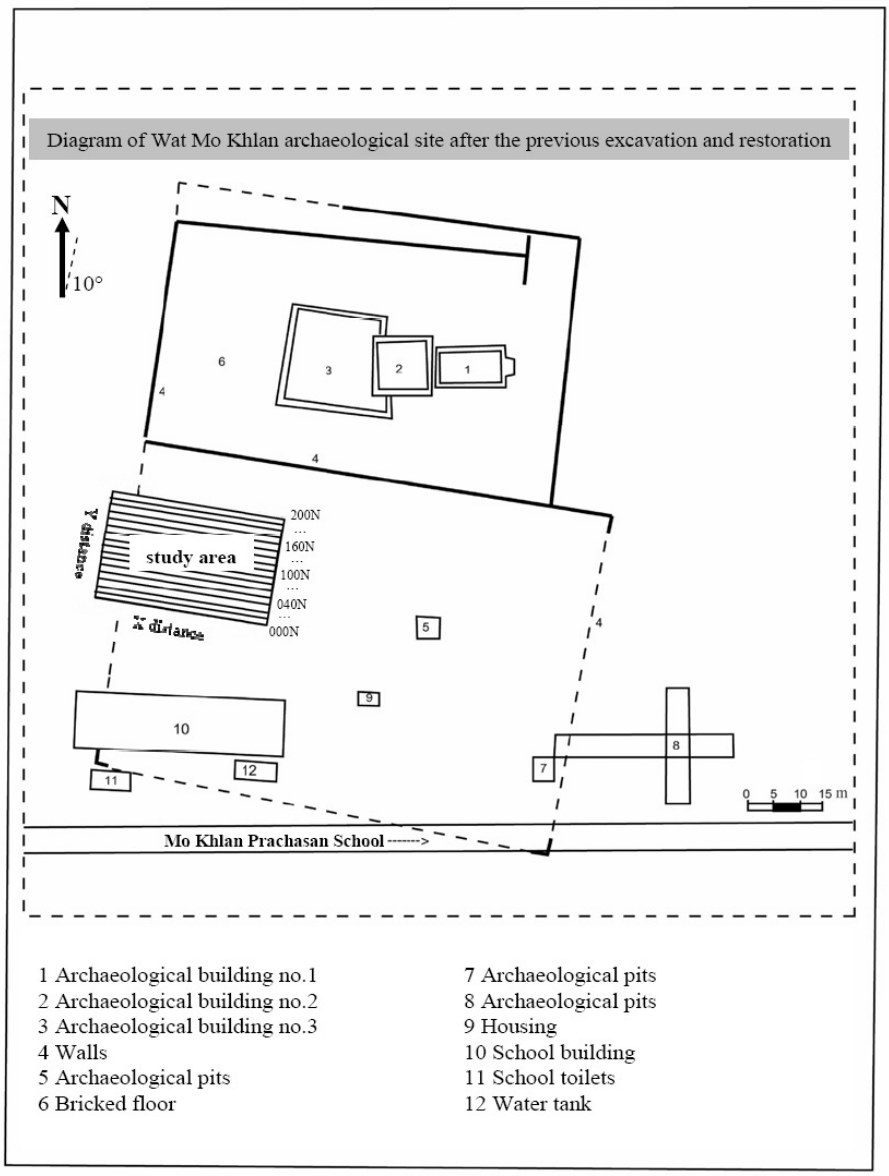

Figure 2. Location of ground penetrating radar profiles in the Wat Mo Khlan archeological site

The most common geophysical methods are electrical, magnetic, electromagnetic, and ground penetrating radar. The use of ground penetrating radar in archaeological investigations is increasingly used due to its non–destructive nature, fast operating time, and high resolution images that permit

buried features of relatively small size to be quickly recognized. The locations, alignments, and depths of burial obtained from ground penetrating radar measurements can be very useful for planning archaeological excavations.

FIELD INSTRUMENTATION AND DATA ACQUISITION

The RAMAC ground penetrating radar system, with a 200-megaheartz center frequency antenna, was used in this study. Ground penetrating radar measurements were made along 101 parallel lines trending N 80° W within a 20-meter x 33-meter area (Figure 2). Acquisition measurement parameters used were: 0.6-meter common antennae offset; 0.2-meter line spacing; 0.1-meter trace spacing; sampling frequencies of 1654.381779 megaheartz and 3124.943360 megaheartz; 256 samples per scan; and recording time window of 154.74 nanosecond.

DATA ANALYSIS

Processing steps applied to the ground penetrating radar data so that anomalies could be observed clearly on recorded sections were:

1. Resampling: Since three-dimensional imaging requires equal time increments, ground penetrating radar data of different profiles with different sampling time intervals were re-sampled to the same time increment (Sandmeier and others, 2007).

2. Trace editing: Shifts in recorded traces are probably caused by an unstable condition of field equipment and resulted in sawtooth ground penetrating radar time sections, as shown in Figure 3a. Trace editing is then necessary to shift all traces to the same starting time, as shown in Figure 3b.

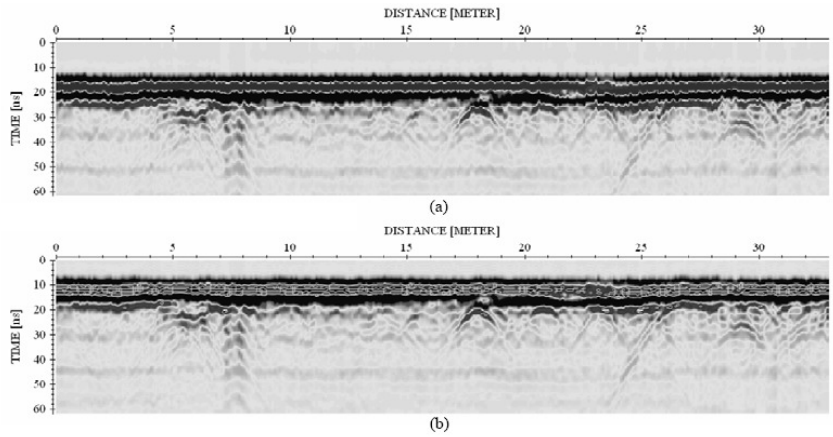

Figure 3. Ground penetrating radar section of profile 168N, (a) before and (b) after trace shift processing

3. Dewow: A dewow filter eliminates a possible low frequency part of the recording signal.

4. Set time zero: In this processing step, the first arrival time of the radar pulse at receiver is set to time zero.

5. Background removal: This processing step eliminates temporally consistent noise from the whole profile and possibly makes signals previously covered by noise visible.

6. Gain filter: This manual filter enhances the amplitude of signals.

7. Notch filter: This filter suppresses nearly mono–frequency noise, which in this study was 100 and 200 megaheartz signals.

8. Kirchhoff two-dimensional velocity migration: Velocity migration was done to trace back the reflection and diffraction energy to their source positions. In case of diffractions, migration contracts diffractions to their apexes.

RADAR WAVE PROPAGATION VELOCITY

Velocity is necessary for converting ground penetrating radar time sections to ground penetrating radar depth sections. In this study the velocity of radar propagation in the medium was obtained from the diffraction hyperbola analysis method. This method is supported by common radar software packages but should be applied if the diffraction hyperbola occurs at least at 20 radar scans (Luecci and Negri, 2006).

Hyperbolic reflections on a ground penetrating radar section and their velocity analysis are shown in Figure 5. The average velocity of radar pulse obtained from the study is about 0.13 meter/nanosecond.

DATA INTERPRETATION

A two-dimensional image of a selected profile, 100N, is shown in Figure 6. Most distinctive anomalies are clearly observed at 6 to 30 nanosecond two–way time, this being about 0.39 to 1.95 meters in depth. Similar anomalies appear in many of the profiles. According to shape and alignment, the anomalies labeled W were interpreted as archaeological structures, such as walls and other building structures. Moreover, a linear anomaly labeled L at 10 nanosecond to 14 nanosecond two–way time, about 0.65 to 0.91 meter, was interpreted as the interface between the present surface soil and an ancient surface soil.

THREE-DIMENSIONAL VISUALIZATION

Three-dimensional visualization of ground penetrating radar images was attempted in order to map continuation of anomalies observed in the study area. Two methods were employed, time–slice maps and iso–amplitude maps.

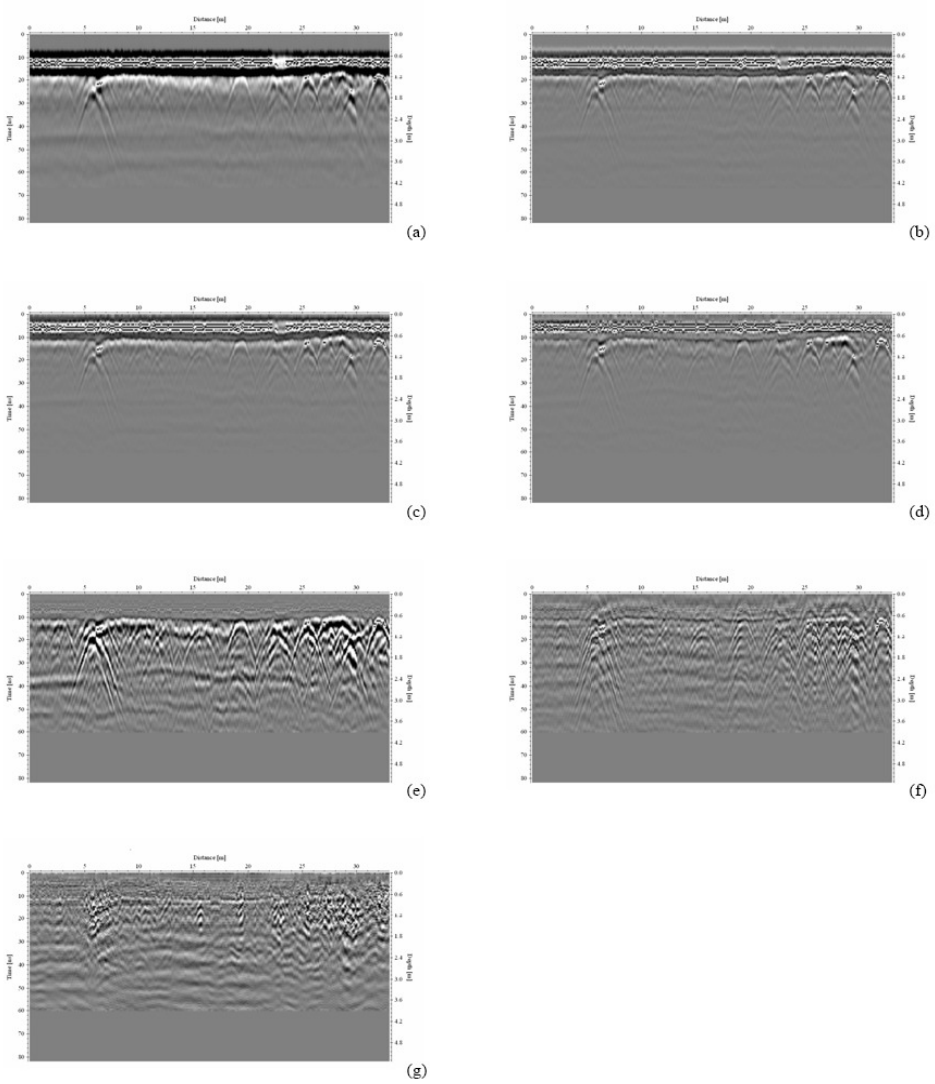

Figure 4. Processing steps applied to ground penetrating radar data of profile 100N, (a) raw data; (b) dewow; (c) set time zero; (d) background removal; (e) gain; (f) notch filter; and (g) migration

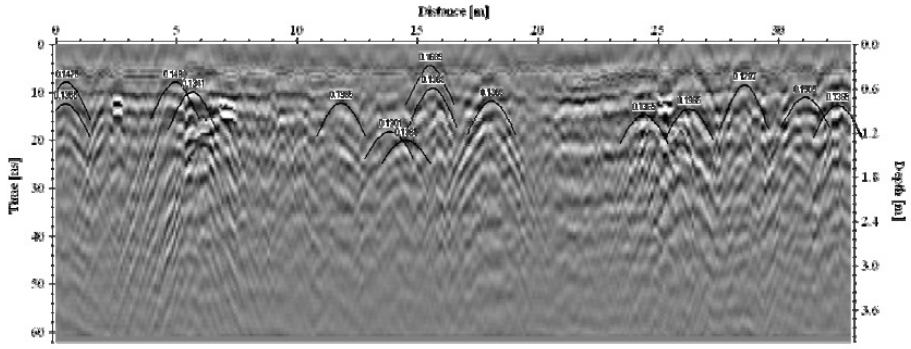

Figure 5 Velocity analyses with the diffraction hyperbolas method on the profile 160N. Labeled numbers over hyperbolas are their corresponding velocity values in m/ns

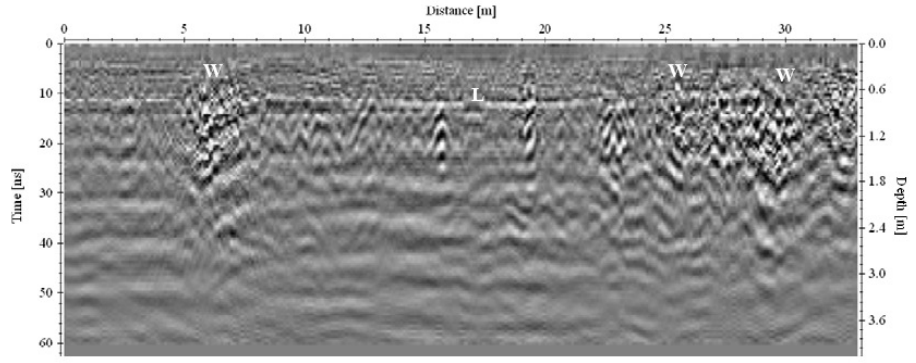

Figure 6. Two-dimensional image of processed ground penetrating radar data on profile 100N

TIME–SLICE MAPS

A time–slice map shows reflected wave amplitude distribution at a particular depth. In any one slice, low–amplitude variations indicate the presence of fairly homogeneous material and high amplitudes indicate significant subsurface discontinuities that, in many cases, relate to buried features. An abrupt change between an area of low and high amplitude can indicate the presence of a major buried interface between two media (Conyers, 2001).

Due to possible changes of velocity, both across the area and with depth, horizontal time slices must be considered as only approximate depth slices. In this study, the time–slice technique was used to display amplitude variations within consecutive soil layers approximately 0.25 meter thick between

the surface and a depth of 2.5 meters. Depth slices are shown in Figure 7. High amplitude anomalies labeled W were interpreted as ancient walls or ancient building remains.

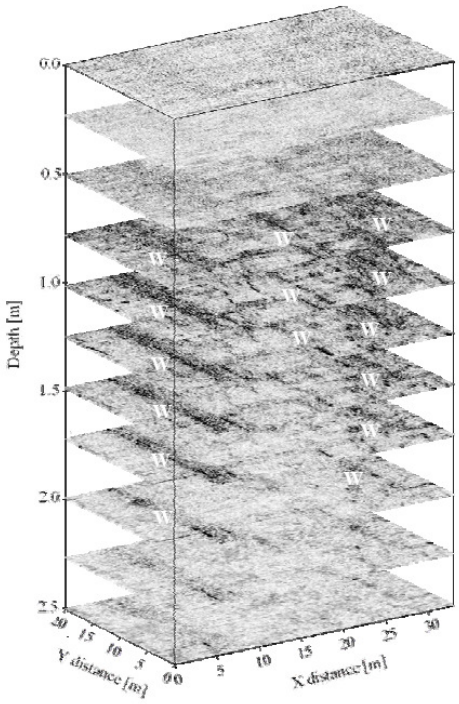

Figure 7. Ground penetrating radar depth slices; high amplitude anomalies labeled W are probably related to subsurface archaeological structures

ISO–AMPLITUDE SURFACE MAPS

In iso–amplitude surface map construction, the gridded data of trace amplitudes are converted to reflection strength. A threshold value is then set and all trace amplitudes greater than, or equal to, this threshold value are used for constructing three-dimensional iso–amplitude surface maps.

Iso–amplitude surface maps of threshold values 60, 70, 80, and 90 percent are shown in Figure 8. These maps show that the lower the threshold values, the more visible are large and small objects.

Most strong and continuous reflections associated with anomalies labeled W in Figure 7 appear clearly in depths between 0.6 and 1.75 meters in the three-dimensional cube threshold volume (Figure 8). Threshold values of 80 percent and 90 percent provide clearer subsurface pictures of archaeological targets than other threshold values. A side view, the x–z plane, and a top view, the x–y plane, of the 80 percent threshold value iso–amplitude surface maps were constructed to facilitate the

interpretation (Figure 9). The shape and alignment of these strong anomalies were interpreted as subsurface archaeological walls or building structure remains.

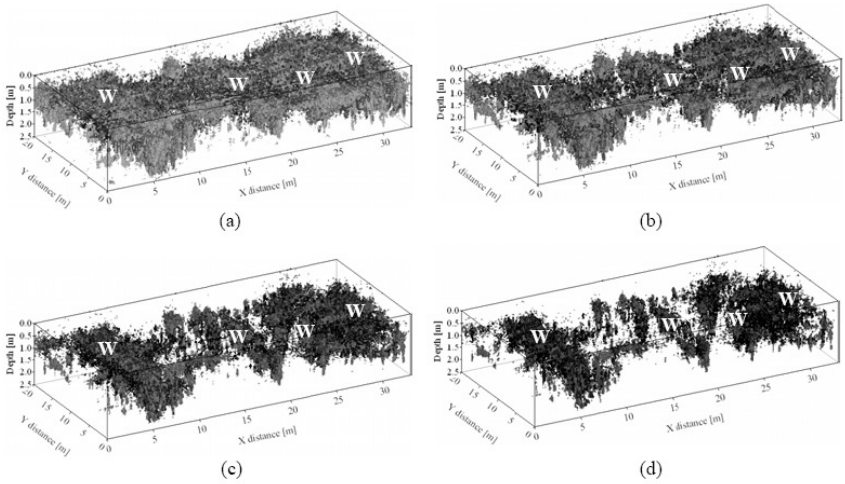

Figure 8. Three-dimensional visualization of ground penetrating radar data by means of iso–amplitude surfaces; views using different threshold values: (a) 60%; (b) 70%; (c) 80%; (d) 90%

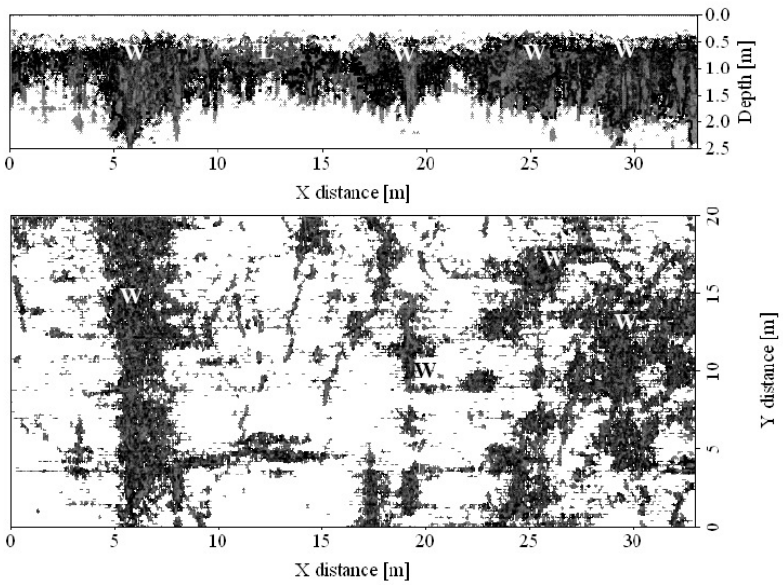

Figure 9. Side view x–z plane and top view x–y plane of ground penetrating radar data of threshold value 80%

Some archaeological test pits were dug in the study area in order to verify anomalies identified from ground penetrating radar measurements. Anomalies labeled W correspond to ancient walls and ancient building structure remains at estimated depths of 0.3 to 0.5 meter. Linear anomaly labeled L corresponds to a ground layer composed of sand and small pieces of ancient bricks (Figure 10).

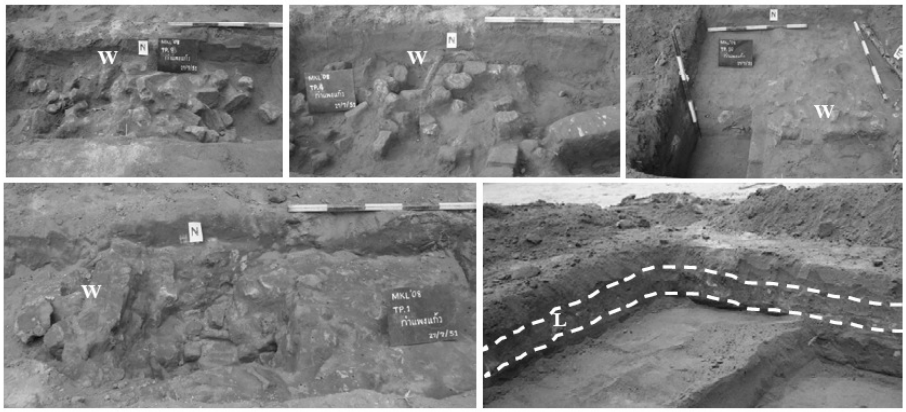

Figure 10. Archaeological test pits for verifying ground penetrating radar anomalies

CONCLUSION

Three-dimensional ground penetrating radar imaging was successfully used in mapping buried archaeological structures of the Wat Mo Klan archaeological site in Nakhon Si Thammarat Province. Buried ancient walls and archaeological structures show as groups of hyperbolic ground penetrating radar anomalies. These anomalies continue across many measuring lines at depths of 0.39 to 1.95 meters. Also on these lines is an interface between present and ancient surface soils. This interface appears as a nearly horizontal linear anomaly at depths of 0.65 to 0.91 meter. Archaeological test pits confirmed the interpretations. Three-dimensional ground penetrating radar imaging is, therefore, considered to be a useful tool in detailed archeological mapping and planning for archaeological excavation pits.

ACKNOWLEDGEMENTS

The authors thank the Graduate School of Prince of Songkla University for the scholarship to carry out this study. Thanks to the IPPS of Uppsala University, Sweden, for the research equipment and interpretation software. Very special thanks to the 14th Regional Office of the Fine Arts Departmant, Nakhon Si Thammarat, for permission to conduct research and for providing related

archaeological information and excavation in the study area. The authors also express their gratitude to the graduate geophysics students at Prince of Songkla University who helped with the fieldwork.

REFERENCES

Acqua, A. D., Sarti, A., Tubaro S., and Zanzi, L. 2004. Detection of linear objects in ground penetrating radar data. *Signal Processing* **84**, 785–799.

Arlsan, E., Biella, G., Boniolo, G., Caporusso, D., Franco, R., Lozej, A. and Veronese, L. 1999. Geophysical investigations of the Olonium Roman site Northern Como Lake. *Journal of Applied Geophysics* **41**, 169–188.

Beres, M., Huggenberger, P., Green, A.G. and Horstmeyer, H. 1999. Using two– and three–dimensional georadar methods to characterize glaciofluvial architecture. *Sedimentary Geology* **129**, 1–24.

Conyers, L. B. 2001. Ground penetrating radar. Encyclopedia of Imaging Science and Technology,New York,USA. 463–476.

Gracia, V.P., Canas, J.A., Pujades, L.G., Clapes, J., Caselles, O., Garcia, F. and Osorio, R. 2000. Ground penetrating radarr survey to confirm the location of ancient structures under the Valencian Cathedral Spain. *Journal of Applied Geophysics* 43, 167–174.

Grasmueck, M., Weger, R. and Horstmeyer, H. 2005. Full–resolution three-dimensional ground penetrating radar imaging. *Geophysics* **70**, K12–K19.

Heincke, B., Green, A.G., Kruk, J. and Horstmeyer, H. 2005. Acquisition and processing strategies for three-dimensional georadar surveying a region characterized by rugged topography. *Geophysics* **70**, K53–K61.

Hruska, J. and Fuchs, G. 1999. Ground penetrating radar prospection in ancient Ephesos. *Journal of Applied Geophysics* **41**, 293–312.

Leucci, G. and Negri, S. 2006. Use of ground penetrating radar to map subsurface archaeological features in an urban area. *Journal of Archaeological Science* **33**, 502–512.

Lohawijarn, W. 2005. Geophysical Investigation at some archaeological sites of Nakhon Si Thammarat province in Peninsular Thailand. Proceeding of the *Seminar on Thailand–Malaysia: Malay Penninsula Archaeology Programme*, 4–10 September 2004, Thailand and Malaysia, 125–132.

Negri, S. and Leucci, G. 2006. Geophysical investigation of the Temple of Apollo (Hierapolis, Turkey). *Journal of Archaeological Science* **33**, 1505–1513.

Pattanaviriyapisan, A. 1999. A study of Archaeology Morphology with High Frequency Electromagnetic Wave, Hat Yai. M.Sc. Thesis, Prince of Songkla University. 157 p. (in Thai)

Ranalli, D., Scozzafava, M. and Tallini, M. 2004. Ground penetrating radar investigations for the restoration of historic buildings: the case study of the Collemaggio Basilica (L'Aquila, Italy). *Journal of Cultural Heritage* **5**, 91–99.

Sambuelli, L., Socco, L.V. and Brecciaroli, L. 1999. Acquisition and processing of electric, magnetic and ground penetrating radar data on a Roman site Victimulae, Salussola, Biella. *Journal of Applied Geophysics* **41**, 189–204.

Sandmeier, K.J. 2007. Reflexw Version 4.5 manual, Sandmeier Software, Zipser Strabe 1, D–76227 Karlsruhe, Germany.

Shaaban, F.F. and Shaaban, F.A. 2001. Use of two–dimensional electric resistivity and ground penetrating radar for archaeological prospecting at the ancient capital of Egypt. *Journal of African Earth Sciences* **33**, 661–671.

Sigurdsson, T. and Overgaard, T. 1998. Application of ground penetrating radar for 3–D visualization of geological and structural variation in a limestone formation. *Journal of Applied Geophysics* **40**, 29–36.

Whiting, B.M., McFarland, D.P., and Hackenberger, S. 2001. Three-dimensional ground penetrating radar study of a prehistoric site in Barbados, West Indies. *Journal of Applied Geophysics* **47**, 217–226.

Zeng, X., McMechan, G.A., Bhattacharya, J.P., Aiken, C.L.V., Xu, X., Hammon, W.S. and Corbeanu, R.M. 2004. Three-dimensional imaging of a reservoir analogue in point bar deposits in the Ferron Sandstone, Utah, using ground–penetrating radar. *Geophysical Prospecting* **52**, 151-163.

VITAE

Name Miss Araya Chansane

Student ID 4910220106

Education

Degree	Name of Institution	Year of Graduation
B.Sc. in Physics	Prince of Songkla University	2005

Scholarship Awards during Enrolment

1. The Development and Promotion of Science and Technology Talents Project (DPST Project) from The Institute for the Promotion of Teaching Science and Technology, Ministry of Education
2. Research Assistant from The Research Fund of Faculty of Science, Prince of Songkla University (2006)

List of Publication and Proceedings

Chansane, A., Lohawijarn, W. and Phongdara, B., 2008. Application of 3D GPR imaging in locating Wat Mo Khlan archaeological site in Nakhon Si Thammarat, Thailand. Proceeding of the Conference on "Proceedings of The International Conference On Applied Geophysics (Geophysics Chiang Mai 2008)", 12^{nd}-13^{rd} Nov 2008, Chiang Mai, Thailand, 29-42.